Transport of Liquid Phase Organic Solutes in Liquid Crystalline Membranes

Sangil Han

Dissertation submitted to the faculty of the Virginia Polytechnic Institute and State University in partial fulfillment of the requirements for the degree of

Doctor of Philosophy
In
Chemical Engineering

Stephen M. Martin, Chair
Eva Marand
Richey M. Davis
Louis A. Madsen

September. 08. 2010
Blacksburg, VA

Keywords: Liquid crystals, membrane, isomers, enantiomers, circular dichroism, chirality

Transport of Liquid Phase Organic Solutes in Liquid Crystalline Membranes

Sangil Han

ABSTRACT

Porous cellulose nitrate membranes were impregnated with 8CB and PCH5 LCs (liquid crystals) and separations of solutes dissolved in aqueous phases were performed while monitoring solute concentration via UV-VIS spectrometry. The diffusing organic solutes, which consist of one aromatic ring and various functional groups, were selected to exclude molecular size effects on the diffusion and sorption.

We studied the effects on solute transport of solute intra-molecular hydrogen bonding and solute/LC intermolecular hydrogen bonding. Hydrogen-bonding effects are a significant factor in the permeation selectivity of positional isomers. The reduction of available hydrogen-bond donors in aromatic ortho-isomers due to intramolecular H-bonding resulted in significant differences in the diffusion relative to the para-isomers which possessed more available H-bond donors. Solutes possessing multiple H-bonding interactions experienced a higher barrier to diffusion and, consequently, lower diffusivities. Diffusing solutes with a single available H-bond donor exhibited faster diffusion than solutes without H-bond donors.

PCH5 embedded membranes showed higher solubility and diffusivity than the 8CB embedded membranes due to less dense molecular packing in PCH5 resulting from the bent cyclohexyl ring. The PCH5 LC membranes demonstrated enhanced permeation selectivity for hydroxybenzoic acid and aminophenol isomers primarily due to increased sorption selectivity. Shape selective absorption of rod-like para-isomers in the nematic phase was observed in both 8CB and PCH5 LCs.

A nonchiral based HPLC-CD (High Performance Liquid Chromatography-CD) system was developed for the characterization of enantioselective separations. An enantioselective cholesteric liquid crystal membrane was fabricated and evaluated using the nonchiral HPLC-CD system. The cholesteric LC membrane showed enantioselectivity in the cholesteric phase where activation energies of permeation for 1-phenylethanol enantiomers were significantly increased

due to the increased interactions between enantiomer and LC phase. The enantioselectivity increased with decreasing pore size of the membrane and increasing chiral dopant compositions. The selectivity decreases when there are no hydrogen bonding interactions between enantiomer and chiral dopant.

Acknowledgements

First, I would like to acknowledge my advisor, Dr. Martin for his guidance to perform research in the right direction. He spent a lot of time not only to advise the research, but also to revise my written English. I also appreciate the opportunity to experience different research areas. Without Dr. Martin, I could have not accomplished my goals.

I would also like to acknowledge my committee, Dr. Marand, Dr. Davis, and Dr. Madsen. Their continued encouragement and suggestions are extremely appreciated. I would also like to express my thanks to Dr. Baird for his guidance in the polymer research.

This is an opportunity to express my sincere thanks to departmental staff for the help over the years, especially Mike Vaught and Riley Chan who helped build the experimental apparatus. I also would like to thank my colleague Mike Heinzer for the successful collaboration performed at Stanford Synchrotron Radiation Laboratory (SSRL). I would like to extend a special thanks to John Pople at SSRL for his help analyzing scattering data and Cynthia Patty for the lab preparation.

My deepest thanks go to my wife, Yeonhee Kim, for her help throughout the graduate school experience, cooking as a wife, learning as a classmate, and guidance as a researcher. Her invaluable support enabled me to accomplish my degree.

To my mother and father, I acknowledge their emotional support at all times.

Table of Contents

List of Figures

Chapter 2

Chapter 3

Chapter 4

Chapter 5

Chapter 6

Chapter 7

List of Tables

Chapter 3

Chapter 4

Chapter 5

Chapter 6

Chapter 1. Introduction

Membrane separation technologies are attractive due to their higher energy efficiency, simplicity, convenience, and continuous operability[1,2] compared to conventional separation techniques such as distillation and chromatography. Chromatographic separations rely on an analyte in a mobile phase passing through a stationary phase; the analyte is separated from other solutes in the mixture based on the differential affinity between the mobile and the stationary phases. Furthermore there are limitations in the ability to separate isomers such as positional isomers (para, ortho, meta) which have similar boiling points[3] using distillation techniques. Similarily, chromatographic separations to produce pure enantiomers[4] such as drugs, have a low production rate. Accordingly, it would be beneficial to find new membrane materials capable of performing these separations.

There have been significant research efforts on liquid crystal (LC) materials for display applications due to their optical activity. In contrast, little work has been conducted on solute transport in LCs. Thermotropic liquid crystals (TLCs) exhibit anisotropic phases such as nematic, smectic and cholesteric phases, which are sensitive to temperature or electric field. We expected interesting transport behavior of dissolved solutes in TLCs due to the oriented LC phases, which affect the intermolecular interactions between the solutes and the LC molecules and the diffusion path.

By adding chiral dopants in the nematic LC phase, LC molecules are reoriented in a helical way known as a cholesteric liquid crystal (ChLC) phase. The ChLC phase has been widely studied in display applications, but separation applications using the ChLC phase have only been demonstrated in gas chromatographic separations[5,6]. No ChLC based membrane separations have been reported. Here we present a novel enantiomer separation membrane using the ChLC phase featuring a membrane chromatography transport mechanism through the membrane pores. The ChLC phase, in which the LC molecules are helically oriented due

to the addition of cholesterol-based chiral dopants to a nematic LC phase, exhibits left-handed chirality[7,8] at temperatures below 40 ℃.

In addition, a methodology for the determination of enantiomer compositions has been developed for enantioselective membrane separations. The technique relies on the use of circular dichroism (CD) in combination with non-chiral phase based HPLC (HPLC-CD). The HPLC-CD method has significant advantages over conventional chiral column based HPLC detection systems, as the HPLC-CD system does not require multiple expensive chiral columns. While the HPLC-CD system has been used for the determination of drug purity and enantioselective syntheses, to our knowledge there have been no reports of using the HPLC-CD system in membrane separation applications.

Chapter 2. Literature Review

2.1 Liquid Crystals

Liquid crystals (LCs) are materials which show liquid crystalline mesophases between the liquid and solid phases. In the liquid crystalline phase, liquid crystal molecules exhibit some order like a solid but also mobility like a liquid. Liquid crystals can be broadly categorized as thermotropic LCs or lyotropic LCs.

2.1.1 Lyotropic Liquid Crystals

Lyotropic LCs are amphiphilic molecules (Figure 2.1) which consist of polar head groups and non-polar organic tail groups.[9] Lyotropic LCs can self-organize upon addition of solvents such as water due to their amphiphilic properties. They show different ordered structures depending on the type of solvent concentration of the LCs.[10]

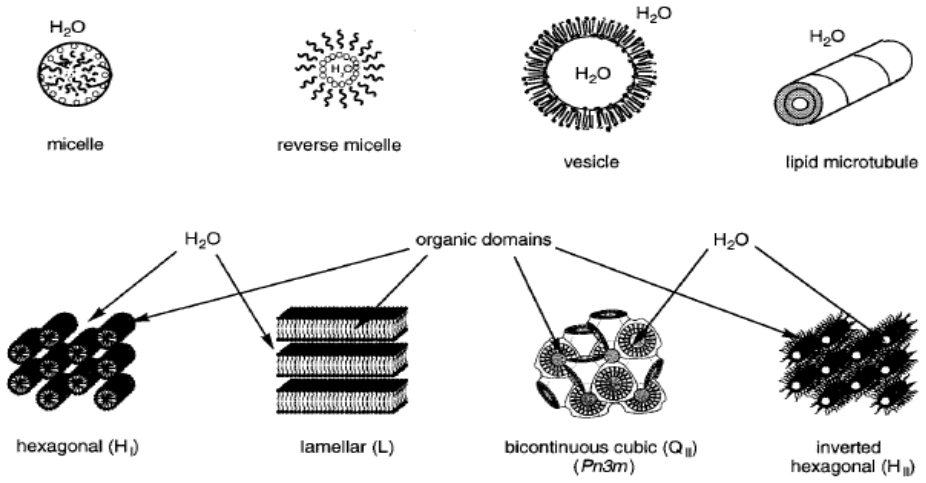

Figure 2.1: Common lyotropic LCs phases[2]

2.1.2 Thermotropic Liquid Crystals

Small molecule thermotropic liquid crystals (LCs) exhibit anisotropic phases that are responsive to various stimuli, including temperature, electric and magnetic fields, and the presence of impurities. Rod-like thermotropic LCs generally consist of a mesogen and two terminal groups (Figure 2.2).[11] The mesogen is a rigid rod-like moiety that consists of two or

more ring systems (aromatic, alicyclic, aromatic heterocycles, saturated heterocycles or condensed ring systems) connected by a central group. The central group can be polar (azogroups, azoxy-groups, imines, esters, thioesters, and amides) or non-polar (alkynes, alkenes or alkanes). The terminal groups are straight or branched alkyl/alkoxy chains which may contain functional groups (alkenes, alkynes, ethers, ketones, esters).

Figure 2.2: Typical shape of thermotropic liquid crystals

Thermotropic LCs can exhibit a variety of temperature-dependent phases (i.e. crystalline, smectic, nematic, cholesteric, isotropic) which are classified according to their orientational order, positional order, and chirality[12,13,14] (Figure 2.3). The LC molecules are aligned along their long axis in the nematic and smectic phases, but randomly oriented in the isotropic phase. Mesogens are aligned along the long axis in the nematic and smectic phases, but there is a layered structure in the smectic phase. The director can be parallel (SmA) or slightly tilted (SmC) to the layer normal direction.

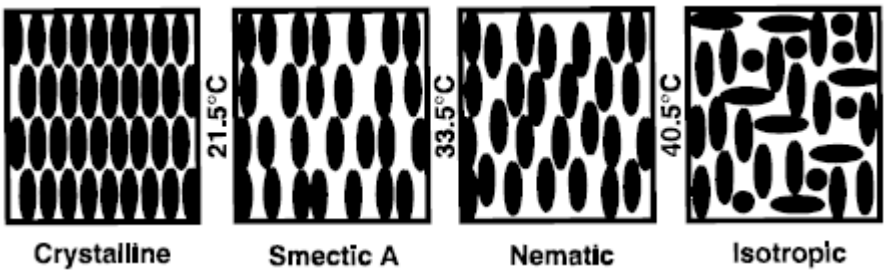

Figure 2.3: Schematic of different phases for octylcyanobiphenyl (8CB) LCs in various temperatures[14]

The tendency of LC molecules to align along a director (long axis) can be measured by the orientational order parameter, which is strongly temperature dependent, assuming the rods to be cylindrical. (Figure 2.4)[15]

Orientational order parameter, $S = (1/2) \times \langle 3\cos 2\theta - 1 \rangle$ (1.1)

θ is the angle between LC molecule and director, angular brackets denote a statistical average. S=0 for a completely random phase (isotropic) and S=1 for a fully ordered phase (crystal).

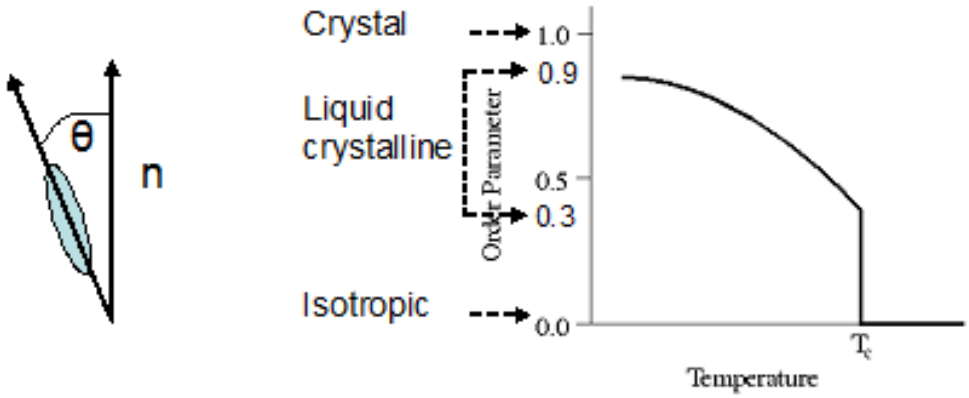

(a) (b)

Figure 2.4: Angle between LC and director (a), temperature versus order parameter (b). Liquid crystalline phase exists between the order parameter 0.9 and 0.3

2.1.3 Cholesteric Liquid Crystals

Cholesteric liquid crystals (ChLC) are liquid crystals which consist of cholesteryl group and a long alkyl group (Figure 2.5), which induces chiral nematic phase, or cholesteric phase (Figure 2.6,) in the nematic liquid crystal phase. The helical sense of cholesteric phase depends on the handedness of chiral dopants and the helical pitch decreases with an increase of chiral dopant composition.

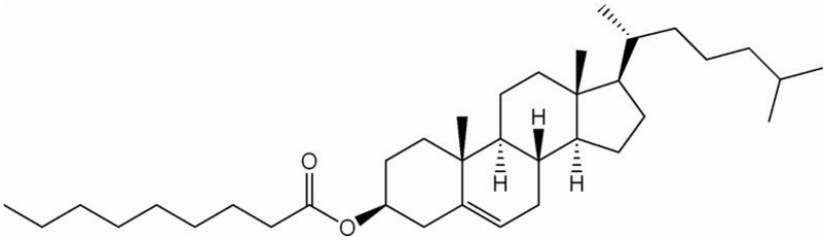

Figure 2.5: Cholesteryl Nonanoate (CN) (solid<79.6 ℃<cholesteric<88.5 ℃<isotropic)

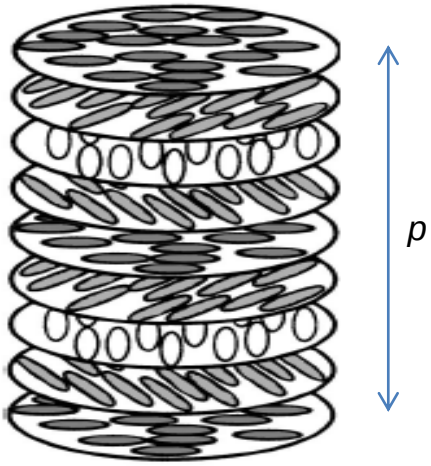

Figure 2.6: Schematic representation of the cholesteric phase.[13] The molecules are shown as elliptical rods. There is a rotation of the orientational ordering of molecules in the layers.

The cholesteric phase can be identified using cross-polarized optical microscopy. Different images, Grand-jean, fingerprint, and focal conic, are obtained depending on the helical axis orientations (Figure 2.7). In Grand-jean and fingerprint planes, the helical axes are aligned vertical and parallel to the substrates respectively. When the helical structures of the LCs are vertically aligned to the substrate surface, the phase will selectively reflect light at a certain wavelength, in which the pitch of the phase is similar to the wavelength of light.[13] The helical axes in the focal conic plane are randomly oriented.

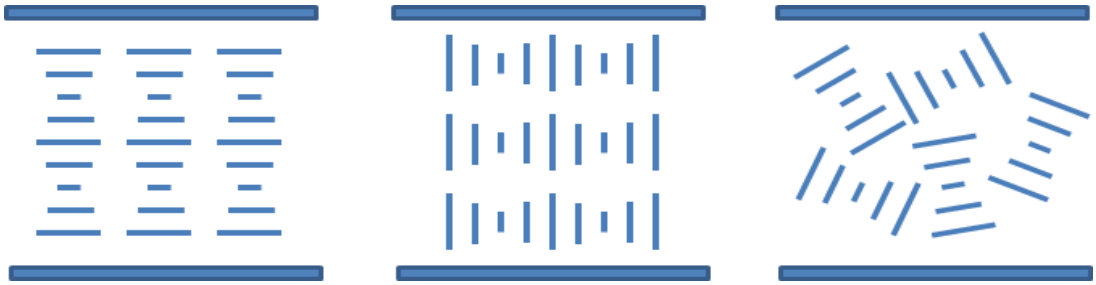

(a) Grand-jean Fingerprint Focal conic

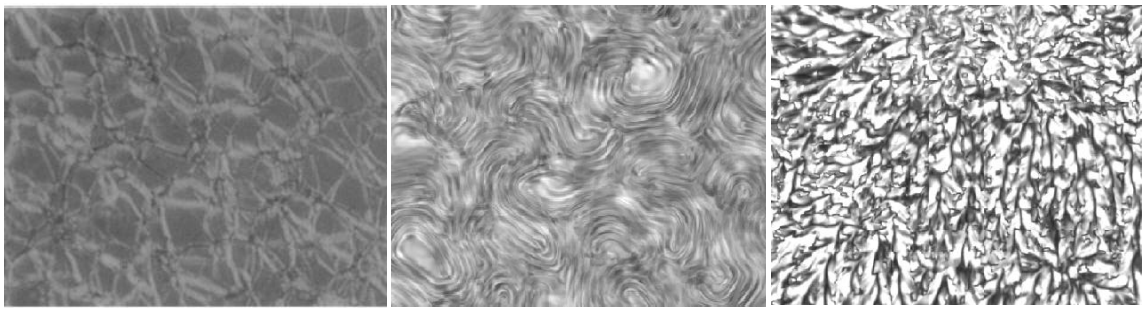

(b) Grand-jean[13] Fingerprint Focal conic

Figure 2.7: Orientations[16] of liquid crystals in cholesteric phase (a) and microscopy images (b) between glass substrates

2.2 Liquid Crystals for Membrane Separations

Most liquid crystal studies have been focused on electro-optical properties for display applications. Thus far, there have been few studies focusing on solute transport and membrane separations. The phase transition properties of LCs were used to develop on-off drug release membranes which can be controlled by temperature changes.[17,18,19,20,21,22] Nozawa et al.[20,21] investigated LCs as a thermoresponsive membrane material for polymer alloyed membranes and LC supported membranes, and concluded that the LC supported membrane could perform a sharp on-off drug control. In addition to the above supported liquid membranes, Inui et al. developed polymerized liquid crystal membranes for size selective separations using their highly ordered nematic phase.[23,24]

2.2.1 Liquid Crystalline Polymer Membranes

Inui et al. made liquid crystalline side-chain polymer membranes (Figure 2.8), which were composed of different mesogenic group compositions, to separate organic mixtures such as a mixture of benzene and cyclohexane and a mixture of ethanol and water using a size selective mechanism. The membranes were fabricated by a casting method and sandwiched between two porous support films to give robustness.

In order to evaluate the membrane performance, a pervaporation technique was used (Figure 2.9), which is an energy efficient combination of membrane permeation and evaporation for the separation of azeotropic mixtures, close-boiling point mixtures, and heat-sensitive mixtures. The permeated product was sampled after steady state was reached from a U-tube at liquid nitrogen temperature, and analyzed by gas chromotography.

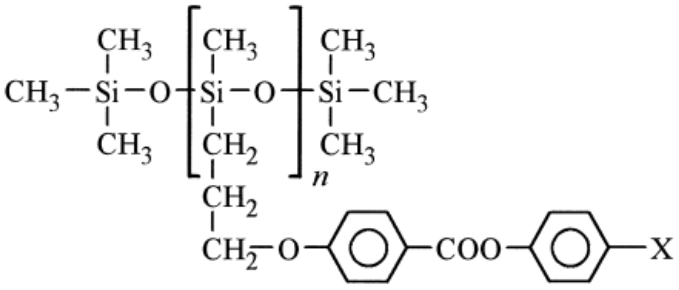

X : OCH_3 (*n*-LCP)
CN (*s*-LCP)

Figure 2.8: Liquid crystalline polymer[23]

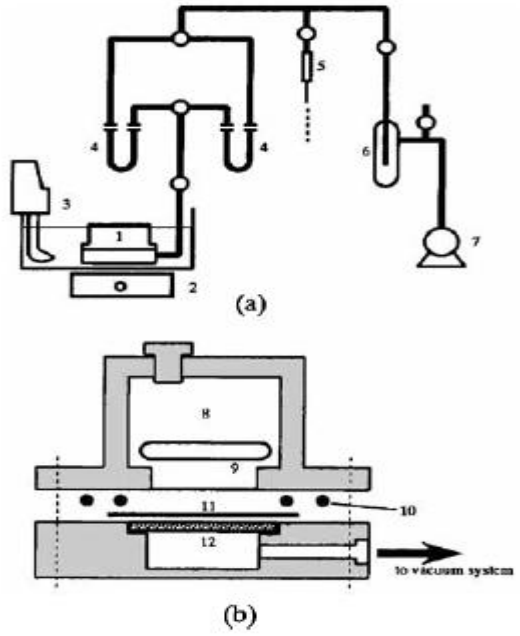

Figure 2.9: Pervaporation apparatus and cross-section of permeation cell[25] (1) permeation cell, (2) magnetic stirrer, (3) water bath, (4) cold U-tube trap, (5) pirani gauge, (6) cold trap, (7) vacuum pump, (8) feed solution, (9), stirring rod, (10) O-ring, (11) membrane, (12) sintered stainless disk.

Figure 2.10 shows the size selective separation mechanism through a liquid crystalline polymer membrane. According to the results, the diffusion selectivity was a major factor for the selective permeation in the liquid crystalline phase due to the size differences. Benzene, with a smaller molar volume (89.4 cm^3/mol), diffused faster than cyclohexane (108.7 cm^3/mol) in the highly ordered liquid crystalline phase. Based on activation energies for the permeations in the different phases, the activation energy was highest in the liquid crystalline phase compared to the glassy and the isotropic phases. This suggested that the diffusion is much more inhibited in the liquid crystalline phase than other phases. In the isotropic phase, the permeation selectivity was reduced as the permeations of both molecules were increased in the absence of the anisotropic orientation.

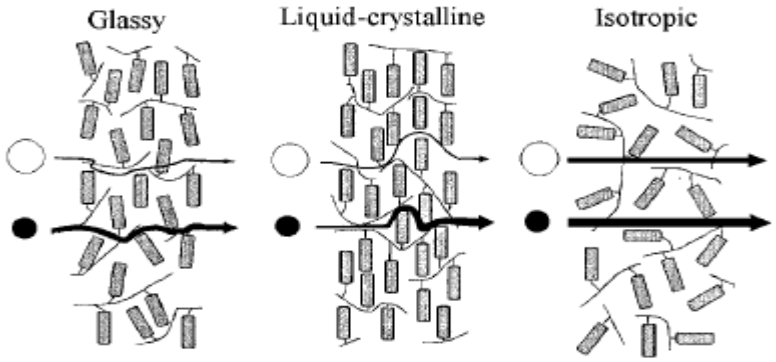

Figure 2.10: Permeation mechanism model for the benzene and the cyclohexane ○: cyclohexane, ●: benzene.[26]

2.2.2 Liquid Crystal Embedded Membrane

Lin et al. employed two cholesteric LCs, cholesteryl oleyl carbonate (COC) and cholesteryl nonanoate (CN), for thermo-responsive drug release membranes (Figure 2.11). The cholesteric LCs consist of a cholesterol moiety and a flexible chain with a chiral center. COC has transition temperatures at 19 °C (smectic-cholesteric) and 38 °C (cholesteric–isotropic), and CN has transition temperatures at 80 °C (crystal-cholesteric) and 89 °C (cholesteric–isotropic). The thermo-responsive release mechanism depended on the solubility differences in the different phases of the LCs.

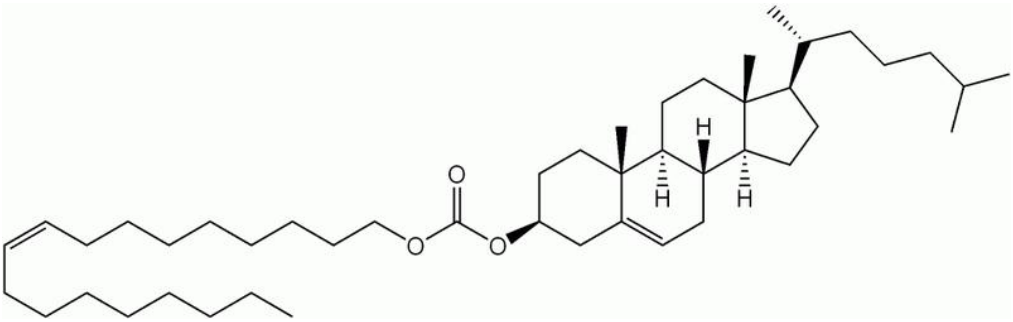

(a) COC

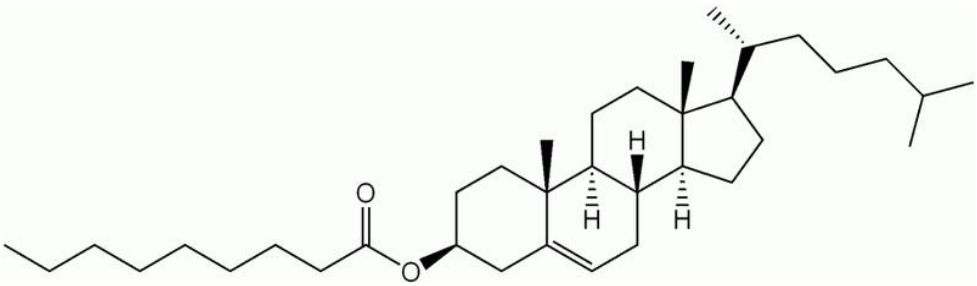

(b) CN

Figure 2.11: Cholesteric liquid crystals used for the thermo-responsive membrane

The transition temperatures for COC and CN mixtures were measured using a differential scanning calorimeter (DSC) with a heating rate of 3 °C/min. The transition temperature gradually increased as the CN concentration increased, (Figure 2.12) as predicted from Schroder-van Laar equations.[27]

$$-\ln x_1 = \frac{\Delta H_{f1}}{R}\left(\frac{1}{T} - \frac{1}{T_1}\right) \qquad (2.1)$$

Where $\Delta H_{f1,}$ T_1, x_1, T are heat of fusion, transition temperature of pure component 1 from crystal to liquid crystalline mesophase, mole fraction of component 1, transition temperature of a binary mixture containing x_1 mole fraction, respectively.

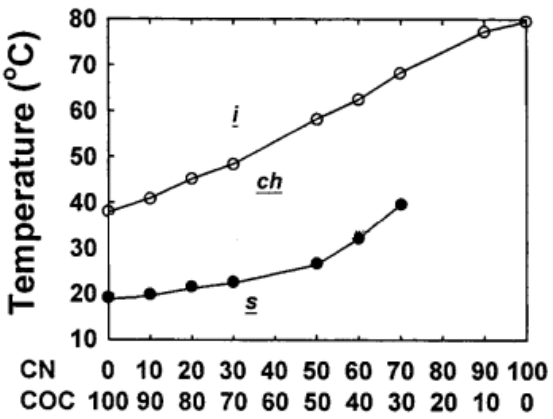

Figure 2.12: Transition temperature vs. LC composition[28]. White and black symbols represent cholesteric to isotropic phase transition and solid to cholesteric phase transition, respectively.

A binary mixture of 36 % COC and 64 % CN was used as the transition temperature of 35.7 °C for this mixture is close to that of body temperature, and is thus suitable for controlled drug release. The liquid crystals were embedded in a cellulose nitrate membrane support (pore size 0.2 μm and 0.45 μm) and tested for permeation of the drug salbutamol sulfate between aqueous phases. The membrane showed on-off drug release controlled by phase transitions (anisotropic and crystal phases) (Figure 2.13).

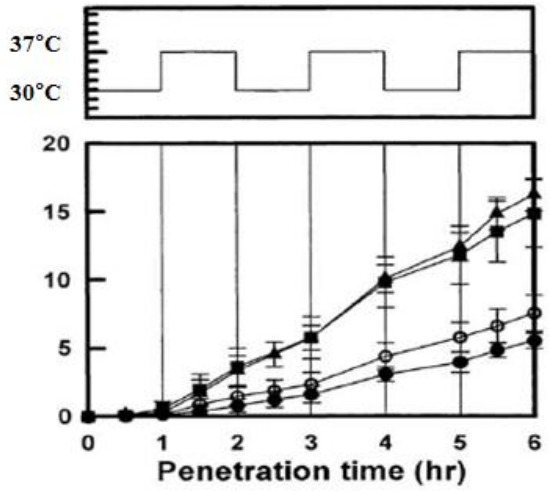

Figure 2.13: Salbutamol sulfate permeation through a mixture of COC and CN supported cellulose nitrate membrane[19]

Dinarvand et al. proposed a triple-layer membrane (Figure 2.14) in which 5CB LCs were placed between two hydrophilic cellulose nitrate membranes. The triple-layer membranes also showed temperature controlled drug release (Figure 2.15) without any LC loss from the membranes during transport.

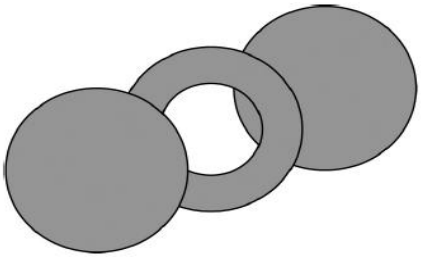

(a) Triple layer membrane

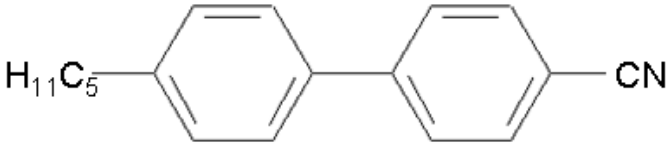

(b) 5CB LC

Figure 2.14: Schematic of triple-layer membrane (a) and 4-cyano-4'-pentylbiphenyl (5CB) liquid crystal (b)[22]

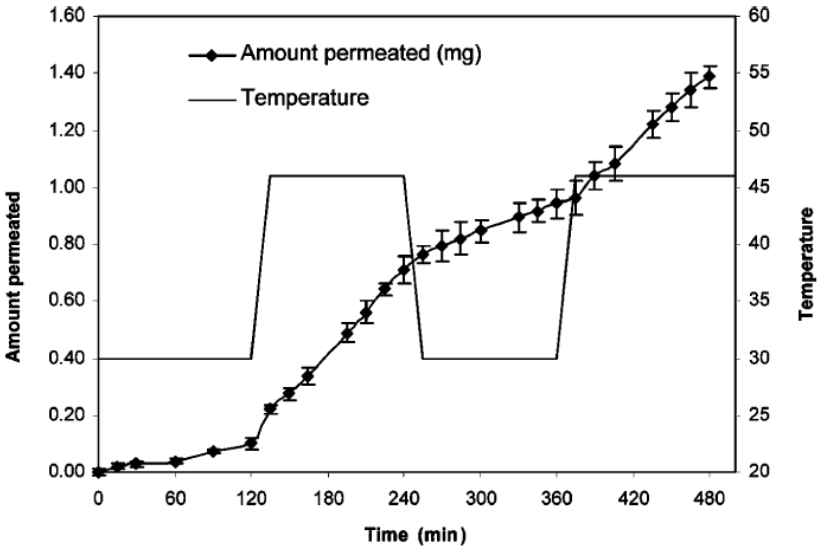

Figure 2.15: Methimazole permeation through triple-layer membrane containing 5CB with a cycling 30 °C (off, liquid crystalline phase) and 46 °C (on, isotropic phase)[22]

2.2.3 Liquid Crystal/Polymer Composite Membranes

Polymer dispersed liquid crystal (PDLC) membranes, where the LC droplets are embedded in a polymer network (Figure 2.16), have been studied for optical activity due to their light scattering properties in the isotropic phase with a field-free state (Figure 2.17). In the electric off state, the LC molecules are aligned isotropically in each droplet, whereas the LC molecules are aligned parallel to the electric field in the electric on state due to the high dipole moments of the LCs.

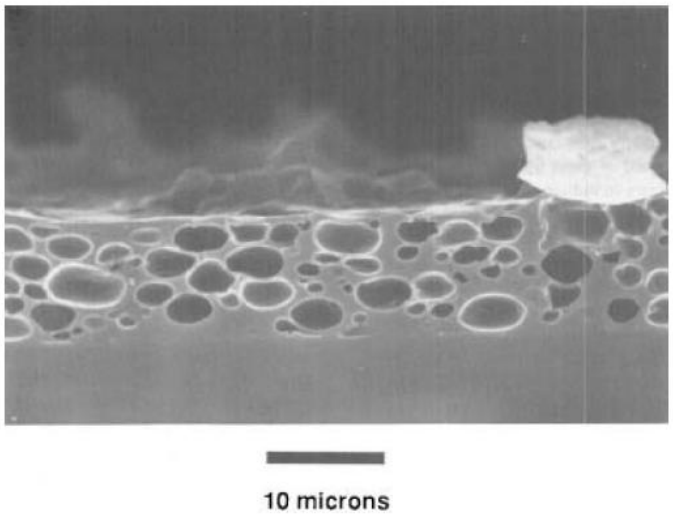

Figure 2.16: Scanning electron micrograph of a polymer/nematic LC film (LC was removed from the polymer network)[29]

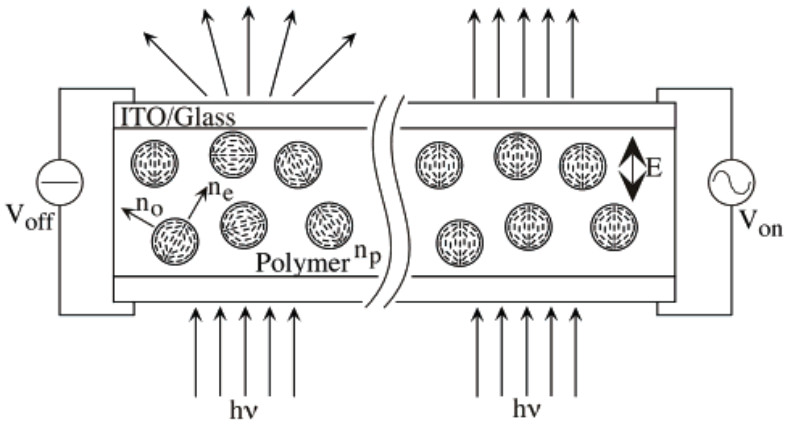

Figure 2.17: Schematic representation of the light transmission of a PDLC membrane in the on and off electric field[30]

In addition, polymer dispersed liquid crystal (PDLC) membranes have been studied for membrane separations[31]. PDLC membranes were fabricated by a solution casting method with polycarbonate and N-(4-ethoxybenzylidene 4'-n-butylaniline) (EBBA) LCs (Figure 2.18). Homogeneous dispersion of EBBA was observed for 15 wt% EBBA blend film, while EBBA LC droplets were observed for 45 wt% and 60 wt% of LC. In gas phase separations through the PDLC membranes, a large increase in permeability was found across the phase transitions of EBBA (Figure 2.19). This resulted from the sorption process of hydrocarbon gases, because permeability increased with an increasing number of carbon atoms in the order of n-C_4H_{10}, i-C_4H_{10}, C_3H_8, and CH_4 above the phase transition temperature. The authors state that the higher permeability for the solutes with higher molecular weight and size can not be understood by a diffusion control mechanism, but can be reasonably explained by a sorption mechanism.

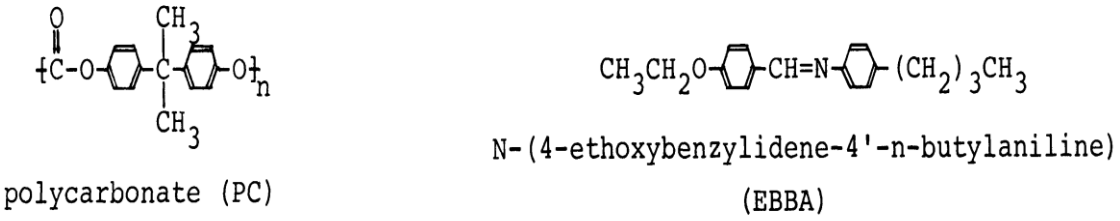

Figure 2.18: Polymer support and thermotropic liquid crystal[31]

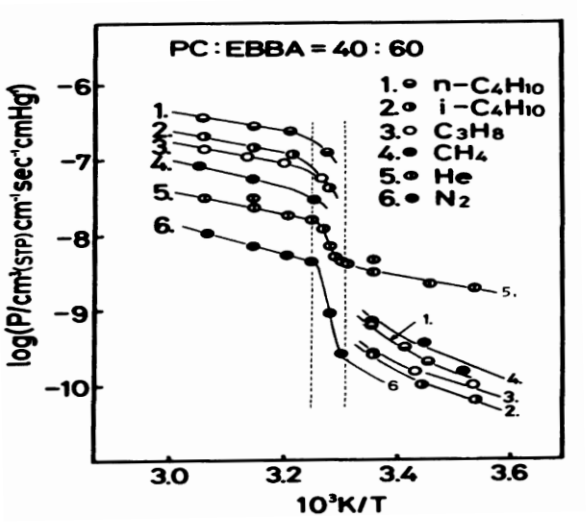

Figure 2.19: Arrhenius plot of permeability for 60wt% EBBA composite membranes[31]

2.3 The Effects of Liquid Crystal Phase Transitions on Transport

Solubility and diffusivity of gas molecules depends on the liquid crystal phase transitions due to physical property changes such as free volume and orientation. In addition, there is a shape-selective adsorption of positional isomers in the anisotropic liquid crystal stationary phases in chromatographic separations.

2.3.1 Transport Behaviors in the Liquid Crystal Phase Transitions

There have been studies[32,33,34] on the sorption and diffusion behavior of gas molecules in thermotropic liquid crystals, methoxybenzilidene butylanaline (MBBA), 4-(trans-4-pentylcyclohexyl)benzonitrile (PCH5), and 1-isothiocyanato-4-(trans-4-octylcyclohexyl) benzene PCH8-CNS (Figure 2.20).

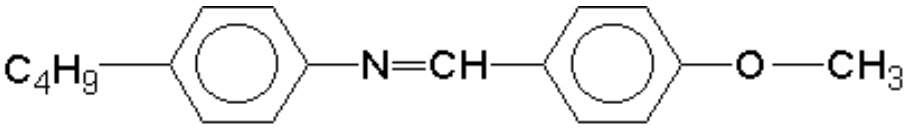

(a) MBBA (Cryst – 21 ℃ – N – 45 ℃ -- Iso)

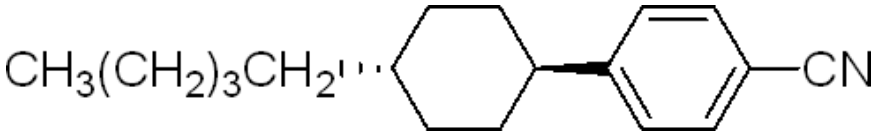

(b) PCH5 (Cryst – 30 ℃ – N – 55.2 ℃ -- Iso)

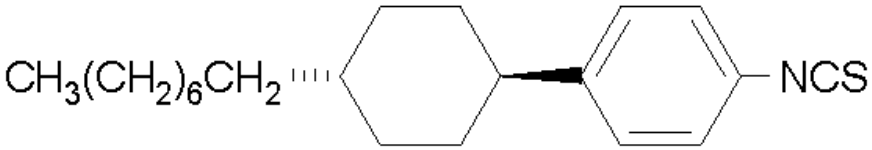

(c) PCH8-CNS

Figure 2.20: Thermotropic liquid crystals used for the gas phase transport

For quantitative analysis, a mathematical model was used (eq. 2.2), which enables calculation of diffusivity and solubility in the one-sided gas sorption process. Liquid crystal samples were placed on a quartz pan to measure the sorbed gas weight (Figure 2.21).

$$\frac{c(t)}{c_e} = \frac{M_t}{M_\infty} = 1 - \sum_{n=0}^{\infty} \frac{8}{(2n+1)^2 \pi^2} \exp\left\{\frac{-D(2n+1)^2 \pi^2 t}{4l^2}\right\}, (n = 0, 1, 2, ...) \qquad (2.2)$$

Where M_t is the total amount of the gas sorbed by the liquid crystals at time t, M_∞ is the equilibrium sorption after infinite time, l is the liquid crystal thickness, D is the diffusivity, and c_e is the equilibrium gas concentration after infinite time.

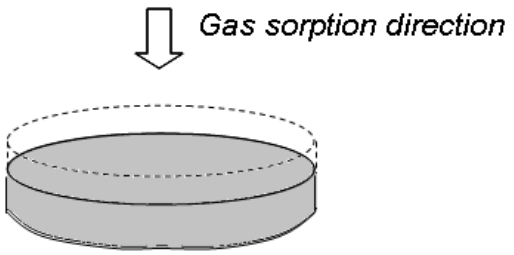

Figure 2.21: Schematic of gas sorption model

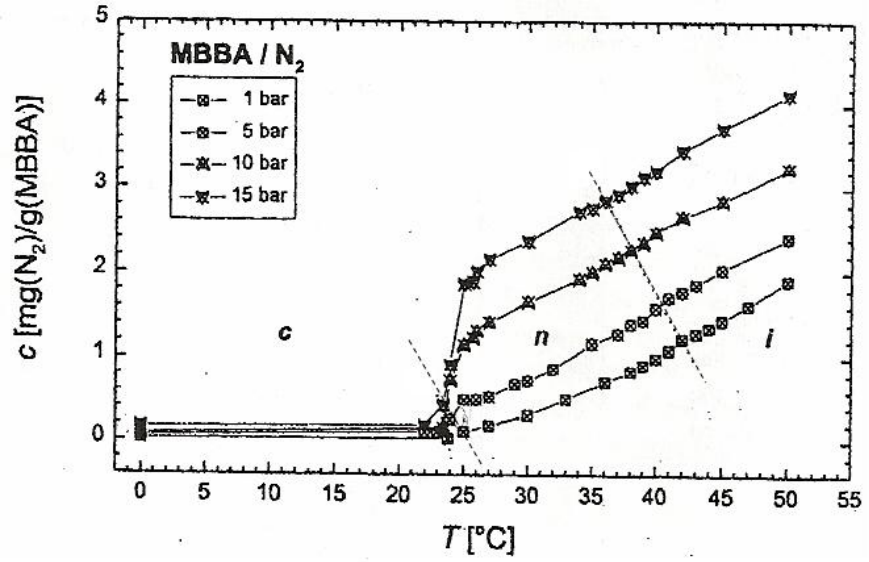

Figure 2.22: Temperature dependence of the sorption of N_2 in MBBA at various pressures.[32] Dashed lines present the liquid crystal phase transitions.

In Figure 2.22, the sorption was very low in the crystal phase due to the limited free volume in the crystal phase, but increased in the nematic and isotropic phases. The LC transition phase temperatures depended on the gas pressure, with the transition temperature decreasing with the increasing gas pressure. In addition, the solubility (maximum sorbed amount) depended on the gas pressure. Among the four gases tested (N_2, CO_2, Ar and He), CO_2 showed the highest solubility, probably due to the interaction of the polar bond of CO_2 with the liquid crystals.

Chen et al.[35] investigated the gas sorption behavior in liquid crystalline side-group polymers (LCP). The LCP membranes showed different sorption behaviors compared to the low-molecular weight liquid crystals. In the smectic and isotropic phases, the LCP membranes showed decreasing sorption with increasing temperature while low-molecular LCs showed increasing sorption amount with increasing temperature (Figure 2.23). They proposed a combination of polymer and low-molecular LCs (Figure 2.24) in which the sorption of gases was not only dependent on the mesogenic groups of LCs, but also the polymer backbone.

In common polymers, the solubility in polymers depends on the van't Hoff relationship:[36]

$$S = S_0 \exp\left[-\frac{\Delta H_S}{RT}\right] \qquad (2.3)$$

$$\Delta H_S = \Delta H_{condensation} + \Delta H_{mixing} \qquad (2.4)$$

where S_0 is a constant, ΔH_S is the partial molar enthalpy of sorption, R is gas constant, T is absolute temperature, $\Delta H_{condensation}$ and ΔH_{mixing} are the enthalpy changes associated with the first and second thermodynamic processes, respectively.

For condensable gases and vapors such as CO_2 and organic vapors, ΔH_S becomes negative as the ΔH_S is governed by the large negative contribution of $\Delta H_{condensation}$. Therefore,

the solubility in common polymers decreases with increasing temperature since the exponential term in equation 2.3 is positive.[36] For low molecular liquid crystals, the solubility mainly depends on the free volume, and as a result the solubility gradually increases with increasing temperatures and significantly increases at the phase transitions.[35] Polymeric liquid crystals possess properties from both common polymer and low molecular liquid crystals. Therefore, the sorption of CO_2 depends on not only the liquid crystal mesogenic group but also the polymer backbone. The polymeric liquid crystals exhibited decreasing solubilities with increasing temperature, but exhibit significantly increased solubility at the phase transition due to the increased free volume due to the liquid crystalline side-groups.[35]

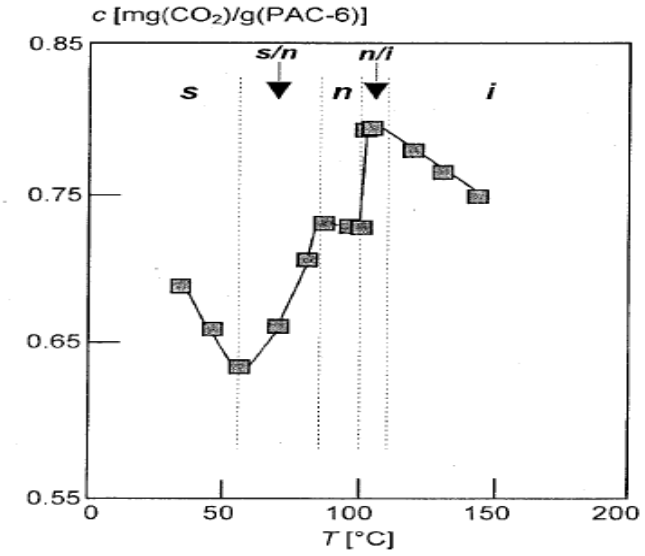

Figure 2.23: CO_2 concentration absorbed in LCP membranes versus temperature in 1.2 bar[35]

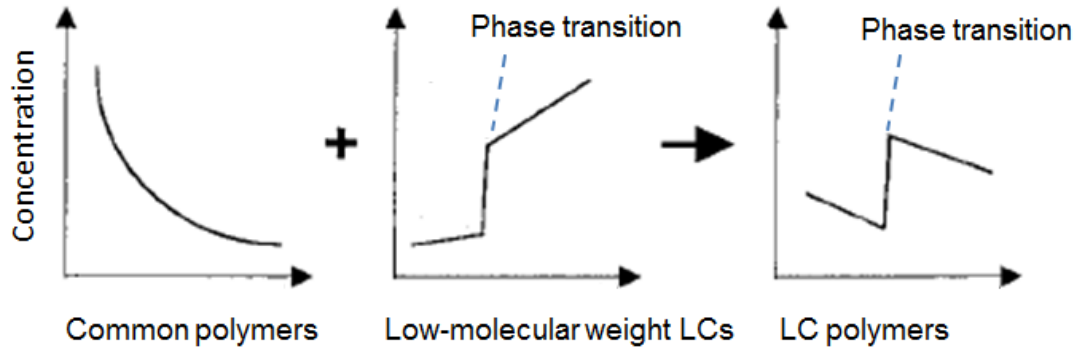

Figure 2.24: Schematic presentation of gas sorption in polymer, low-molecular LCs, and LCP[35]

2.3.2 Column Chromatography Separations using a Liquid Crystal Stationary Phase

Due to the anisotropic orientations of liquid crystals, there have been studies on liquid crystalline stationary phases for chromatographic separations. Most of the studies have been conducted on gas chromatography[37,38,39] but recently more studies have been reported using liquid chromatography.

Chromatography separations are influenced by different interactions between the stationary phases and the analytes. Separations of mixtures which possess similar polarities are difficult in conventional stationary phases because the separation abilities are associated with polarity differences in the analytes. On the other hand, liquid crystalline stationary phases performed enhanced separations for mixtures of similar polarities, as separations with liquid crystalline phases were dependent on the molecular shapes of the analytes.

Figure 2.25 shows data reported for liquid crystals used as stationary phases and chromatograms for several positional isomers. The LC molecules were coated on the packing material, 100-120 mesh Chromosorb W HP, by using chloroform as solvent with a coating concentration of 2.5 wt%. For the positional isomers which are different in molecular shape, para isomers showed longer retention times than meta isomers due to the shape selective

adsorption between the anisotropic nematic LC phases and the rod-like para isomers. In addition, it was reported[40] that steroid epimer separations were improved with nematic LC phases in gas chromatography separations which were associated with shape selective adsorption in the nematic LC phases. Longer retention times were observed for steroid epimers with higher length-to-breadth ratios.

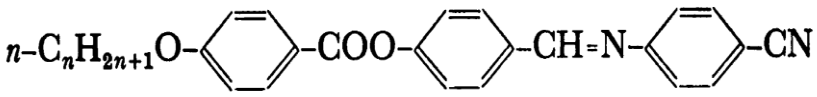

(n=7, 9, and 12)

n	Re-entrant nematic	Smectic C	Smectic A	Nematic	Isotropic
7			(72)	113	264
9	(92)		95	224	246
12		(74)	83		245

(a) Thermotropic liquid crystals and transition temperatures.

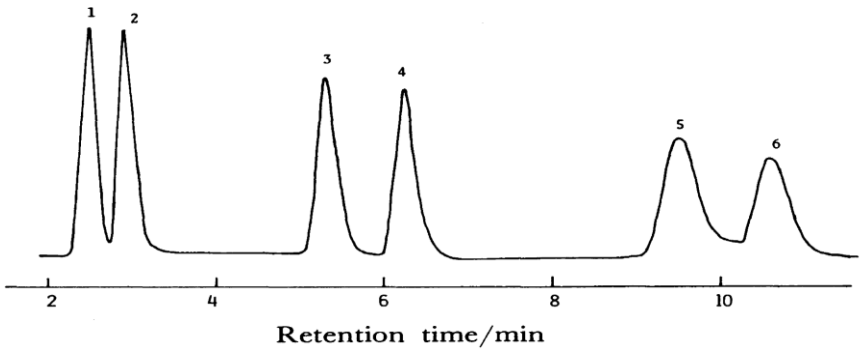

(b) Gas chromatogram of a mixture of dibromobenzenes, chloroacetophenones and chloronaphthalenes observed in the nematic phase on a C_7 (n=7) column. Peaks 1 and 2: *m*- and *p*- dibromobenzene, peaks 3 and 4: *m*- and *p*-chloroacetophenone, peaks 5 and 6: 1- and 2-chloronaphthalene.

Figure 2.25: Liquid crystals and gas chromatograms for three different positional isomers[41]

Medina[42] determined the diffusivities of positional isomers using gas chromatography separations with cholesteric liquid crystals. Among the smectic, cholesteric, and isotropic LC phases, the diffusion coefficients were lower in the smectic phase because of the highly ordered LC orientations and lower free volumes. *Para*-isomers with higher length-to-breadth ratios were retained longer than other positional isomers in the liquid crystalline mesophases due to shape selective adsorption, as described above.

Chapter 3. Diffusivity and Solubility of Organic Solutes in Supported Liquid Crystal Membranes

NOTE: The contents of this section have been adapted from the work previously published in the Journal of Physical Chemistry B [43]

3.1 Chapter Summary

The electro-optical properties of thermotropic liquid crystalline (LC) materials have been the subject of significant research effort due to their well-established applications in display technology; however, relatively little work has been done concerning the transport of dissolved solutes in LC phases, limiting their potential use in applications including chemical separation and sensing. Supported liquid crystal membranes were synthesized by impregnating porous cellulose nitrate (CN) membranes with 4-cyano-4′-octylbiphenyl (8CB) from chloroform solutions under vacuum. The resulting membranes were stable under aqueous conditions. Measurements of the 8CB-CN membrane transport properties were performed at 38 ℃ (nematic) and 44 ℃ (isotropic) for eleven aromatic solutes, including positional isomers, in aqueous solution. Solute diffusivity and solubility were calculated using a time-lag technique based on the study of the transient (unsteady state) and steady-state permeation regimes. The solubility and diffusivity of aqueous aromatic solutes in 8CB LCs depended significantly on intra- and intermolecular hydrogen bonding, and more specifically the number of hydrogen-bonding sites on a solute that are available for interactions with the aqueous and LC phases. In the nematic phase of 8CB, shape specific affinity was observed for *para* isomers and other rod-like solutes. A decreased activation energy for diffusion was observed at the isotropic to nematic phase transition for *o*-hydroxybenzoic acid, as expected based on the increased order in the nematic phase. Permeation selectivities for the separation of positional isomers by the 8CB-CN membranes

indicated high selectivity only for the hydroxybenzoic acid isomers, due to the propensity of o-hydroxybenzoic acid to form intramolecular hydrogen bonds.

3.2 Introduction

Small molecule thermotropic liquid crystals (LCs) exhibit anisotropic phases that are responsive to various stimuli, including temperature, electric and magnetic fields, and the presence of impurities. Rod-like thermotropic LCs consist of rigid moieties (mesogens), usually consisting of aromatic groups, and flexible moieties, often alkane chains. The LCs can exhibit a variety of temperature-dependent phases (i.e. smectic, nematic, cholesteric, isotropic) which are classified according to their orientational order, positional order, and chirality.[12,13] The LC molecules are aligned along their long axis in the nematic and smectic phases, but randomly oriented in the isotropic phase. We expect that the increased intermolecular interactions caused by the molecular alignment will lead to observable differences in the solubility and diffusivity of organic solutes in the LC materials.

Membrane separation technologies are attractive as they enable higher energy efficiency, simplicity, convenience, and continuous operability[1,2] compared to conventional energy intensive distillation separation or chromatographic separation techniques. Furthermore there are some chemical separations that are difficult to perform with existing methods, such as the separation of isomers that have similar boiling points[3], including positional isomers (para, ortho, meta) and optical isomer[4] (enantiomers). Accordingly, it would be beneficial to find new membrane materials capable of performing these separations.

Generally, transport behavior through a membrane is dominated by the solubility and diffusivity of solutes in the membrane materials.[44] These quantities are dependent on intermolecular interactions, such as hydrogen bonding, Van der Waals forces, and pi-pi stacking between the solutes molecules and the LC materials. Therefore, a thorough

understanding of the transport parameters (diffusivity, solubility, permeability) of organic molecules in LCs is essential for the application of LCs as membrane materials.

Due to their unique optical properties LCs have widespread applications in display technology. As a result, the chemistry and electro-optical properties of a large number of LC materials have been reported.[45,46] Despite this intense scrutiny, thus far there have been few studies conducted on the solubility and diffusivity of diffusing solutes in LC materials. The diffusivity and solubility of inert gas molecules in several LC materials have been studied using gas sorption measurements.[33,34,32] Gas solubility and permeability were shown to depend on the LC phase (smectic, nematic, isotropic) and on the nature of the dissolved gas, CO2 exhibiting higher diffusivities than N_2 or Ar.

Several studies in aqueous phases have been published using liquid crystals embedded in porous supports as a temperature sensitive controlled drug release mechanism. This work relied on the difference in permeability of a solute through the membrane depending on whether the system is held at a temperature above or below a LC transition. A thermo-responsive membrane embedded with a single cholesteric oleyl carbonate or a binary mixture of cholesteric oleyl carbonate and cholesteryl nonanoate was studied by Lin et al. in two different phases, crystal (off-state) and liquid crystalline phase (on-state).[17,18,19] Nozawa et al. investigated LCs as a thermoresponsive membrane material for polymer alloyed and LC adsorbed membranes, and concluded that LC-adsorbed membrane could perform a sharp on-off drug control.[20] In addition to the above supported liquid and polymer membranes, Nozawa et al. and Dinarvand et al. also fabricated a ‘sandwich’ membrane in which LCs were entrapped between two polymer membranes.[21,22] They found that the sandwich membrane had a better thermal-response efficacy than the supported liquid membrane.[21] Unfortunately, none of these studies reported quantitative values for drug transport in liquid crystals, and relied only on a qualitative analysis of membrane permeability.

Herein we report a preliminary study of the transport of various water soluble organic molecules passing through 4-cyano-4′-octylbiphenyl (8CB) LC embedded membranes immersed in aqueous solution under the nematic and isotropic phases of 8CB. The LC embedded membrane is classified as a supported liquid membrane (SLM) which offers the advantages such as the use of small amounts of expensive carriers, high selectivity, and easy scale-up, etc.[47] In order to provide a quantitative analysis of the transport kinetics we employed a time-lag method,[48,49,50] a macroscopic technique based on the time necessary to achieve steady state transport, to estimate the solute diffusivity in the membrane material.[51] Subsequently, solubility and permeability were calculated from the transport experiments for the supported LC membrane according to Fick's law.[52] For positional isomers, the selectivity for each pair of isomers was calculated from the single component transport experiments.

3.3 Experimental

3.3.1 Materials and Equipment

4-cyano-4′-octylbiphenyl (8CB) was obtained from Wako Chemicals (Japan), which exhibits multiple liquid crystalline phases with transition temperatures of 21.5 ℃ (Crystal-Smectic A), 33.5 ℃ (Smectic A-Nematic), and 40.5 ℃ (Nematic-Isotropic).[53] Phenol, pyridine, chloroform, *p*-, *m*- and *o*-cresol, *p*- and *o*-hydroxybenzoic acid, *p*- and *o*-aminophenol, *p*- and *o*-aminobenzoic acid were purchased from Sigma Aldrich (St. Louis, MO, USA). Flat sheet cellulose nitrate membranes (pore size 0.22 μm, porosity 70~80 %, diameter 47 mm) were obtained from Whatman (Dassel, Germany). In preliminary experiments, the smaller pore size membranes (0.22 μm) showed more liquid crystal amount impregnated in the cellulose nitrate membrane than the larger pore size membranes (0.45 μm). The 18.2 MΩ deionized water was produced by an E-pure deionization system (Barnstead, USA). All chemicals were reagent grade and used without further purification.

Polarized light microscopy was performed using an Olympus BX51 microscope (Olympus USA) with a Linkam LTS-350 hot stage (Linkam Co, UK). Scanning electron microscopy (SEM) was performed using a LEO (Zeiss) 1550; samples were prepared by coating with a gold layer (15 nm) or by freezing in liquid nitrogen, fracturing and coating with a gold layer (15 nm) for cross-sectional images. Fourier-transform Infrared spectroscopy (FTIR) was performed using a BioRad FTS-40A (Cambridge, MA, USA). FTIR samples were prepared by dissolving solutes in 8CB LCs at 60 ℃ (isotropic phase) onto a clean KBr plate. Ultraviolet-Visible light spectra were recorded using a USB-4000 UV-VIS spectrophotometer (Ocean Optics) equipped with a z-type flow cell (1 cm path length) and a peristaltic pump.

3.3.2 Membrane Preparation

LC embedded membranes were prepared by impregnating the porous cellulose nitrate membrane with 8CB via vacuum filtration. 25 % (w/v) 8CB chloroform solution was filtered through the porous membrane support in which 8CB LCs were kept in membrane pores by capillary forces. The resulting LC embedded membranes were immersed in deionized water overnight at room temperature to remove excess 8CB remaining on the membrane surface and then dried under vacuum for 1 hour at 70 ℃. The membranes were trimmed to final size and sandwiched between two rings of aluminum tape to provide added support. Finally, the 8CB embedded membranes were washed in deionized water, stirred (150 rpm) at 38 ℃ for 45 min during which any leaching of 8CB from the membrane was monitored via UV-VIS. The amount of 8CB in the impregnated membranes following the vacuum drying step was 100.7 ± 2.6 mg (n=8) and the final membrane thickness was 122 μm, the same as the unfilled membrane support. The membrane pores of 98 vol% were filled with 8CB LCs according to a calculation based on cylindrical pore structure, porosity (70 %) and 8CB density (0.99 g/cm^3)[80].

It has previously been reported that small molecule nematic LCs arrange themselves in a parallel orientation (planar or homogenous) to various substrates. This is the case for 4-pentyl-4′-cyanobiphenyl (5CB) in a cellulose nitrate support[54]; 8CB in random porous glass[55]; and 5CB in 4,4′-bis(acryloyloxy)biphenyl (BAB) [58]. Based on these results, we assume that the 8CB molecules will be oriented parallel to the cellulose nitrate substrate surfaces; however, since the cellulose nitrate support consists of a randomly oriented network of pores, there is no preferred macroscopic LC orientation. This allows us to treat diffusion across the membrane as essentially isotropic.

3.3.3 Permeation in 8CB-CN Membranes

8CB embedded membranes with an effective permeation area of 7.55 cm^2 were placed between two glass half cells. The feed cell was filled with 200 ml of a 5 mM aqueous solution of a particular solute molecule and the receiving cell was filled with 200 ml of deionized water. The membrane permeation cell was immersed in a recirculating water bath to control system temperature and the solution in each half cell was stirred at 150 rpm, a speed determined to be fast enough to prevent concentration gradients (Figure 3.1). The transport experiments were performed at 38 ℃ (nematic phase) and 44 ℃ (isotropic phase). During the experiments, samples of the model molecules in the receiving cell were circulated continuously by a peristaltic pump through a cuvette cell in which solute concentrations were monitored by a UV spectrometer (USB-4000, Ocean Optics, USA). Diffusivities and solubilities of the solute molecules in 8CB were calculated based on the average of three separate transport experiments for each solute molecule. New membranes were used for each solute.

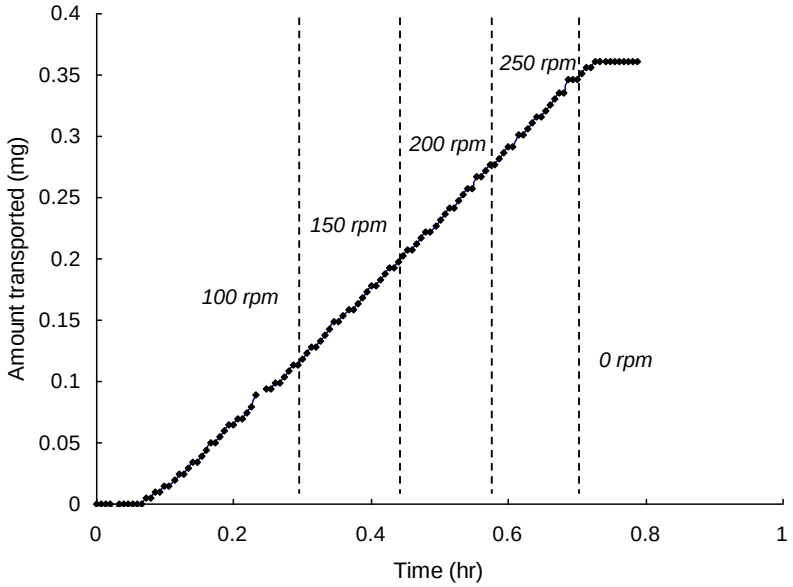

Figure 3.1: Pyridine transport through 4-(trans-4′-pentylcyclohexyl)-benzonitrile LCs embedded CN (PCH5-CN) membrane at 35 ℃ by varying solution mixing speeds. (Initial concentration: 1mmol pyridine in 200 ml deionized water in the feed side and 200 ml deionized water in the receiving side)

3.3.4 Calculation of Diffusivity and Solubility

The steady state concentration gradient driven diffusive transport of a solute across a membrane is described by Fick's law. The measured permeability is related to the solubility and diffusivity as follows:[48]

$$P = D\,S \qquad (3.1)$$

where P is permeability (mmol/cms); D is diffusivity (cm^2/s); S is solubility ($mmol/cm^3$).

In order to calculate the solubility from the above equation, two parameters, the permeability and diffusivity must be calculated from experimental data. The permeability is defined as:[48]

$$P = \frac{dM_t}{dt}\frac{L}{A} \qquad (3.2)$$

dM_t/dt is the rate of solute mass transport (determined from the slope of the plot of mass transported vs time at steady state regime); L is membrane thickness (cm); A is membrane area (cm^2).

The mathematical analysis of diffusion and solubility using the time-lag method[52,56] assumes that there is no boundary layer resistance at the membrane interfaces and no convective flow through the membrane. These conditions are achieved experimentally by stirring inside the diffusion cells and immobilizing the liquid crystals in a porous membrane. Under these conditions the concentration profile used for the measurement of solubility and diffusivity can be found by Fick's law.

$$\frac{\partial C_i}{\partial t} = D\frac{\partial^2 C_i}{\partial z^2} \qquad (3.3)$$

Where C_i is the concentration of species i, D is its diffusivity, and z is the direction of transport perpendicular to the membrane surfaces. At time zero, diffusing species are injected into the donor side and it is assumed that the concentration on the receiving side will be negligible, leading to the following boundary conditions.

$$\begin{aligned} &At\ t = 0 \text{ and } 0 \le z \le L, && C_i(z,0) = 0 \\ &At\ t > 0 \text{ and } z = 0, && C_i(0,t) = C_{i0} \\ &At\ t > 0 \text{ and } z = L, && C_{iL}(L,t) = C_{iL} \approx 0 \end{aligned} \qquad (3.4)$$

The solution of eq (3.3) subject to the boundary conditions (3.4) is given by:

$$C_i = C_{i0}\left(1-\frac{z}{L}\right) + \frac{2C_{i0}}{\pi}\sum_{n=1}^{\infty}\frac{1}{n}\sin\left(\frac{n\pi z}{L}\right)\exp\left(-\frac{Dn^2\pi^2 t}{L^2}\right) \qquad (3.5)$$

Flux, J, is obtained from eq. (3.5) by applying Fick's law (eq. (3.3)) and the flux at the membrane interface (L) at time, t, is follows.

$$J_L(t) = \frac{DC_{i0}}{L} + \frac{2DC_{i0}}{L}\sum_{n=1}^{\infty}\cos(n\pi)\exp\left(-\frac{Dn^2\pi^2 t}{L^2}\right) \qquad (3.6)$$

After integration of eq. (3.6) with respect to time, the total amount of diffusing molecules through the membrane is;

$$Q_L(t) = \frac{ADC_{i0}}{L}\left[t - \frac{L^2}{6D} + \frac{2L^2}{\pi^2 D}\sum_{n=1}^{\infty}\frac{(-1)^{n+1}}{n^2}\exp\left(-\frac{Dn^2\pi^2 t}{L^2}\right)\right] \qquad (3.7)$$

The concentration change in the receiving side is obtained from eq. (3.7).

$$C_{iL}(t) = \frac{ADC_{i0}}{VL}\left[t - \frac{L^2}{6D} + \frac{2L^2}{\pi^2 D}\sum_{n=1}^{\infty}\frac{(-1)^{n+1}}{n^2}\exp\left(-\frac{Dn^2\pi^2 t}{L^2}\right)\right] \qquad (3.8)$$

The steady state solution for eq. (3.8) as time goes infinity,

$$\lim_{t\to\infty} C_{iL}(t) = \frac{ADC_{i0}}{VL}\left(t - \frac{L^2}{6D}\right) \qquad (3.9)$$

Solving the unsteady-state diffusion problem results in the following equation for solute diffusivity:

$$t_g = \frac{L^2}{6D} \qquad (3.10)$$

where t_g is the time-lag (s); L is membrane thickness (cm); D is diffusion coefficient or diffusivity (cm^2/s). Using the permeability and diffusivity calculated from eqs. (3.2) and (3.10), the solubility of diffusing species in the 8CB embedded cellulose nitrate membrane can be obtained using eqn. (1).

3.4 Results and Discussion

Permeability measurements were carried out on supported liquid crystal membranes consisting of 4-cyano-4′-octylbiphenyl (8CB) embedded in porous cellulose nitrate (CN) membranes (denoted 8CB-CN). Scanning electron microscopy (SEM) images for surface and cross-section of 8CB-CN showed that 8CB LC fills all the CN membrane pores except for larger defects (Figure 3.2). The feed side of the diffusion cell contained 5 mM aqueous solutions of aromatic solutes respectively (phenol; pyridine; *p*-, *m*- and *o*-cresol; *p*- and *o*-aminophenol; *p*- and *o*- aminobenzoic acid; *p*- and *o*-hydroxybenzoic acid) and the receiving side contained deionized water.

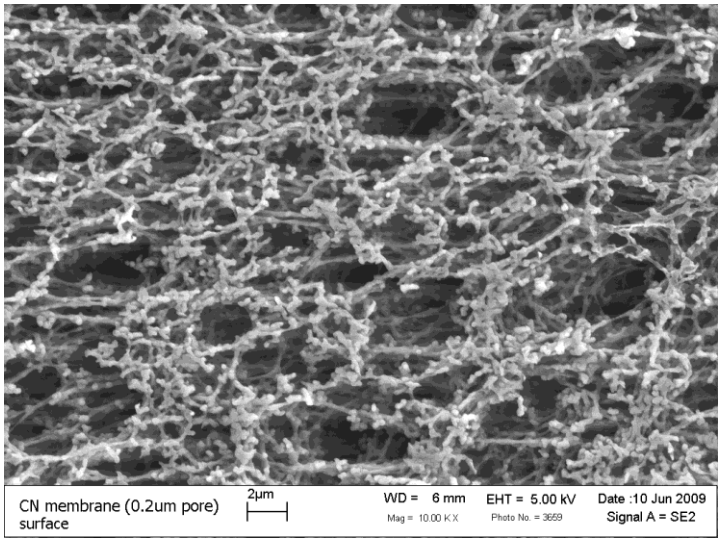

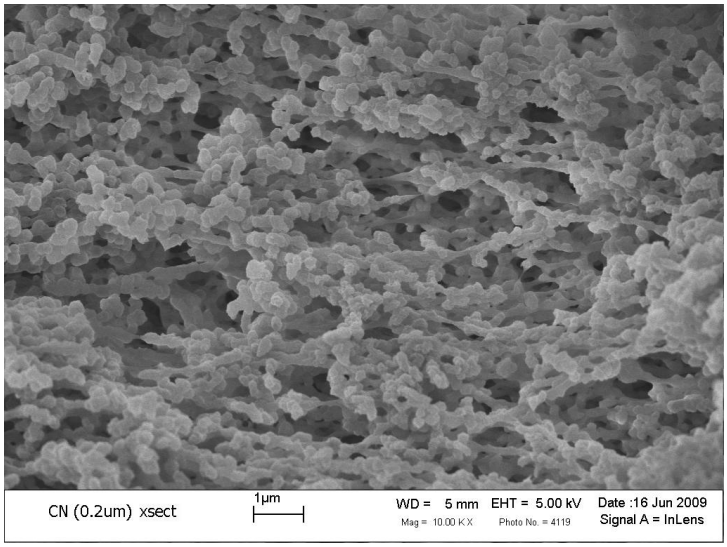

(a) Surface and cross-sectional images for CN membrane without 8CB LCs

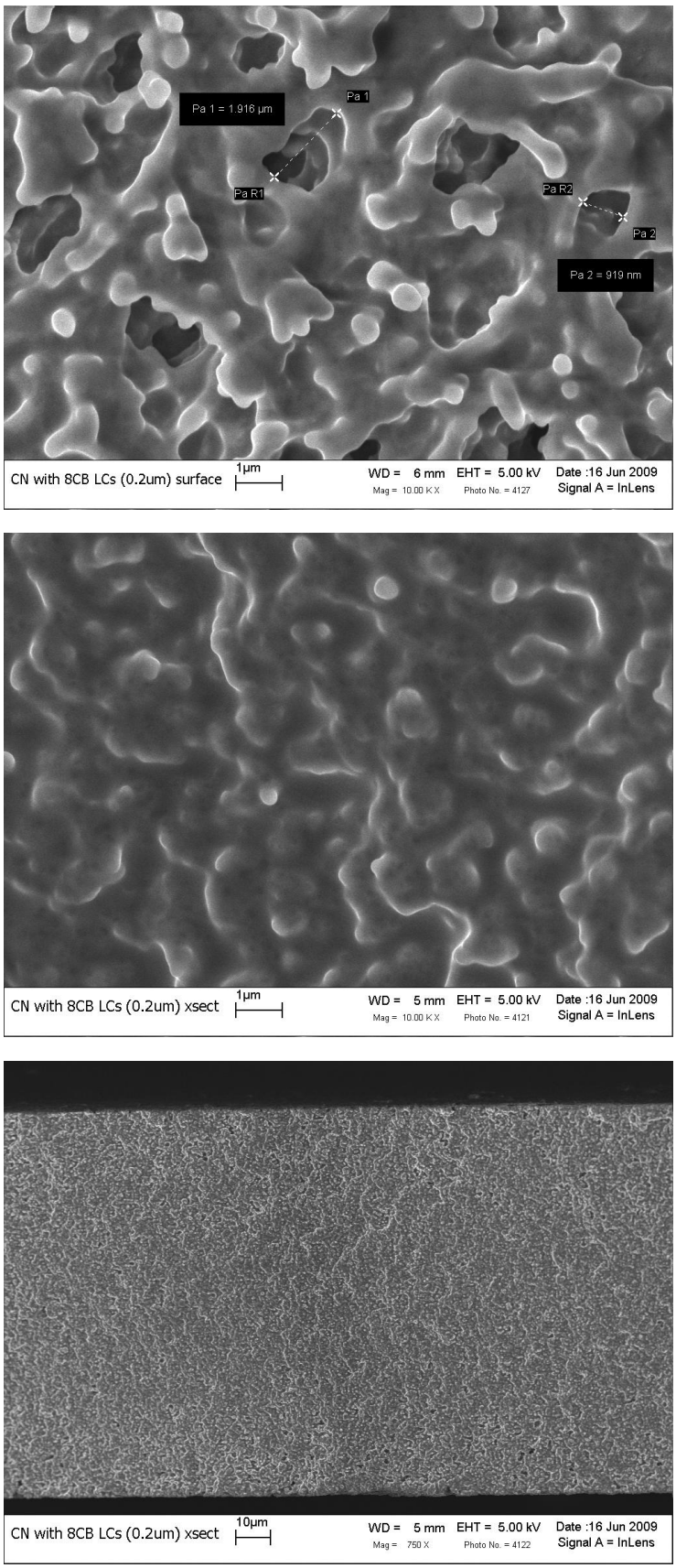

(b) Surface and cross-sectional images for 8CB-CN membrane

Figure 3.2: Scanning electron micrographs for CN without 8CBs and 8CB-CN membrane. Cellulose nitrate (CN, 0.2 μm pore) membrane without 8CBs (a) and CN membrane embedded with 8CBs (b). (The samples for cross-sectional images were prepared by dipping in liquid nitrogen)

3.4.1 Supported LC Membrane Stability

The 8CB-CN membranes were tested for leaching by immersion in DI water for 3 hours while monitoring the UV-VIS spectrum for any increase in the 8CB peak intensity in the aqueous phase (260~280 nm). The 8CB-CN membranes exhibited no significant leaching. An example of a time-lag plot of the transport of *p*- and *o*-hydroxybenzoic acid through an 8CB-CN membrane at 38 ^{o}C (nematic phase) is depicted in Figure 3.3. The time-lag plot shows the increase of solute in the receiving side of the permeation cell with respect to time. Multiple measurements were performed using the same membrane, and there was little change in membrane performance between runs.

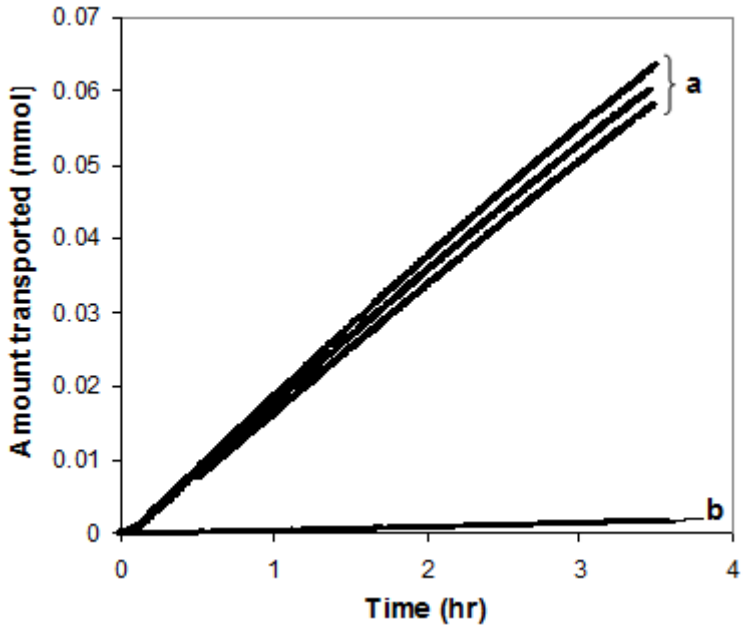

Figure 3.3: Concentration change in the receiving side plotted versus time for (a) *o*-hydroxybenzoic acid and (b) *p*-hydroxybenzoic acid transport in an 8CB-CN membrane

3.4.2 Phase Transition of 8CB-CN Membranes and Solute Impacts

It has been reported that transition temperatures of LCs in confined geometries decrease slightly (up to 2 ℃) or do not change when compared with the bulk.[57,58] The LC transitions in the 8CB-CN membranes were examined using polarized light microscopy. Transition from the nematic phase to the isotropic phase was observed between 40.5 ℃ and 41 ℃ during both heating and cooling (Figure 3.4). These are consistent with the nematic-isotropic transition temperature for bulk 8CB (40.5 ℃.)

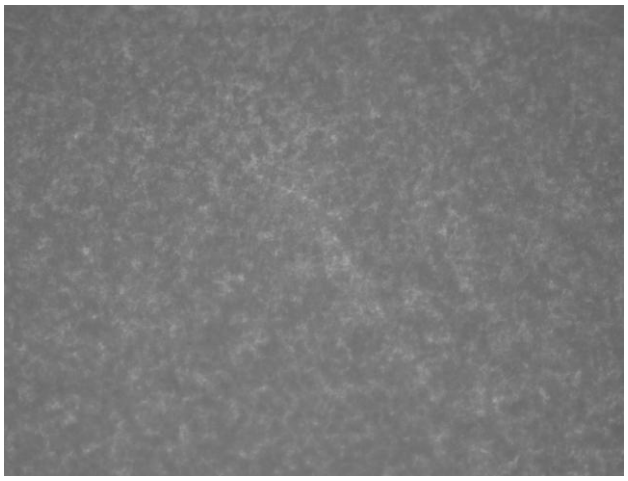

(a) 8CB-CN at 38 ^{o}C (anisotropic)

(b) 8CB-CN at 41 ^{o}C (isotropic)

Figure 3.4: Optical microscopy images for 8CB-CN in the anisotropic (a) and isotropic (b) phases under cross polarization (polarizer and analyzer angled at 90). To prevent heat loss, 8CB-CN sample was sandwiched between two glass slides

To determine the effect of a dissolved solute on the phase transition of 8CB-CN, a 8CB-CN membrane was examined using polarized light microscopy following a permeation experiment using 1-fluoro-2-nitrobenzene. The nematic-isotropic phase transition occurred between 40 ℃ and 40.5 ℃, 1 ℃ lower than in the unadulterated 8CB-CN membrane (Figure 3.5). This result is in accordance with previous studies[59] in which the transition temperature decreased slightly with increasing biphenyl and cyclohexane solute concentrations in 8CB at low mole fractions. The temperatures used for permeability measurements, 38 ℃ and 44 ℃, are clearly in the nematic and isotropic phases respectively.

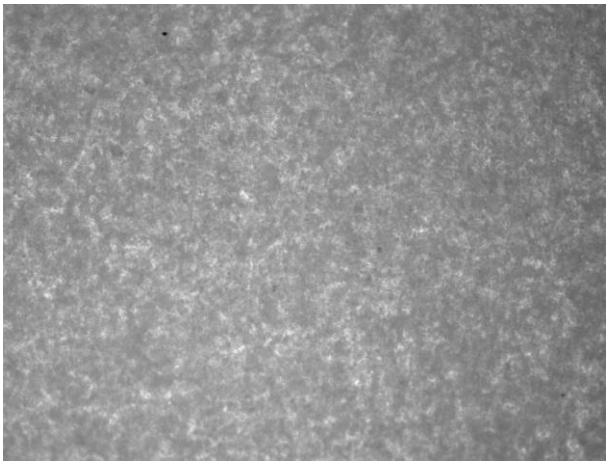

(a) 8CB-CN saturated with 1-fluoro-2-nitrobenzene at 38 ^{o}C (anisotropic)

(b) 8CB-CN saturated with 1-fluoro-2-nitrobenzene at 41 ^{o}C (isotropic)

Figure 3.5: Optical microscopy images for 8CB-CN saturated with 1-fluoro-2-nitrobenzene in the anisotropic and isotropic phases under cross polarization (polarizer and analyzer angled at 90). To prevent heat loss, 8CB-CN sample was sandwiched between two glass slides

3.4.3 Solute Diffusion in 8CB-CN Membranes

Table 3.1 shows the time lag, diffusivity, and solubility for organic solutes through 8CB-CN membranes at 38 ^{o}C (nematic phase) calculated using the time-lag method. In general, solute diffusivity is affected by factors including molecular size, molecular weight, and molecular interactions. In this study, we attempted to minimize the effect of molecular size by selecting similar solute molecules: each solute consists of a single aromatic ring to which small functional groups are attached.

Table 3.1: Time lag, diffusivity and solubility calculated from permeation through 8CB-CN membrane at 38 ^{o}C

Diffusing molecules	Time lag, T_g (s)	Diffusivity, D x 10^8 (cm^2/s)	Solubility, S ($mmol/cm^3$)
Phenol	143.1 ±1.5	17.3 ±1.5	0.049 ±0.1
Pyridine	209.9 ±8.1	11.9 ±8.1	0.042 ±5.2
o-cresol	239.8 ±4.5	10.3 ±3.7	0.147 ±5.6
m-cresol	236.7 ±1.6	10.5 ±1.3	0.130 ±3.9
p-cresol	258.3 ±1	5.7 ±1.7	0.212 ±5.7
o-aminophenol	503.4 ±10.8	5.0 ±8.3	0.014 ±6.3
p-aminophenol	3261.9 ±13.5	0.7 ±9.5	0.022 ±1.4
o-aminobenzoic acid	324.6 ±5.6	7.7 ±4.5	0.033 ±8.3
p-aminobenzoic acid	1478.5 ±2.8	1.7 ±2.3	0.023 ±7.3
o-hydroxybenzoic acid	257.3 ±4.0	9.8 ±2.8	0.078 ±0.1
p-hydroxybenzoic acid	1366.2 ±5.5	1.8 ±4.3	0.012 ±4.2

Errors reported are one standard deviation.

The solute diffusivities in the nematic phase were plotted as a function of molecular weight in Figure 3.6. The diffusivities generally decreased as the molecular weight increased, however phenol exhibited faster diffusion than pyridine despite having a higher molecular weight. Aminophenol exhibited a significantly lower diffusivity than all the other compounds.

o-aminophenol and *o*-cresol have similar molecular weights, 108.14 and 109.13 respectively; however the diffusivity of o-cresol was two times higher than of *o*-aminophenol. We attribute this significant difference to the influence of hydrogen bonding interactions. *o*-cresol possesses a single hydroxyl group capable of intermolecular hydrogen bonding while *o*-aminophenol possesses one hydroxyl and one amine group. Thus the cresol isomers have a maximum of one hydrogen-bond donor, while the aminophenol isomers have up to three available for interactions with valence eletrons of cyano groups or electrons in the aromatic rings of the 8CB liquid crystal molecules. It is clear that chemical functionality, and specifically hydrogen-bonding, plays an important role in the determination of transport properties.

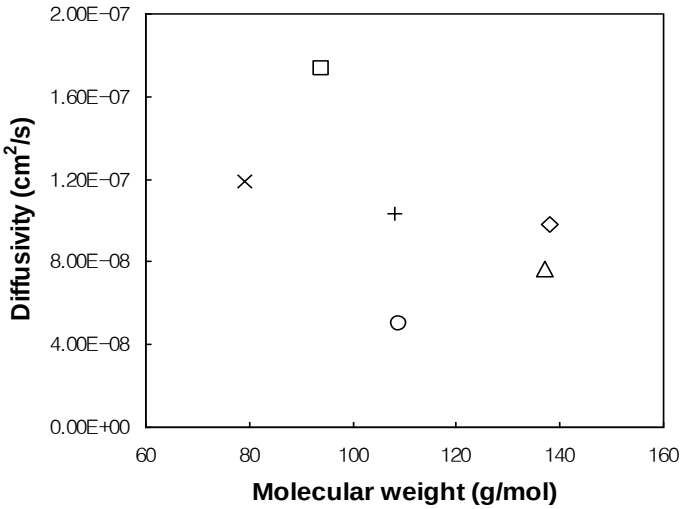

Figure 3.6: Diffusivity in 8CB as a function of solute molecular weight measured at 38 ^{o}C (nematic phase) for (◊) *o*-hydroxybenzoic acid, (□) phenol, (x) pyridine, (+) *o*-cresol, (o) *o*-aminophenol, and (Δ) *o*-aminobenzoic acid

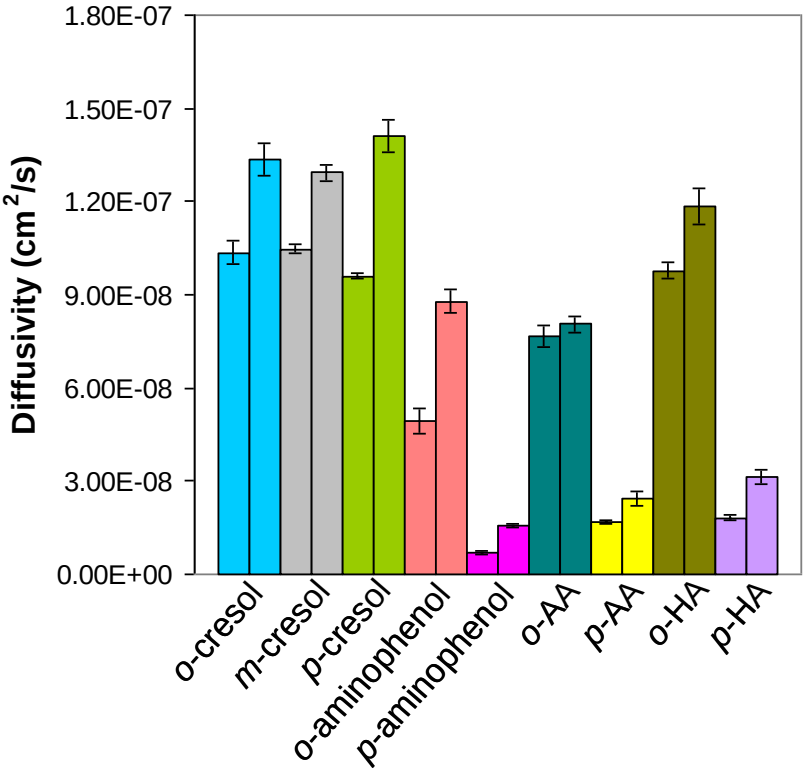

Figure 3.7: Diffusivity of isomers in the nematic and isotropic phases determined from the transport experiments through the 8CB-CN membranes. AA and HA represent aminobenzoic acid and hydroxybenzoic acid respectively. The left and right bars for each molecule represent data obtained at 38 ℃ and 44 ℃ respectively

3.4.4 Isomer Diffusion in 8CB-CN Membranes

The diffusion coefficients for the ortho and para isomers of aminophenol, aminobenzoic acid, and hydroxybenzoic acid are compared in Figure 3.7. The diffusion coefficients of ortho isomers were higher than para isomers for all three solutes (D_{ortho}/D_{para}= 7.2, 4.6, 5.4 for aminophenol, aminobenzoic acid, and hydroxybenzoic acid respectively). We attribute the differences in diffusivity between positional isomers to the relative capacity for intermolecular hydrogen-bonding.[60,61] In the ortho configuration, the two functional groups are ideally arranged to participate in intramolecular hydrogen bonding. The existence of a strained five-membered ring for *o*-aminophenol and six-membered ring for, *o*-aminobenzoic

acid and *o*-hydroxybenzoic acid due to intramolecular hydrogen bonding has previously been reported.[61,62,63](Figure 3.8) Weaker hydrogen bonding interactions between the ortho isomers and the 8CB liquid crystals lead to a decreased barrier to diffusion. On the contrary, the positional isomers of cresol, which possess only a single hydrogen-bond donor and cannot participate in intramolecular hydrogen bonding, exhibited similar diffusivities (D_{ortho}/D_{para}= 1.1 and D_{ortho}/D_{meta}= 0.99 at 38 ℃).

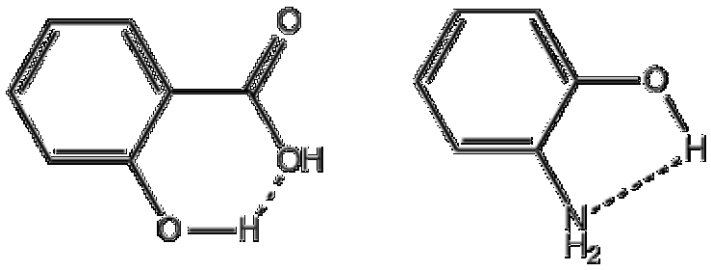

Figure 3.8: Six-membered ring for *o*-hydroxybenzoic acid and five-membered ring for *o*-aminophenol formed by an intramolecular HB. The stability of the intramolecular HB is dependent on the HB donor ability, acceptor ability, and their spatial arrangement.[57]

Table 3.2 shows the time lag, diffusivity, and solubility obtained from the transport experiments through the 8CB-CN membranes at 44 ^{o}C (isotropic phase). Diffusion coefficients increased in the isotropic phase for all diffusing species. Similar behavior has been reported for the diffusion of inert gases (N_2, CO_2, Ar) in thermotropic liquid crystals.[32] The effects of intramolecular and intermolecular hydrogen-bonding interactions on solubility and diffusivity, previously observed in the nematic phase, were also demonstrated in the isotropic phase (D_{ortho}/D_{para}= 5.7, 3.31, and 3.8 for aminophenol, aminobenzoic acid, hydroxybenzoic acid respectively). Cresol isomers exhibited little difference in diffusion coefficients (D_{ortho}/D_{para}= 0.95; D_{ortho}/D_{meta}= 1.03) due to the lack of intramolecular hydrogen-bonding interactions in the ortho configuration.

Table 3.2: Time lag, diffusivity and solubility calculated from permeation through 8CB-CN membrane at 44 ^{o}C

Diffusing molecules	Time lag, T_g (s)	Diffusivity, D x 10^8 (cm^2/s)	Solubility, S ($mmol/cm^3$)
Phenol	122.6 ± 5.3	20.3 ± 5.3	0.040 ± 2.1
Pyridine	165.7 ± 3.8	15.0 ± 3.8	0.044 ± 5.3
o-cresol	185.8 ± 4.1	13.4 ± 4.1	0.149 ± 2.1
m-cresol	191.7 ± 2.0	12.9 ± 2.0	0.131 ± 3.3
p-cresol	175.9 ± 0.5	14.1 ± 1.5	0.152 ± 5.6
o-aminophenol	282.4 ± 12.3	8.8 ± 4.4	0.017 ± 3.1
p-aminophenol	1600.3 ± 4.5	1.6 ± 4.5	0.020 ± 5.3
o-aminobenzoic acid	307.9 ± 3.1	8.1 ± 3.2	0.039 ± 5.9
p-aminobenzoic acid	1024.7 ± 8.9	2.4 ± 8.4	0.021 ± 4.9
o-hydroxybenzoic acid	207.45 ± 4.9	11.9 ± 4.9	0.079 ± 2
p-hydroxybenzoic acid	793.2 ± 7.7	3.1 ± 6.5	0.010 ± 1.8

Errors reported are one standard deviation.

3.4.5 Hydrogen Bonding Interactions with 8CB LCs

The intermolecular hydrogen bonding interactions between 4-cyano-4′-pentylbiphenyl (5CB) LCs, in which the cyano group acts as the hydrogen-bond acceptor, and various hydrogen-bond donor molecules (e.g. hexanol) have previously been studied using FTIR spectroscopy.[64,65] To identify hydrogen bonding interactions between 8CB LCs and solutes, samples containing 19 % (mol/mol) of phenol, *o*-hydroxybenzoic acid, and 1-fluoro-4-nitrobenzene in 8CB were studied using FTIR (Figure 3.9). The C-N stretching peak[66,67] of the 8CB molecule (2200-2250 cm^{-1}) exhibits a shift to a higher wave number when the cyano group acts as a hydrogen-bond acceptor. This shift is evident in the sample containing phenol and o-hydroxybenzoic acid, both of which contain hydrogen-bond donor groups; these groups are absent in the pure 8CB sample and the sample containing 1-fluoro-

4-nitrobenzene. Relative strengths of the hydrogen-bond interactions for the different solutes studied are difficult to assess, as some of the solutes exhibit low solubility in 8CB (below the detection threshold in the FTIR spectra).

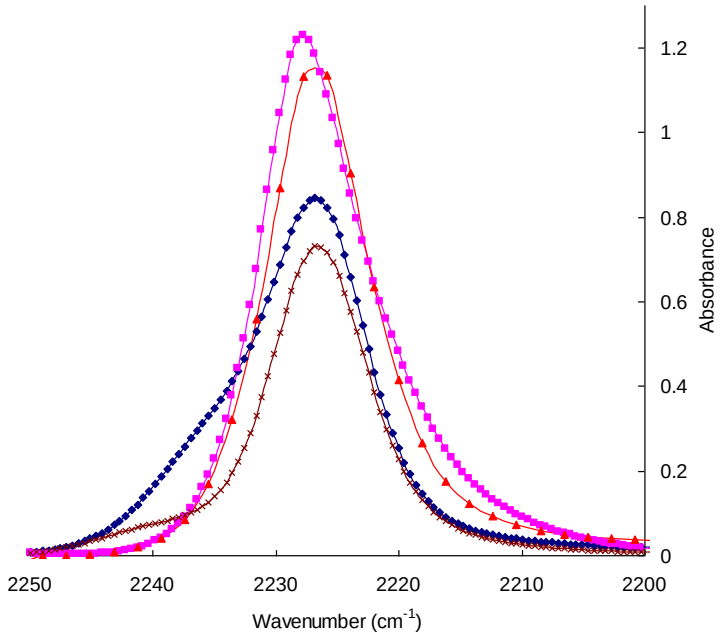

Figure 3.9: FTIR for pure 8CB LCs (▲), o-hydroxybenzoic acid in 8CB LCs (x), phenol in 8CB LCs (◆), 1-fluro-4-nitrobenzene (■) in 8CB LCs (The same concentration samples of 19 % mol/mol). According to the references66,67, the hydrogen bonded C-N has a shifted peak to higher frequency. For *o*-hydroxybenzoic acid and phenol in 8CB LCs, there were the broad peaks (2250~2235) due to the hydrogen bonding interactions. 20% of the cyano group of LCs participate in the hydrogen-bonding with phenol or *o*-hydroxybenzoic acid on time scale of IR.

3.4.6 Solute Partition in 8CB-CN Membranes

Cresol isomers exhibited the highest solubility in 8CB of the solutes studied. When compared with phenol, the addition of one methyl group increased the solubility nearly three

times ($k_{o\text{-}cesol}/k_{phenol}$=2.96 at 38 ℃; 3.79 at 44 ℃). The hydrophobic nature of the methyl group makes cresol less soluble in the aqueous phase and is responsible for the higher solubility in the hydrophobic 8CB LC phase. Generally, molecules having a higher number of available hydrogen-bonding sites, such as the aminophenol isomers, aminobenzoic acid isomers, and *p*-hydroxybenzoic acid, exhibited lower solubility than phenol and cresol as shown in Figure 3.10. Increased hydrogen-bonding interactions with water mean that there is a greater energy barrier for partition into the liquid crystal phase.

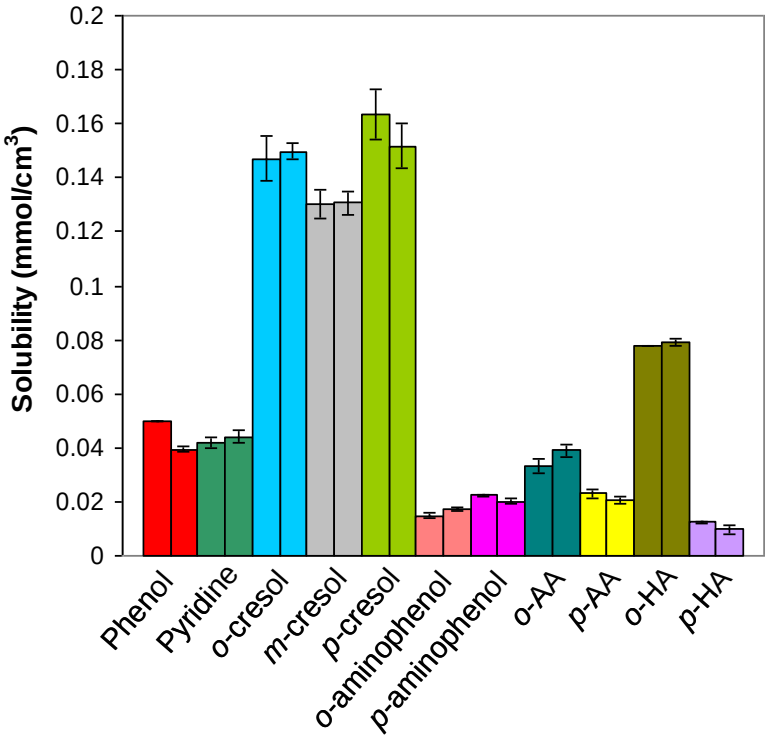

Figure 3.10: Solubility in the nematic and isotropic phases determined from the transport experiments through the 8CB-CN membranes. AA and HA represent aminobenzoic acid and hydroxybenzoic acid respectively. The left and right bars of the same molecules, presented by the same color, were obtained at 38 ℃ and 44 ℃ respectively.

3.4.7 Isomer Solubility in 8CB-CN Membranes

The solubility of *o*-hydroxybenzoic acid is significantly higher than that of *p*-hydroxybenzoic acid (k_{ortho}/k_{para}=6.29 at 38 ℃; 8.05 at 44 ℃) due to the aforementioned intramolecular hydrogen-bonding in the ortho isomer. Fewer hydrogen-bonding interactions with water lead to a lower energy barrier for partition into the LC phase. Similarly, the ortho isomer of aminobenzoic acid exhibited higher solubility than the para isomer (k_{ortho}/k_{para}=1.44 at 38 ℃; 1.89 at 44 ℃). *o*-hydroxybenzoic acid exhibited the highest solubility in 8CB, only next to the cresol isomers. The presence of polar C=O and O-H groups[32] as well as decreased intermolecular hydrogen-bonding are responsible for the relatively high solubility in the 8CB LC phase. In addition, the formation of a six-membered ring due to intramolecular hydrogen-bonding in *o*-hydroxybenzoic acid could lead to enhanced Van der Waal's interactions and solubility in 8CB LCs phase due to the greater contact area.[68]

3.4.8 Shape Selectivity in 8CB-CN Membranes

Previous work on the solubility of gases in liquid crystals reported that solubility was dependent on both temperature and liquid crystal phase.[33,34,35] The sorption coefficients of N_2, CO_2, and Ar increased dramatically at the crystal to nematic phase transition and gradually increased up to and beyond the isotropic transition. In the present study, the para isomers and phenol exhibited either no increase or a decrease in solubility when going from the nematic (38 ^{o}C) to the isotropic phase (44 ^{o}C) as depicted in Figure 3.10. Decreases of 21 %, 7 %, 21 %, 11 %, 11 % were observed for phenol, *p*-cresol, *p*-hydroxybenzoic acid, *p*-aminophenol, *p*-aminobenzoic acid respectively. The para isomer of cresol exhibited a 7 % decrease in solubility at the phase transition from the nematic to isotropic phase while the ortho and meta isomers exhibited no difference ($k_{isotropic}/k_{nematic}$=1.02 for *o*-cresol; 1.00 for *m*-cresol). The increased solubility of the para isomers in the nematic phase indicates a favorable interaction,

likely due to the shape of the molecule, between the solutes and the ordered liquid crystal structure.

It has been reported that when thermotropic calamitic (rod-like) liquid crystals were used as stationary phase in gas-liquid chromatography, retention times of para isomers were longer than that of other isomers in the nematic phase because para isomers, which are more rod-like in shape (higher length to breadth ratio), have a higher affinity for the nematic phase due to similar shape of the solutes and the liquid crystal phase.[41,69]Therefore, the increased solubility in the nematic phase is likely due to the unidirectionally oriented structures of the liquid crystal, which has a higher affinity for the rod-like para isomers than the disordered isotropic phase. Similarly, the solubility of phenol in the nematic phase was higher than that of pyridine despite the fact that pyridine has fewer hydrogen bonding sites, suggesting that molecular shape is a factor.

3.4.9 Diffusivity Temperature Dependence

To investigate further the effect of the smectic-nematic-isotropic phase transitions on diffusivity and solubility, transport experiments of *o*-hydroxybenzoic acid in 8CB-CN membranes were carried out at temperatures ranging from the smectic to isotropic phase (Figure 3.11). The expected behavior is that the slope of the Arrhenius plot of ln (D) vs. 1/T (related to the activation energy for diffusion according to equation 3.11) will change if there are dissimilar physical properties such as viscosity and ordered structure in the different liquid crystal phases.[51,24]

$$D = D_0 \exp\left(\frac{-E_a}{RT}\right) \qquad (3.11)$$

where D is diffusion coefficient or diffusivity (cm^2/s), R is ideal gas constant (8.314 J/mol·K), T is temperature (K), E_a is activation energy for diffusion (kJ/mol), and D_0 is Arrhenius constant (cm^2/s)

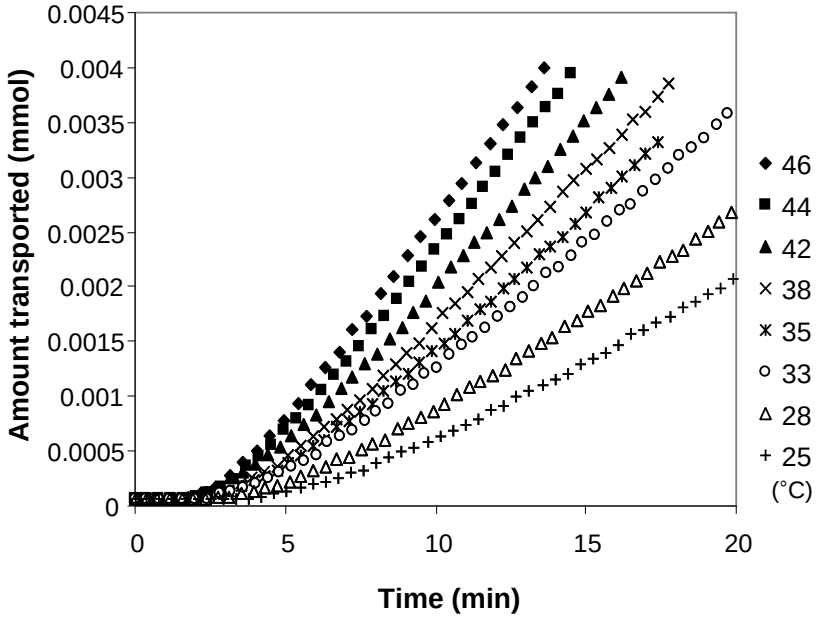

Figure 3.11: Transport of *o*-hydroxybenzoic acid through 8CB-CN membranes at different temperatures (Permeation rate is decreasing and time lag is increasing, as temperature decreases)

Figure 3.12 depicts the Arrhenius plot of *o*-hydroxybenzoic acid for an 8CB-CN membrane in the isotropic, nematic and smectic phases. The diffusion coefficients demonstrated Arrhenius-like temperature dependence with a slightly increased slope a the phase transition. There was no apparent difference in the slope at the nematic/smectic transition. The liquid crystalline phases exhibited an activation energy of 27.02 kJ/mol while the isotropic phase exhibited an activation energy of 39.33 kJ/mol. These values were consistent with the literature values calculated from self-diffusion data (33 kJ/mol for the nematic and isotropic phase of 4-cyano-4′-pentylbiphenyl (5CB)[70]; 31 kJ/mol for the isotropic phase and 23 kJ/mol for the nematic phase of *N*-(*p*-methoxy-benzylidene)-*p*-*n*-

butylaniline (MBBA)[71]). They are also consistent with previous research indicating that activation energies increase as the ordering of the liquid crystal decreases through the smectic or nematic phase to the isotropic phase as determined by nuclear magnetic resonance (NMR).[70,71,72] For the NMR measurements, the liquid crystal molecules are loaded in track-etched membranes such as Anopore or thin film capillaries, which result in LC orientations along the cylindrical pore axis in the smectic or nematic phases. As the nematic phase forms, diffusion parallel to the cylindrical axis dominates over diffusion perpendicular to the cylindrical axis, resulting in a lower diffusion barrier and lower activation energy in the nematic phase than in the isotropic phase.[71]

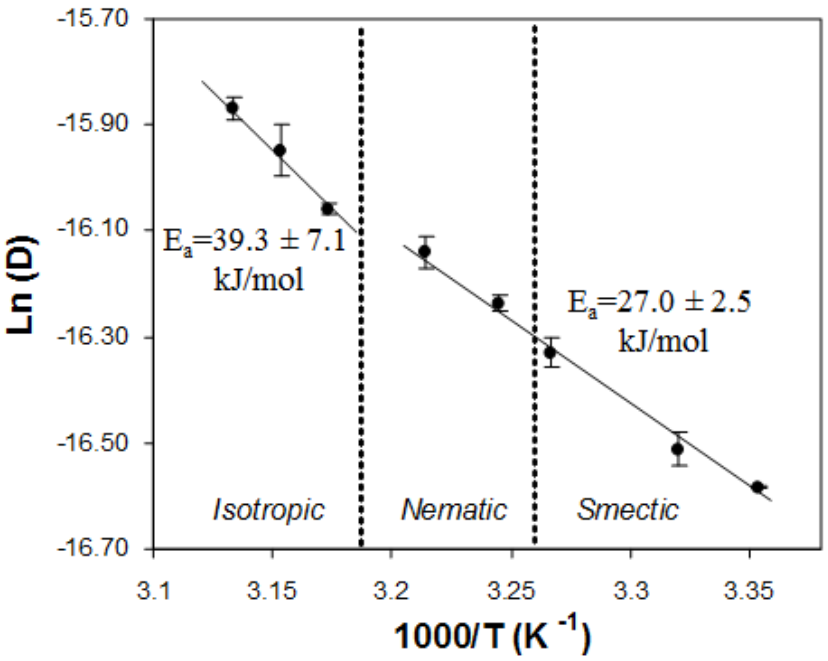

Figure 3.12: Arrhenius plot of diffusivity for *o*-hydroxybenzoic acid through 8CB-CN membranes. Errors reported are one standard deviation.

When Vilfan et al.[70] studied the self-diffusion coefficients of 5CB using NMR, a discontinuous jump in the self-diffusivity for the same activation energy was found at the isotropic to nematic phase transition for bulk 5CB due to anisotropy in the nematic phase (where only the anisotropic self-diffusion tensor along the nematic director was considered).

In contrast to bulk 5CB, no discontinuity in diffusivity was observed for 5CB confined within randomly oriented pores (7.5, 100, 140 nm). Since the distribution of pore directions is isotropic, the measured diffusion coefficients can be treated as isotropic even if the phase is changed to nematic. In the present study, there was no increase in diffusivity at the isotropic to nematic phase transition as observed in the NMR study[70,71] due to the isotropic pore distributions of the CN membrane support. Further study, employing porous supports with anisotropic pore distributions, is necessary to determine the effect of anisotropic diffusion on solute transport in liquid crystals.

3.4.10 Solubility Temperature Dependence

The solubility of *o*-hydroxybenzoic acid was studied as a function of temperature (Figure 3.13). Solubility decreased only slightly with temperature in the isotropic and nematic phases, but exhibited an increased temperature dependence in the smectic phase (T < 307 K). This trend is analogous to that reported for the solubility of gas molecules (N_2, CO_2, Ar) in thermotropic nematic liquid crystals.[32] The lower solubility is due to the increased order and structural rigidity in the smectic phase.[32]

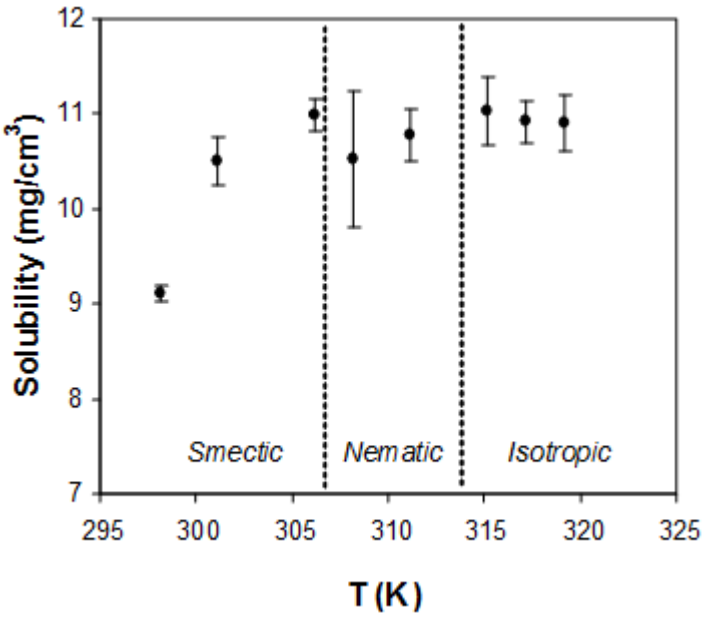

Figure 3.13: Solubility for *o*-hydroxybenzoic acid at different temperatures

3.4.11 Positional Isomer Permselectivity

The selectivity for various positional isomers measured in the isotropic and nematic phases of 8CB LCs are listed in Table 3.3. In general, only small changes in selectivity were observed above and below the nematic-isotropic transition. Selectivity was higher in the nematic phase for all solutes (with hydroxybenzoic acid exhibiting an 11 % increase) with the exception of aminophenol, which exhibited a 4 % increase in selectivity in the isotropic phase. In particular, the 8CB-CN membrane showed the highest selectivity (33.9) for the separation of *o*- and *p*-hydroxybenzoic acid isomers in the nematic phase.

Table 3.3: Permeability and selectivity for positional isomers at different phases

	Permeability, P x 10^8		Selectivity, $S_{o/p}$ or $S_{o/m}$	
	38 ^oC	44 ^oC	38 ^oC	44 ^oC
o-cresol	1.52	2.00		
m-cresol	1.36	1.69	1.12	1.18
p-cresol	1.57	2.14	0.97	0.93
o-aminophenol	0.07	0.15		
p-aminophenol	0.02	0.03	4.71	4.90
o-aminobenzoic acid	0.26	0.32		
p-aminobenzoic acid	0.04	0.05	6.59	6.26
o-hydroxybenzoic acid	0.76	0.94		
p-hydroxybenzoic acid	0.02	0.03	33.87	30.42

38^oC and 44^oC correspond to the nematic and isotropic phases respectively.

3.5 Conclusions

In conclusion, the transport behavior (permeability, diffusivity, and solubility) of a series of water-soluble aromatic solutes, including multiple isomeric compounds, in a calamitic (rod-like) thermotropic liquid crystal were studied. As these measurements were

performed using aqueous solutions on either side of the 8CB-CN membrane, the intramolecular and intermolecular (primarily solute-water) hydrogen-bonding interactions had a significant influence on the observed solubility in the 8CB-CN membranes. This behavior is in accordance with previously reported studies[62] of the partitioning of organic solutes between aqueous and immiscible organic phases. In addition, solubility also depended on the molecular structure of the solute, including the presence of aromatic moieties and polar functional groups. Organic solutes containing multiple available hydrogen-bonding sites (OH, NH_2, etc), such as *p*-hydroxybenzoic acid, exhibited markedly lower solubilities in the 8CB-CN membranes due to their higher propensity to form hydrogen-bonds with water molecules.

A comparison of the solubilities of solutes above and below the nematic-isotropic transition temperature revealed slight increases in solubility in the nematic phase for *para* isomers and other rod-like solutes. This suggests that there is an affinity between the uniaxially oriented nematic phase and the rod-like *para* isomers caused by similarities in molecular shape.

Solute diffusion in 8CB-CN membranes also exhibited a marked dependence on the ability of the isomers to participate in intermolecular hydrogen-bonding. In contrast, the effects of the liquid crystal orientations on the diffusion are limited compared to the intermolecular hydrogen-bonding interactions. This is illustrated by the small differences in diffusivity between the nematic and the isotropic phases and the significant differences in diffusivity between isomers of hydroxybenzoic acid, aminobenzoic acid, and aminophenol, whose *ortho* isomers can form ring structures through intramolecular hydrogen-bonding, thereby limiting the number of hydrogen-bonding sites available for interactions with the 8CB molecules.

Selectivities for the separation of structural isomers measured from their single component permeabilities, varied widely, and were primarily related to the partitioning of the

isomers between the aqueous and organic phases. As such, the observed selectivities can be attributed primarily to the ability of the certain ortho isomers to form intramolecular hydrogen-bonds and limit their available intermolecular hydrogen-bonding sites. Only small differences in selectivity were observed between the nematic and isotropic phases of 8CB.

To our knowledge, this is the first quantitative research on the diffusion and solubility of aqueous organic solutes in a thermotropic liquid crystal. Further work is needed to determine the effects of the molecular structure of the liquid crystal (presence of aromatic groups and other functionalities) on solute transport. LC materials available, we anticipate that selectivity can be enhanced via the judicious selection of specific solute-LC combinations. In addition, the study of LC orientation effects on the diffusion is limited due to the isotropic pore orientations in the cellulose nitrate support, and could lead to more effective control over solute transport by using membranes with cylindrical pore structures, which allows the anisotropic LC orientations through the membrane pores. Finally, chiral LC-forming materials hold the promise of supported LC membranes capable of performing enantiomeric separations.

Chapter 4. Effect of Molecular Packing and Intermolecular Interactions on Solute Transport in Supported Liquid Crystalline Membranes

NOTE: The contents of this section have been submitted to Journal of Chemical & Engineering Data.

4.1 Chapter Summary

The electro-optical properties of thermotropic liquid crystalline (LC) materials have been the subject of significant research effort due to their well-established applications in display technology. Until recently, relatively little work has been concentrated on the transport of dissolved solutes in LC phases for applications in separations and sensing. Recently, we reported on the transport behavior of organic solutes in 4-cyano-4'-octylbiphenyl (8CB) supported liquid crystal membranes. Herein we report on the transport of organic solutes in 4-(trans-4'-4'-n-pentylcyclohexy)-benzonitrile (PCH5) and 8CB supported liquid crystal membranes in order to broaden the understanding of the mechanisms for solute transport kinetics. PCH5 was chosen as it exhibits a lower packing density than 8CB but retains a similar molecular structure. Supported liquid crystal membranes were synthesized by impregnating porous cellulose nitrate (CN) membranes with 8CB and PCH5 from chloroform solutions under vacuum. Measurements of solute permeation through 8CB-CN and the PCH5-CN membranes were performed in the nematic and isotropic phases for aromatic solutes with different functional groups, including positional isomers. Solute diffusivity and solubility were calculated using a time-lag technique based on the study of the transient (unsteady state) and steady-state permeation regimes. The Wilke-Chang correlation was used to examine the diffusivity deviations due to the presence of solute/LC intermolecular interactions. According to the Wilke-Chang correlation fitting, solutes without hydrogen donor showed negative diffusivity deviations compared to solutes with single hydrogen

donor, proposing enhanced diffusivity by the single hydrogen interactions. Higher sorption and diffusion coefficients were found in PCH5, compared to 8CB, due primarily to the lower packing density in the PCH5 nematic phase. Shape selective absorption, in which rod-like para- isomers (e.g. p-ethylphenol) exhibited higher solubility in the anisotropic nematic phases, was observed in both PCH5 and 8CB. Aromatic solutes possessing more functional groups exhibited decreased solubility. Diffusing solutes with multiple hydrogen donors exhibited significantly decreased diffusivities in both 8CB and PCH5, leading to large selectivities for the separation of isomers that form intramolecular hydrogen-bonds in the ortho conformation. The PCH5-CN membranes demonstrated enhanced selectivities for hydroxybenzoic acid (3 %) and the aminophenol isomers (29 %) compared to 8CB-CN membranes resulting from a significant increase in sorption selectivity.

4.2 Introduction

Small molecule thermotropic liquid crystals (LCs) exhibit anisotropic phases that are responsive to various stimuli, including temperature, electric and magnetic fields, and the presence of impurities. Rod-like thermotropic LCs consist of rigid moieties (mesogens), usually consisting of aromatic groups, and flexible moieties, often alkane chains. The LCs can exhibit a variety of temperature-dependent phases (i.e. smectic, nematic, cholesteric, isotropic) which are classified according to their orientational order, positional order, and chirality.[12,13] The LC molecules are aligned along their long axis in the nematic and smectic phases, but randomly oriented in the isotropic phase.

The molecular packing in thermotropic LC phases depends on the chemical structure of the mesogenic moieties and the length of pendant alkyl chains.[73] Increases in alkyl chain length and higher temperatures have been reported to lower the molecular packing coefficient (defined as the sphere volume divided by the unit cell volume) indicating a decreased molecular packing density. When a phenyl ring in a biphenyl mesogen is replaced by a

cyclohexyl ring (e.g. 4-cyano-4'-pentylbiphenyl, 5CB → 4-(trans-4'-4'-n-pentylcyclohexy)-benzonitrile, PCH-5), the packing coefficient decreases by 0.02 due to an increased steric repulsion as revealed by a decrease in the activation energy of rotational viscosity (0.41 eV for PCH-5 and 0.55 eV for 5CB).[73]

Membrane separation techniques provide advantages such as increased energy efficiency, simplicity, and ease of scale-up when compared to conventional distillation and chromatographic separation methods which are more complex and energy intensive processes. Furthermore, conventional separation processes have limited applicability for the separation of positional (ortho, meta, and para) and optical isomers[74] (left- and right-handed) due to their similar physical properties. Currently, chromatography[68,75] and capillary electrophoresis[76,77] techniques using different electrophoretic mobilities related to molecular shape have applied in positional isomer separations. Few membrane materials for positional isomer separations have been reported. It would be advantageous to find a novel membrane material capable of performing isomeric separations in order to replace conventional energy intensive separation techniques.

We have previously reported on the solubility and diffusivity of aromatic organic solutes consisting of one phenyl ring and a variety of appended functional groups in the nematic and isotropic phases of 4-cyano-4'-pentylbiphenyl (8CB) using a membrane permeation technique.[43] Multiple solute/LC hydrogen bonding interactions and shape specific affinity were identified as important considerations for the sorption and diffusion behavior of organic solutes in 8CB LCs.

Herein we report on the transport properties of aromatic organic solutes in membranes consisting of 8CB and PCH-5 liquid crystals. PCH-5, whose mesogenic core consists of one cyclohexyl ring and one phenyl ring, was selected in order to understand the effect of LC molecular packing and decreased aromatic interactions on solute transport. We expected that the decreased molecular packing coefficient in PCH-5 would result in

decreased solute-LC interactions and would affect both the diffusion and sorption selectivity between different LC materials and phases (nematic and isotropic).

4.3 Experimental

4.3.1 Materials and Equipment

4-cyano-4′-octylbiphenyl (8CB) was obtained from Wako Chemicals (Japan), which exhibits multiple liquid crystalline phases with transition temperatures of 21.5 ℃ (Crystal-Smectic A), 33.5 ℃ (Smectic A-Nematic), and 40.5 ℃ (Nematic-Isotropic).[53] Phenol, pyridine, chloroform, kerosene, *p*-, *m*- and *o*-cresol, *p*- ,m- and *o*-hydroxybenzoic acid (salicylic acid), *p*- and *o*-aminophenol, *p*- and *o*-aminobenzoic acid, *o*- and *p*-nitrophenol, *o*- and *p*-ethylphenol, 5-nitrosalicylic acid, 1-fluoro-2-nitrobenzene, 1-fluoro-4-nitrobenzene, 4-(trans-4'-4'-n-pentylcyclohexy)-benzonitrile (PCH5) were purchased from Sigma Aldrich (St. Louis, MO, USA). Flat sheet cellulose nitrate membranes (pore size 0.22 μm, porosity 70~80 %, diameter 47 mm) were obtained from Whatman (Dassel, Germany). Polypropylene membranes (pore size 0.22 μm) were obtained from Sterlitech (USA). 18.2 MΩ deionized water was produced by an E-pure deionization system (Barnstead, USA). All chemicals were of reagent grade and used without further purification.

Polarized light microscopy was performed using an Olympus BX51 microscope (Olympus USA) with a Linkam LTS-350 hot stage (Linkam Co, UK). Scanning electron microscopy (SEM) was performed using a LEO (Zeiss) 1550; samples were prepared by coating with a gold layer (15 nm) or by freezing in liquid nitrogen, fracturing and coating with a gold layer (15 nm) for cross-sectional images. Fourier-transform Infrared spectroscopy (FTIR) was performed using a BioRad FTS-40A (Cambridge, MA, USA). FTIR samples were prepared by dissolving solutes in 8CB LCs and PCH5 LCs at 60 ℃ (isotropic phase) onto a clean KBr plate. Ultraviolet-Visible light spectra were recorded using a USB-4000

UV-VIS spectrophotometer (Ocean Optics) equipped with a z-type flow cell (1 cm path length) and a peristaltic pump.

4.3.2 Membrane Preparation

LC embedded membranes were prepared by impregnating the porous cellulose nitrate membrane with 8CB or PCH5 via vacuum filtration. 25 % (w/v) 8CB or PCH5 chloroform solution was filtered through the porous membrane support in which 8CB LCs or PCH5 LCs were kept in membrane pores by capillary forces. The resulting LC embedded membranes were immersed in deionized water overnight at room temperature to remove excess LCs remaining on the membrane surface and then dried under vacuum for 1 hour at 70 ℃. The membranes were trimmed to final size and sandwiched between two rings of aluminum tape to provide added support. Finally, the 8CB embedded membranes (8CB-CN) and PCH5 embedded membranes (PCH5-CN) were washed in deionized water stirred (150 rpm) at 38 ℃ for 45 min during which any leaching of 8CB or PCH5 from the membrane was monitored using UV-VIS specroscopy. The membranes were then dried in a vacuum oven. Kerosene, a mixture of saturated hydrocarbon chains, which has been commonly used as an organic phase for supported liquid membranes,[78,79] was embedded in polypropylene membrane supports using the same procedure without the rinsing and drying steps. The kerosene embedded polypropylene membrane was compared with 8CB or PCH5 LC embedded membranes in terms of salicylic acid solubility as there is no pi-pi stacking interaction between kerosene and salicylic acid.

The amount of 8CB and PCH5 in the impregnated membranes following the vacuum drying step was 100.7 ± 2.6 mg (n=8) (2.7 mmol/cm^3) and 92.2 ± 3.5 mg (n=6) (2.5 mmol/cm^3) respectively. The final membrane thicknesses were 122 μm, the same as the unfilled membrane support. The volume of liquid crystal in the membranes (calculated based on densities of 0.96 g/cm^3 for PCH5 at 30 ℃ and 0.99 g/cm^3 for 8CB at 33 ℃)[80] was 0.096

cm^3 for PCH5 and 0.101 cm^3 for 8CB. These values are very close to the CN membrane void volume of 0.095 cm^3, indicating that most of the membrane void space was filled with LC. Scanning electron microscopy (SEM) images (Figure 4.1) of the surface and cross-sections of the 8CB-CN[43] and PCH5-CN membranes showed that 8CB and PCH5 LCs fills all the CN membrane pores except for larger defects in the porous supports.

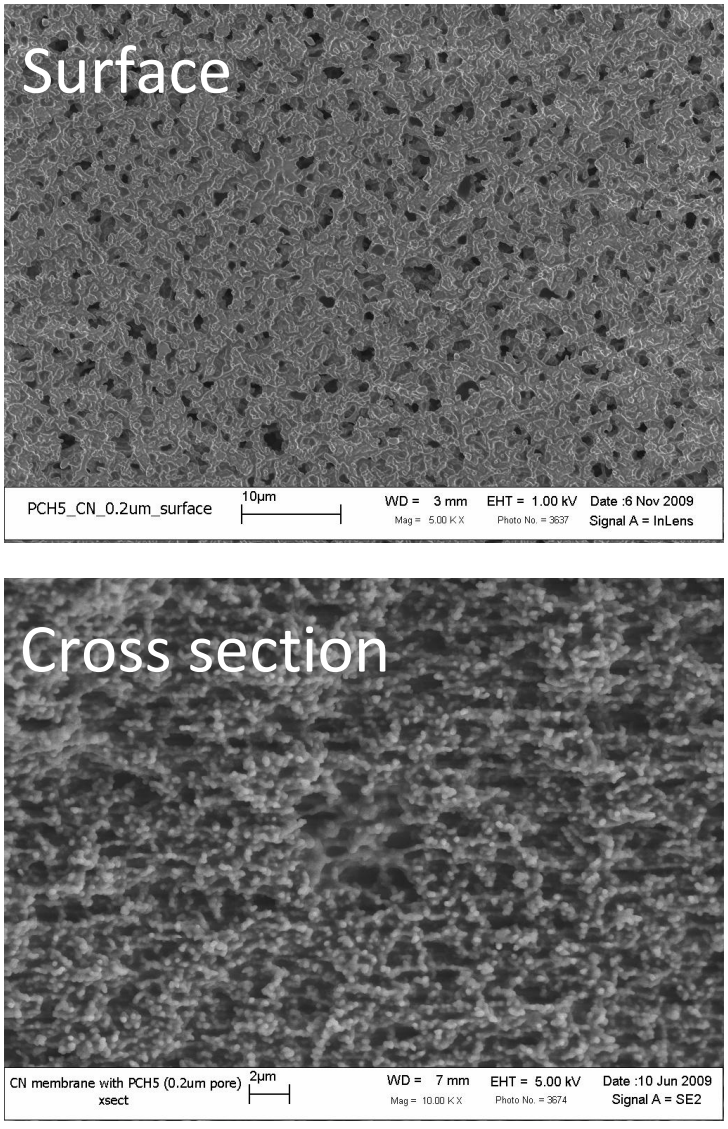

Figure 4.1: SEM images of PCH5 LCs embedded cellulose nitrate membranes

It has previously been reported that small molecule nematic LCs arrange themselves in a parallel orientation (planar or homogenous) to certain substrates. This is the case for 4-

cyano-4'-pentylbiphenyl (5CB) in a cellulose nitrate support[54]; 8CB in random porous glass[55]; 5CB in polymer dispersed liquid crystals[58] and 5CB in 4,4′-bis(acryloyloxy)biphenyl (BAB).[58] Based on these results, we assume that the 8CB and PCH5 molecules orient parallel to the cellulose nitrate pore walls. Since the cellulose nitrate support consists of a randomly oriented network of pores there is no macroscopic preferred LC orientation. This allows us to treat diffusion across the membrane as essentially isotropic.

4.3.3 Permeation Measurements in 8CB-CN and PCH5-CN Membranes

8CB or PCH5 embedded membranes with an effective permeation area of 7.55 cm^2 were placed between two glass half cells. The feed cell was filled with 200 ml of a 5 mM aqueous solution of a solute molecule (except for 5-nitrosalicylic acid, 1-fluoro-2-nitrobenzene and 1-fluoro-4-nitrobenzene whose feeds contained 2.5 mM, and 1 mM respectively due to low water solubility.) The receiving cell was filled with 200 ml of deionized water. The membrane permeation cell was immersed in a recirculating water bath to control the system temperature and the solution in each half cell was stirred at 150 rpm, a speed determined to be fast enough to prevent concentration gradients. The transport experiments were performed at 38 ℃ (nematic phase) and 44 ℃ (isotropic phase) for 8CB and at 48 ℃ (nematic phase) and 52 ℃ (isotropic phase) for PCH5. During the experiment, the solute concentration in the receiving cell was continuously monitored using a UV spectrometer (USB-4000, Ocean Optics, USA). Diffusivities and solubilities of the solute molecules in 8CB and PCH5 were calculated based on the average of three separate transport experiments for each solute molecule and new membranes were used for each solute. The membranes were washed in deionized water at 38 °C prior to and between the transport experiments to remove any dissolved solute molecules remaining in the membranes.

4.3.4 Calculation of Diffusivity and Solubility

For a quantitative analysis of the transport kinetics, a time-lag method was employed for the membrane permeation experiments. The time-lag method is a macroscopic technique based on the time required to reach steady-state transport regime, which enables the estimation of the diffusivity of organic solutes passing through the membranes. The solubility can then be obtained using the measured permeability and the calculated diffusivity.

The steady state concentration gradient driven diffusive transport of a solute across a membrane is described by Fick's law. The measured permeability is related to the solubility and diffusivity as follows:[48]

$$P = D\,S \qquad (4.1)$$

where P is permeability (mmol/cms); D is diffusivity (cm^2/s); S is solubility ($mmol/cm^3$).

In order to calculate the solubility from the above equation, two parameters, the permeability and diffusivity must be calculated from experimental data. The permeability is defined as:

$$P = \frac{dM_t}{dt}\frac{L}{A} \qquad (4.2)$$

dM_t/dt is the rate of solute mass transport (determined from the slope of the plot of mass transported vs time in the steady state regime); L is membrane thickness (cm); A is membrane area (cm^2).

The mathematical analysis of diffusion and solubility using the time-lag method assumes that there is no boundary layer resistance at the membrane interfaces and no convective flow through the membrane.[52,56] These conditions are achieved experimentally by stirring in the diffusion cells and immobilizing the liquid crystal in a porous membrane. Under these conditions the concentration profile used for the measurement of solubility and diffusivity can be found by Fick's law where transport is assumed to take place in z-direction only (e.g. perpendicular to the membrane surface):

$$\frac{\partial C_i}{\partial t} = D\frac{\partial^2 C_i}{\partial z^2} \qquad (4.3)$$

where C_i is the concentration of species *i*, *D* is its diffusivity, and *z* is the direction of transport perpendicular to the membrane surfaces.

At the time zero, diffusing molecules are injected into the feed side with a concentration which is assumed to be constant during the transport. In addition, the diffusing molecule concentration in the receiving side will remain small enough to influence no effects on the diffusivity, leading to the following boundary conditions:

$$\begin{aligned} &t = 0 \text{ and } 0 \le z \le L, && C_i(z,0) = 0 \\ &t > 0 \text{ and } z = 0, && C_{i0}(0,t) = C_{i0} = \text{constant} \\ &t > 0 \text{ and } z = L, && C_{iL}(L,t) = C_{iL} \approx 0 \end{aligned} \qquad (4.4)$$

where *L* is membrane thickness; C_i is concentration of diffusing molecules *i*.

Solving the unsteady-state diffusion problem results in the following equation for solute diffusivity:

$$t_g = \frac{L^2}{6D} \qquad (4.5)$$

where t_g is the time-lag (s); *L* is membrane thickness (cm); *D* is diffusion coefficient or diffusivity (cm^2/s). Using the permeability and diffusivity calculated from eqs. (4.2) and (4.5), the solubilities of diffusing species in the 8CB and PCH5 embedded cellulose nitrate membrane were obtained using eq. (4.1).

4.4 Results and Discussion

4.4.1 Supported Liquid Crystal Membrane Stability

Membranes were immersed in deionized water at 38 °C and the UV-VIS spectrum of the aqueous phase was monitored for any increase in the PCH5 peak intensity (290~310 nm). The PCH5-CN membranes exhibited no significant leaching of the PCH5 into the aqueous phase. Multiple experiments for the permeation of *o*-nitrobenzoic acid through PCH5-CN at

38 °C performed using the same membrane exhibited only slight changes in membrane performance between runs indicating that the membranes are stable under experimental conditions. The stability of 8CB-CN membranes has been reported previously.[43,81]

4.4.2 Phase Behavior in 8CB-CN and PCH5-CN Membranes

The existence of nematic-isotropic phase transitions were confirmed using polarized optical microscopy of membrane samples immersed in a temperature controlled deionized water bath. 8CB-CN and PCH5-CN membranes showed nematic-isotropic phase transitions at 40 °C and 51 °C, respectively. The observed transition temperatures are the same as those for bulk 8CB and PCH5 indicating that confinement in the membrane pores and the presence of a neighboring aqueous phase do not change the liquid crystal phase behavior.[57]

4.4.3 Diffusivity and Solubility Behavior of Organic Solutes in 8CB and PCH5 Membranes

4.4.3.1 Diffusivity and Solubility in 8CB-CN and PCH5-CN Membranes

The diffusivities and solubilities for organic solutes in 8CB and PCH5 as determined from membrane permeability measurements in the nematic phase (38 °C) are shown in Table 4.1 and depicted in Figures 4.2 and 4.3. The values for diffusivity and solubility of organic solutes were higher in PCH5 than in 8CB with the exception of *m*-nitrobenzoic acid, which exhibited a slight decrease in diffusivity, and *p*-hydroxybenzoic acid and *p*-aminophenol, which exhibited slight decreases in solubility. This behavior can be attributed to differences in free volume between 8CB and PCH5. PCH5 molecules in the nematic phase do not pack as densely as 8CB molecules due to decreased intermolecular interactions and increased steric hindrance.[97] The resulting increase in free volume leads to the observed increases in sorption and diffusion of organic solutes in PCH5. Increased solubility has also been reported in CO_2

gas absorption experiments in the nematic and isotropic phases of PCH5 compared to n-4′-methoxybenzylidene-n-butylaniline (MBBA)[32] as a result of increased free volume (ρ_{PCH5} = 0.9634 g/cm^3 at 30 °C;[73] ρ_{MBBA} = 1.049 g/cm^3 at 22 °C[82]).

Table 4.1: Measured time lag, and calculated diffusivity and solubility from measurements of solute permeation through 8CB-CN and PCH5-CN membranes at 38 ^{o}C

Diffusing molecules	Time lag, T_g (s)		Diffusivity, D x 10^8 (cm^2/s)		Solubility, S (mmol/cm^3) x 10	
	8CB	PCH5	8CB	PCH5	8CB	PCH5
Phenol	168.7[a]	149.4	14.7 ±3.8[a]	16.5 ±2.1	0.48 ±0.1[a]	0.61 ±6.2
Pyridine	258.1[a]	227.2	9.6 ±8.1[a]	10.5 ±2.9	0.39 ±1.5[a]	0.41 ±4.6
o-aminophenol	503.4[a]	316.4	5.0 ±8.3[a]	7.8 ±3.4	0.14 ±6.3[a]	0.19 ±9.1
p-aminophenol	3261.9[a]	1641.6	0.7 ±9.5[a]	1.8 ±10.2	0.22 ±1.4[a]	0.18 ±6.2
o-aminobenzoic acid	324.6[a]	279.0	7.7 ±4.5[a]	8.9 ±2.0	0.33 ±8.3[a]	0.38 ±6.2
p-aminobenzoic acid	1478.5[a]	869.3	1.7 ±2.3[a]	2.85 ±3.7	0.23 ±7.3[a]	0.25 ±2.7
o-hydroxybenzoic acid	257.3[a]	208.9	9.8 ±2.8[a]	11.8 ±0.7	0.78 ±0.1[a]	1.03 ±2.4
p-hydroxybenzoic acid	1366.2[a]	476.9	1.8 ±4.3[a]	5.2 ±2.0	0.12 ±4.2[a]	0.09 ±2.6
o-nitrophenol	367.7	363.9	6.2 ±8.5	6.8 ±4.6	4.67 ±12.2	5.49 ±5.9
p-nitrophenol	286.5	239.7	8.7 ±2.3	10.3 ±3.2	1.41 ±2.2	1.68 ±1.3
o-nitrobenzoic acid	606.1	726.1	3.1 ±6.3	3.4 ±2.9	0.21 ±8.3	0.25 ±5.3
m-nitrobenzoic acid	295.4	392.4	6.4 ±4.6	6.3 ±2.6	0.80 ±2.4	1.08 ±3.3

Errors reported are one standard deviation percentage.

[a] previously published results

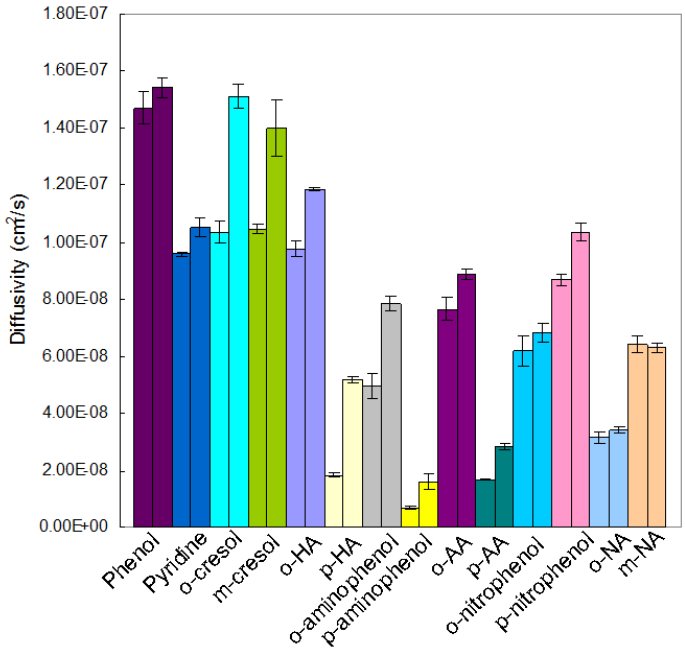

Figure 4.2: Nematic phase diffusivities of organic solutes in 8CB-CN and PCH5-CN membranes measured at 38 ℃. Left and right-hand bars for each solute represent data for 8CB-CN and PCH5-CN membranes respectively. HA, AA, and NA represent hydroxybenzoic acid, aminobenzoic acid, and nitrobenzoic acid, respectively.

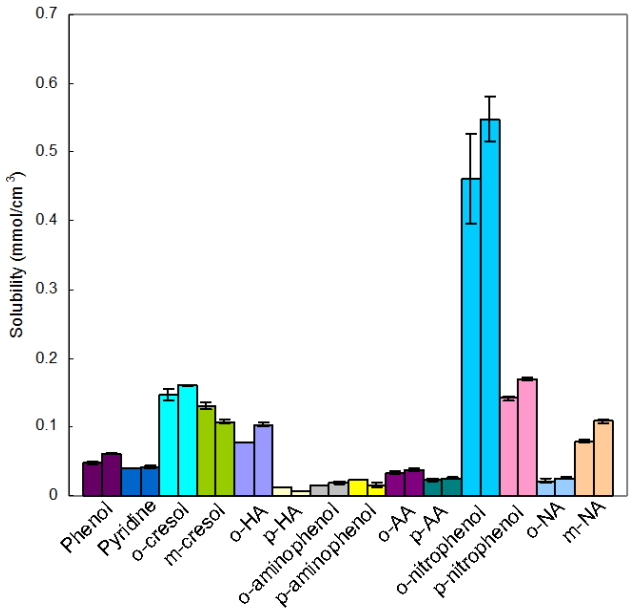

Figure 4.3: Nematic phase solubilities of organic solutes in 8CB-CN and PCH5-CN membranes measured at 38 ℃. Left and right-hand bars for each solute represent data for 8CB and PCH5 respectively. HA, AA, and NA represent hydroxybenzoic acid, aminobenzoic acid, and nitrobenzoic acid, respectively.

The PCH5-CN and 8CB-CN membranes exhibited significant differences in the diffusivities of positional isomers, with the exception of methylphenol (cresol) and ethylphenol isomers. The aberrant behavior of the phenol derivatives (*p*- and *o*-isomers) is attributed to the fact that they have only one hydroxyl group and are incapable of forming intramolecular hydrogen-bonds and capable of only one hydrogen-bonding interaction with the surrounding LC molecules. As reported previously[43], the slow diffusion of para-isomers was attributed to the formation of multiple hydrogen bonding interactions with cyano groups of the LCs. Similar effects of solute-solvent hydrogen bonding on diffusion have also been reported for organic solutes in non-LC organic solvents,[83,84] in which decreased diffusivities were observed with increased intermolecular hydrogen bonding interactions between the solute and the solvent.

The measured solubilities of organic solutes in the LC membranes were strongly dependent on the solubility of the organic solutes in the aqueous phase. The aqueous phase solubility is related to the number of available intermolecular hydrogen bonding sites; for example, para-isomers exhibited lower solubility in the LCs than their corresponding ortho-isomers due to the presence of more available sites for hydrogen bonding with water molecules. One exception is *m*-nitrobenzoic acid which was more soluble in the LCs than *o*-nitrobenzoic acid due to its lower aqueous phase solubility. This behavior is consistent with the prior studies on the partitioning of organic solutes between aqueous and immiscible organic phases.[62]

4.4.3.2 Activation Energy of Diffusion for PCH5

Higher measured diffusivities in PCH5 membranes compared to 8CB membranes suggest that a lower activation energy for diffusion exists in PCH5 due to increased intermolecular distances and free volume. Measurements of salicylic acid permeation through

PCH5-CN membranes were performed at various temperatures ranging from 32 °C to 55 °C. The activation energy for diffusion was obtained from an Arrhenius-like relation which describes the diffusivity dependence on temperatures as follows:[85]

$$D = D_0 \exp\left(\frac{-E_a}{RT}\right) \quad (4.6)$$

where D is the diffusion coefficient or diffusivity (cm^2/s); R is the ideal gas constant (8.314 J/mol·K); T is the temperature (K); E_a is the activation energy for diffusion (kJ/mol); and D_0 is the Arrhenius constant (cm^2/s)

Figure 4.4 shows the diffusivity dependence on the temperature for the permeation of salicylic acid in a PCH5-CN membrane. The slopes of the fitted lines correspond to the activation energy for diffusion. The nematic and isotropic phases of PCH5 exhibit activation energies for diffusion of 25.73 kJ/mol and 36.49 kJ/mol respectively. A decreased activation energy for diffusion in the nematic phase has been previously reported[70,71] and is caused by the anisotropic nature of the nematic phase. We have previously reported activation energies for diffusion of salicylic acid in 8CB-CN membranes (27.02 and 39.33 kJ/mol for the nematic phase and isotropic phases respectively); these values are higher than the PCH5 values by 4 % in the nematic phase and 9 % in the isotropic phase. The lower activation energies for diffusion in PCH5 are consistent with the increased diffusivities observed and are attributed to increased free volume and intermolecular spacing in the PCH5 liquid crystal molecules.

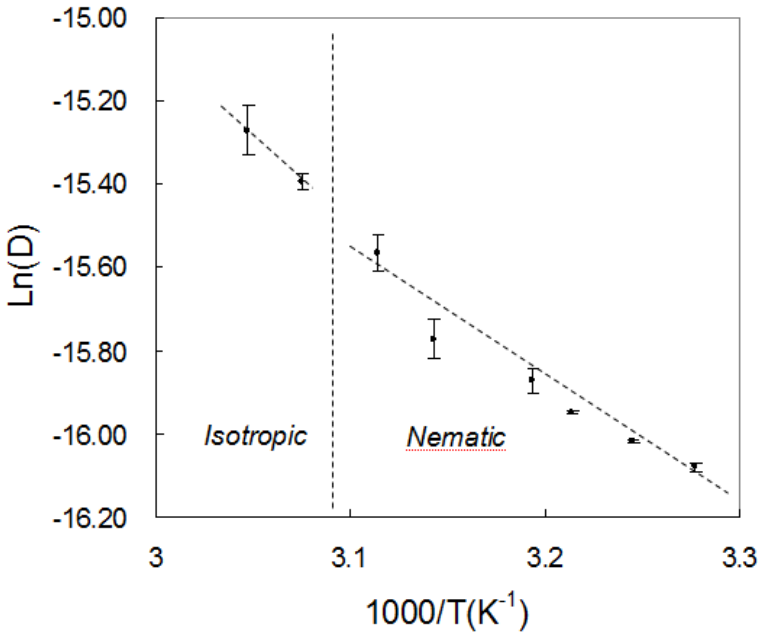

Figure 4.4: Arrhenius plot for the diffusion of *o*-hydroxybenzoic acid through a PCH5-CN membrane (initial concentration; 5 mM). Dashed lines represent linear fits of the data.

4.4.3.3 Shape Selective Absorption in the Nematic Phase of 8CB and PCH5

Our group has previously reported the shape selective absorption of rod-like molecules in the nematic phase of 8CB. Rod-like para isomers such as cresol, hydroxybenzoic acid, aminophenol, aminobenzoic acid exhibited increased solubility in the nematic phase compared to ortho and meta isomers. Thefefore, we investigated the shape selective absorption for PCH5 with ethylphenol isomers including rod-like *p*-ethylphenol.

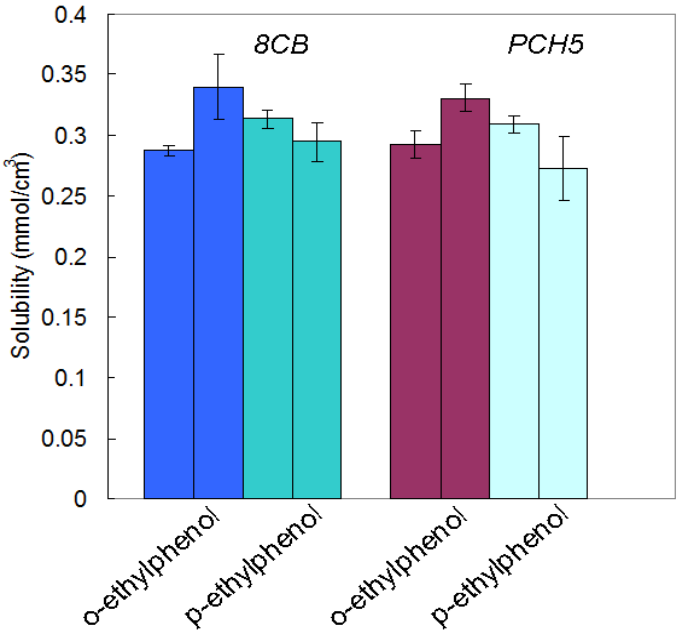

Figure 4.5: Solubilities of ethylphenol isomers in the nematic and isotropic phases of 8CB and PCH5. For each solute, the left and right-hand bars represent data obtained in the nematic and isotropic phases of 8CB (38 ℃ and 44 ℃) and PCH5 (48 ℃ and 52 ℃) respectively.

The solubilities of *o*-ethylphenol were greater in the isotropic phases of 8CB and PCH5 (Figure 4.5), wheareas the solubility of *p*-ethylphenol in the nematic phases of 8CB and PCH5 were greater (6 % and 13 % respectively), despite the lower temperature and decreased free volume in the nematic phase. Similarly, *p*-hydroxybenzoic acid solubility in PCH5-CN membranes was higher in the nematic phase than in the isotropic phase, while *o*-hydroxybenzoic acid exhibited higher solubility in the isotropic phase. This data indicates that shape selective absorption occurs in both PCH5 and 8CB nematic phases due to the favorable interactions between the rod-like para isomers and the ordered liquid crystalline phase.

4.4.3.4 Solubility Comparisons of Various Organic Solutes for 8CB and PCH5

According to the solubility data (Figure 4.3), the solubilities for 8CB and PCH5 mainly depended on the water solubility of organic solutes and could not be compared in terms of the molecular shapes and functional groups. Thus, organic solutes with similar solubility in water (salicylic acid and 5-nitrosalicylic acid) were selected in order to isolate the effect of molecular structure and functionality on solubility in the LC membranes from the effect of solute solubility in the aqueous phase. In comparison with salicylic acid and 5-nitrosalicylic acid which has additional nitro group in the phenyl ring 5-position of salicylic acid, the solubility of salicylic acid in 8CB-CN membranes was 2 times higher than of 5-nitrosalicylic acid even though salicylic acid has more association interactions with water according to the water solubility (4.55 g/l for salicylic acid at 313 K[86]; 0.622 g/l for 5-nitrosalicylic acid at 293 K[87]). The more surrounded phenyl ring is expected to bring into decreased interactions with the liquid crystals due to the steric hindrance.

The solubility measurements of salicylic acid for kerosene were performed using a kerosene embedded polypropylene membrane. Salicylic acid exhibited 11 and 15 times greater solubilities in 8CB and PCH5 respectively than in kerosene. Kerosene[88], which is a mixture of 80 % saturated hydrocarbon and 20 % aromatics, interacts less strongly with salicylic acid due to a lack of hydrogen bonding interactions and decreased pi-pi interactions between the saturated hydrocarbon and the salicylic acid, as previously reported.[68,89] These results demonstrate that solute partitioning between aqueous and LC phases depends not only on the relative aqueous phase solute solubilities but also on specific solute/LC intermolecular interactions such as hydrogen-bonding and pi-pi stacking.

4.4.3.5 Diffusion and Sorption Selectivities of Positional Isomers for 8CB and PCH5 LCs

Our group has previously reported that 8CB-CN membranes showed permeation selectivity for positional isomers based on differences in the number of available solute hydrogen bonding sites. PCH5-CN membranes also exhibited permeation selectivity (Table 4.2) as determined using single component transport experiments. This behavior can also be attributed to the presence of the cyano group in PCH5 which acts as a hydrogen-bond acceptor for interactions with organic solutes. Multiple available solute hydrogen bonding sites lead to the slower diffusion.

Table 4.2: Permeation selectivity[a] in 8CB-CN and PCH5-CN membranes measured at 38 °C (nematic phase)

	8CB	PCH5	% Change
Hydroxybenzoic acid	33.90	35.01	3.27
Aminophenol	4.71	6.07	28.87
Nitrobenzoic acid	7.65	7.81	2.09
Aminobenzoic acid	6.58	4.60	-30.09
Nitrophenol	2.23	2.14	-4.04

[a]Permeation selectivity is the ratio of measured permeabilities of the ortho and para isomers.

Table 4.3: Diffusion and sorption selectivity in 8CB-CN and PCH5-CN membranes measured at 38 °C (nematic phase)

	Diffusion selectivity[a]			Sorption selectivity[a]		
	8CB	PCH5	% Change	8CB	PCH5	% Change
HA[b]	5.38	2.28	-57.62	6.3	15.35	143.65
Ap	7.19	4.91	-31.71	0.65	1.24	90.77
NA	3.5	3.03	-13.43	2.19	2.58	17.81
AA	4.56	3.11	-31.8	1.44	1.48	2.78
Np	0.67	0.66	-1.49	3.35	3.25	-2.99

[a]Diffusion and sorption selectivity are ratios of the diffusivities and solubilities of the ortho and para isomers.

[b]HA, Ap, NA, AA, and Np represent hydroxybenzoic acid, aminophenol, nitrobenzoic acid, aminobenzoic acid, and nitrophenol respectively.

To understand the factors influencing the permeation selectivities in 8CB-CN and PCH5-CN membranes, the diffusion and sorption selectivities for positional isomers were calculated (Table 4.3). For all isomers tested, the PCH5-CN membranes exhibited lower diffusion selectivities than the 8CB-CN membranes. This behavior is a result of differences in the intermolecular distance and void fraction in 8CB and PCH5. 8CB LCs have closer intermolecular distances than PCH5 due to strong intermolecular interactions between biphenyl moieties. The denser molecular packing in 8CB results in the decreased diffusivities and increased diffusion selectivities due to the narrow diffusion path and increased solute/LC interactions.

In contrast, the sorption selectivities observed for PCH5 were higher for all solutes except the nitrophenol isomers. In particular, the sorption selectivities for the hydroxybenzoic acid and aminophenol isomers were greatly increased (143.7 and 90.8 respectively) leading to the improved permeation selectivities for PCH5 (Table 4.2) despite decreased diffusion selectivities.

Table 4.4: Diffusion and sorption selectivity in the nematic and isotropic phases for 8CB

	Diffusion selectivity[a]			Sorption selectivity[a]		
	Nematic	Isotropic	% Change	Nematic	Isotropic	% Change
HA[b]	5.38	3.78	-29.74	6.3	8.05	27.78
Ap	7.19	5.67	-21.14	0.65	5.67	0.87
NA	2.05	1.81	-11.71	2.19	3.89	77.63
AA	4.56	3.31	-27.41	1.44	1.89	31.25

[a]Data for the nematic and isotropic phases were measured at 38 ˚C and 44 ˚C respectively.

Similar behavior for the diffusion and sorption selectivities were found in both the nematic and isortopic phases of 8CB and PCH5. The diffusion selectivities decreased in the isotropic phase of 8CB while the sorption selectivities increased (Table 4.4). In particular, when the permeation of *o*- and *p*-hydroxybenzoic acids were measured in PCH5-CN membranes in the nematic and isotropic phases, they showed a 17 % increase in diffusion selectivity and a 27 % decrease in sorption selectivity in the nematic phase. The closer intermolecular distances and ordered packing of the nematic phases resulted in the higher diffusion selectivities than those observed in the isotropic phases of both 8CB and PCH5. The higher sorption selectivities for positional isomer separation in the isotropic phases of 8CB and PCH5 are a result of the decrease in solubility of the para isomers when going from the nematic to the isotropic phase. This higher solubility in the nematic phase is a result of shape-selective sorption of the rod-like para- isomers described above.

4.4.4 Effects of Hydrogen Bonding and Dipole-Dipole Interactions on Diffusion in 8CB and PCH5 Membranes

4.4.4.1 Hydrogen Bonding Interactions of Organic Solutes with LCs

It has been reported that thermotropic liquid crystals possessing cyano groups can form hydrogen bonding interactions with the hydrogen bond donors such as hexanol.[64] In addition, we have previously reported on the presence of hydrogen bonding interactions between the cyano groups of 8CB LCs and organic solutes as determined by FTIR.[43] Significant differences in diffusivity between o- and p- positional isomers were observed in both PCH5-CN and 8CB-CN membranes (Figure 4.2). The ortho isomers of hydroxybenzoic acid (HA), aminobenzoic acid (AA), and aminophenol (AP) exhibit higher diffusivities than the corresponding para- isomers. In contrast, the ortho- isomers of nitrophenol (NP) and nitrobenzoic acid (NA) exhibited lower diffusivities in both 8CB and PCH5. HA, AA, and AP possess multiple hydrogen bond donor groups, while NP and NA possess only a single

hydrogen bond donor group. The hydrogen bonding interactions between the PCH5 molecules and the organic solute molecules were examined using FTIR in order to further elucidate the effect of hydrogen bonding on solute diffusion.

Mixtures of aminobenzoic acid isomers in PCH5 LCs exhibited a shifted CN stretching peak (2250~2230 cm^{-1}) due to the presence of solute-LC hydrogen bonding interactions (Figure 4.6 - the peaks were normalized according to the C-H stretching peak[90] at 3100~2800 cm^{-1} of the LCs). *p*-aminobenzoic acid showed a more intense shifted peak than *o*-aminobenzoic acid. The *p*-isomer has more hydrogen donor groups available to interact with the PCH5 cyano groups because of intramolecular hydrogen bonding and steric hindrance in *o*-aminobenzoic acid. As a result, the *p*-isomers which have increased hydrogen bonding interaction with the LC exhibited the slower diffusions (Figure 4.2).

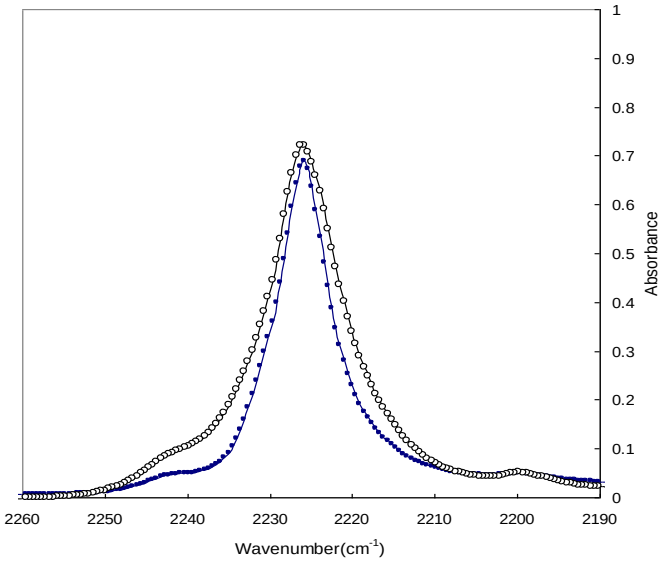

Figure 4.6: FTIR spectra of 25 % mol/mol mixtures of o- (●) and p-aminobenzoic acid (○) in PCH5

Unlike the other isomers studied, *o*-nitrobenzoic acid diffuses more slowly than *m*-nitrobenzoic acid. In the FTIR analysis, *o*-nitrobenzoic acid/PCH5 samples exhibited a shifted CN stretching peak of similar intensity to the *m*-nitrobenzoic acid/PCH5 samples as

no intramolecular hydrogen bonding[97] occurs in *o*-nitrobenzoic acid and the same number of hydrogen bond donors are present in both isomers (Figure 4.7 - the peaks were normalized). Since there were no observable differences in the strength of hydrogen bonding interactions between nitrobenzoic acid isomers and PCH5 we have focused on other effects to explain differences in diffusivity.

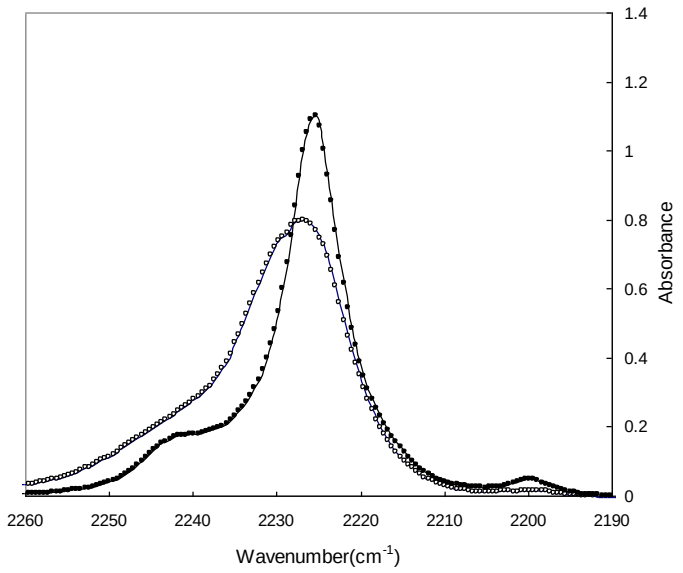

Figure 4.7: FTIR spectra of 25 % mol/mol mixtures of *o*- (●) and *m*-nitrobenzoic acid (○) in PCH5

4.4.4.2 Dipole-Dipole Interactions of Organic Solutes with LCs

It has been reported that diffusing solutes with high dipole moments have higher diffusion barriers in high dipole moment solvent conditions,[91] such as those found in LCs (4.5 D for 8CB[92] and 4.1D for PCH5[93] as a result of the presence of the cyano group oriented along the long molecular axis) due to strong solute-solvent dipole-dipole interactions which induces a molecular spinning aligned with a molecular z-axis. We observed lower diffusivity with higher dipole-dipole interactions in 1-fluoro-2-nitrobenzene and 1-fluoro-4-nitrobenzene transport experiments through 8CB-CN membranes in which the former showed 23 % lower

diffusivity due to the higher dipole-dipole interactions (4.6D for the 1-fluoro-2-nitrobenzene[94]; 2.6D for the 1-fluoro-4-nitrobenzene[94]). In addition, it has been reported that the more linear para-isomers exhibit higher diffusivity than ortho and meta isomers based on solute shape effects. [95] In the case of *o*-nitrobenzoic acid, in which the nitro group induces large dipole moments via formation of a zwitterion, has a higher barrier to diffusion due to a strong dipole-dipole interaction with the LCs (7.1 D for the *o*-isomer[97]; 5.5 D for the *m*-isomer[96]).

The FTIR spectra of *o*-nitrophenol in PCH5 showed no evidence of solute/LC hydrogen bonding due to the presence of intramolecular hydrogen bonding and steric hindrance.[97] *p*-nitrophenol in PCH5 exhibited a shifted CN stretching peak due to the interaction of the single hydroxyl group with the cyano group of PCH5. In the case of phenol, *o*-hydroxybenzoic acid, and cresol isomers, which possess only a single hydrogen-bond donor, hydrogen bonding interactions with the LCs do not appear to significantly decrease diffusivity when compared to isomers with multiple hydrogen-bond donor groups such as *p*-hydroxybenzoic acid and *p*-aminobenzoic acid (Figure 4.2). Furthermore, pyridine and benzene exhibited a lower diffusivity in the LCs than phenol, *o*-hydroxybenzoic acid, and the cresol isomers despite having the lowest molecular weight and no hydrogen bond donor groups. This suggests that a single hydrogen bonding interaction may even increase the rate of diffusion in the LC materials. As a result, the diffusion of *p*-nitrophenol isomers, which possess a single hydrogen bond donor group, could be enhanced by the formation of a hydrogen-bond with PCH5. *o*-nitrophenol is incapable of forming hydrogen bonds with PCH5 and does not benefit from this enhanced diffusion effect. *p*-nitrobenzoic acid, which exhibits a stronger single hydrogen bond interaction, as shown in the FTIR spectra also exhibits enhanced diffusion.

4.4.4.3 Wilke-Chang Correlation Fitting of Solute Diffusion in 8CB-CN and PCH-5-CN Membranes

The Wilke-Chang equation, a well-known empirical correlation developed for the prediction of the diffusion coefficients for organic solutes in a binary solution at infinite dilution, is given by:[98,99]

$$D_{AB} = 7.4\times10^{-12}\frac{\mathrm{T}\sqrt{\Phi M_B}}{\eta_B V_A^{0.6}} \qquad (4.7)$$

where D_{AB} is the diffusivity of solute A in solvent B; M_B is the molecular weight of the solvent; η_B is the viscosity of the solvent at temperature T; V_A is the molar hard core volume of the solute; Φ is an association factor for the solvent which is a dimensionless empirical parameter.

Organic solutes were selected to avoid significant intermolecular interactions with the LC molecules, such as multiple hydrogen bonding interactions, that would serve to slow down solute diffusion because the Wilke-Chang correlation assumes that diffusivity is governed solely by viscosity, solute size, and temperature. The diffusion coefficients for non-hydrogen bonding or singly hydrogen bonding solutes (phenol, *o*-, *m*-, and *p*-cresol, pyridine, *o*-nitrophenol, *o*-ethylphenol, and *o*-hydroxybenzoic acid) in 8CB reported previously showed a dependence on the solute molecular weight. For these solutes we have attempted to quantify the deviation of the measured diffusivities from those predicted by the Wilke-Chang correlation due to solute/LC intermolecular hydrogen bonding interactions. The molar hard core volume, V_A, for each solute was obtained from the literature[99] with the exception of the molar volumes for *o*-ethylphenol and *o*-hydroxybenzoic acid, which were calculated based on atomic volumes.[100]

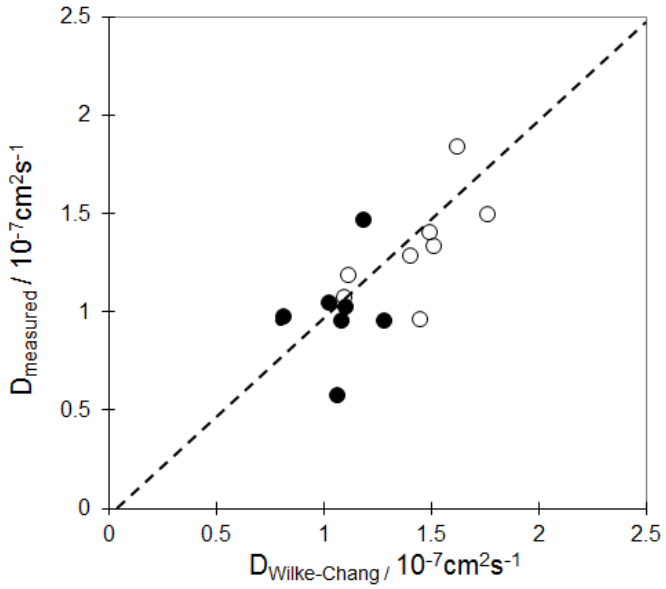

Figure 4.8: Comparison of the measured diffusivities of organic solutes in 8CB-CN membranes those calculated using the Wilke-Chang correlation. Filled and open circles represent data obtained in the nematic (38 ℃) and isotropic (44 ℃) phases respectively.

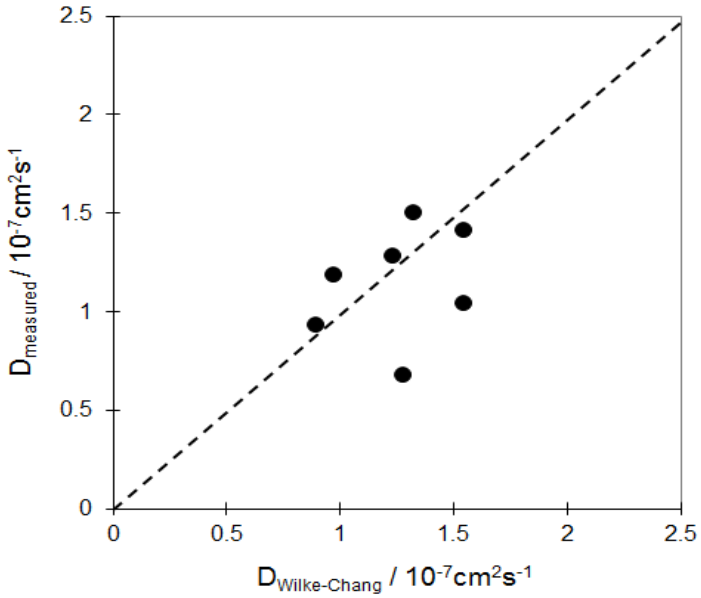

Figure 4.9: Comparison of the measured diffusivities of organic solutes in PCH5-CN membranes to those calculated using the Wilke-Chang correlation. Data was obtained in the nematic phase (38 ℃)

Association factors of Φ = 0.088 and Φ = 0.014 were obtained for the nematic and isotropic phases of 8CB respectively, based on viscosities of 73 cP (nematic, 310 K)[101] and 22 cP (isotropic, 318 K).[102] A value of Φ = 0.099 was obtained for the nematic phase of PCH5 based on a viscosity of 61 cP (nematic, 308 K). [103] Based on these association factors, the correlations for the diffusion of solutes in 8CB had a 20 % average deviation and those in PCH5 had a 21 % average deviation as shown in Figures 4.8 and 4.9 (for comparison, a 16 % average deviation has been reported for 756 different diffusivity measurements[104]). These values neglect the data for pyridine and *o*-nitrophenol which exhibited -25 and -45 % deviations in 8CB (Table 4.5) and -31 and -46 % deviations in PCH5. These negative deviations from the estimated diffusivity are attributed to the absence of available hydrogen bond donors in pyridine and *o*-nitrophenol. The association factors in this model were based primarily on organic solutes containing a single available hydrogen bonding donor. The behavior of pyridine and o-nitrophenol supports the assertion that a single solute/LC hydrogen bonding interaction can serve enhanced diffusion.

Table 4.5: Calculated diffusivity and relative deviation for transport in 8CB-CN membranes as determined using the Wilke-Chang correlation

	Nematic Phase Diffusivity ($x10^{-7}$)			Isotropic Phase Diffusivity ($x10^{-7}$)		
	Calculated	Measured	Deviation,%	Calculated	Measured	Deviation,%
Phenol	1.18	1.47 [a]	24.37	1.62	1.84 [a]	13.45
o-cresol	1.1	1.03 [a]	-6.3	1.51	1.34 [a]	-11.17
m-cresol	1.02	1.05 [a]	2.92	1.4	1.29 [a]	-7.86
pyridine	1.28	0.96 [a]	-25.01	1.76	1.50 [a]	-14.61
p-cresol	1.09	0.96 [a]	-11.73	1.49	1.41 [a]	-5.42
salicylic acid[b]	0.81	0.98 [a]	21.03	1.11	1.19 [a]	7.32
o-ethylphenol	0.79	9.96	20.52	1.09	1.08	-0.99
o-nitrophenol	1.06	0.58	-45.41	1.46	0.96	-33.76

[a] previously reported data

[b]Salicylic acid is *o*-hydroxybenzoic acid

Solutes possessing multiple available hydrogen bond donors exhibit large negative deviations from the Wilke-Chang model. The measured diffusivity of *p*-hydroxybenzoic acid in 8CB showed a -348 % relative deviation with respect to the predicted Wilke-Chang value due to existence of multiple hydrogen bonding interactions with the 8CB molecules. In comparison, *o*-hydroxybenzoic acid, which has a single available hydrogen bond donor, exhibited a 16 % relative deviation from the Wilke-Chang predicted value. Thus, while a single available hydrogen bond donor group serves to facilitate solute diffusion, multiple hydrogen bond donor groups act as a barrier to solute diffusion[84].

The Wilke-Chang correlation produced a better fit for solute diffusion in the isotropic phase of 8CB (12 % average deviation) than in the nematic phase of 8CB (20 % average deviation; Table 4.5). We attribute this difference to the existence of molecular order in the nematic phase that leads to increases in interactions between the solute and LC molecules, and thus, to larger deviations from the Wilke-Change correlation predictions.

4.5 Conclusions

The current study has examined the effect of molecular packing and solute/LC interactions on the transport behavior of aromatic solutes in nematic and isotropic PCH-5 and 8CB supported membranes. Higher solubilities and diffusivities observed in the nematic phase of PCH5, compared to those in the nematic phase of 8CB, were due to increased free volume[73] in the nematic phase of PCH5. PCH-5 exhibited lower activation energies for diffusion in the nematic phase than 8CB, indicating that increased intermolecular distances in nematic PCH-5 resulted in decreased barriers to diffusion. Shape selective absorption was

observed for rod-like *p*-ethylphenol and *p*-hydroxybenzoic acid in the nematic phase of both 8CB and PCH-5.

FTIR studies of the hydrogen bonding interactions between aromatic solutes and PCH5 indicated that the solutes with multiple available hydrogen bond donors had stronger solute/LC hydrogen-bond interactions than solutes with a single available hydrogen bond donor. The results of the FTIR were correlated to differences in solute diffusivity leading to the conclusion that multiple solute/LC hydrogen bonds, such as those exhibited by *p*-hydroxybenzoic acid, resulted in decreased diffusion while single solute/LC hydrogen bonds resulted in facilitated diffusion relative to the diffusion of solutes incapable of solute/LC hydrogen bonding. These conclusions were further confirmed through the analysis of solute diffusion data using the Wilke-Chang correlation which considers solvent viscosity, solute size, and temperature. Experimental diffusion data for solutes with multiple solute/LC hydrogen bonding interactions showed significant negative deviations with respect to the predicted Wilke-Chang model values which are independent of hydrogen bonding while solutes with a single solute/LC hydrogen bonding interaction was fitted well by the data.

The 8CB and PCH5 impregnated cellulose nitrate membranes exhibit promising performance for the separation of positional isomers. 8CB-CN membranes showed the better diffusion selectivities than PCH5-CN membranes due to the decreased molecular packing density in PCH-5. Correspondingly, the PCH5-CN membranes showed better sorption selectivities. Enhanced permeability selectivities for PCH5 compared to 8CB were observed for both hydroxybenzoic acid (3 %) and aminophenol isomers (29 %) due to a significant increase in sorption selectivity.

Chapter 5. Nonchiral HPLC with Circular Dichroism Detection for the Evaluation of Optical Resolution in Chiral Liquid Crystalline Membranes

NOTE: The contents of this section have been accepted for publication in the Journal of Membrane Science.

5.1 Chapter Summary

Novel porous membranes for optical resolution consisting of cholesteric liquid crystalline (LC) phases (mixtures of 4-pentyl-4'-cyanobiphenyl – 5CB – and cholesteryl oleyl carbonate – COC) impregnated in porous cellulose nitrate supports were prepared, and their permeability and selectivity for 1-phenylethanol were studied. The 5CB/COC membranes exhibited 1-phenylethanol enantiomer selectivities between 1.02 (isotropic phase) and 1.27 (cholesteric phase), and increased permeability and stability of operation compared to other sorption enantioselective membranes. Significantly decreased activation energies for diffusion were observed at temperatures above the cholesteric-isotropic phase transition, indicating reduced interactions between diffusing molecules and the LC-coated pore walls in the absence of an ordered helical LC phase. Higher activation energy for permeation was observed for S-1-phenylethanol than R-1-phenylethanol, consistent with increased interactions between the S-enantiomer and the cholesteric LC phase. Membranes produced with the undoped nematic phase of 5CB exhibited higher permeabilities than the 5CB/COC membranes and no chiral selectivity.

The feasibility of using circular dichroism (CD) detection in combination with non-chiral HPLC separation (non-chiral HPLC-CD) to monitor the concentrations and ratios of enantiomers transported through enantioselective membranes was demonstrated. Non-chiral

HPLC-CD has previously been used as an assay for drug purity and to monitor enantioselective syntheses but has not previously been reported for the characterization of enantioselective separations. The non-chiral HPLC-CD system was able to determine the compositions of 1-phenylethanol enantiomers on the receiving side of the permeation cell with detection limits of 0.07 mg/ml for the CD signal and 0.005 mg/ml for the UV signal.

5.2 Introduction

Optical purity is a critical issue in various industries, most notably in the development and production of pharmaceuticals. Often, only one drug enantiomer is safe and effective, whereas the other enantiomer can be either ineffective or toxic[105]. As a result, there is an increasing need for methods to separate pure enantiomers from racemic mixtures. Conventional chiral separation techniques, such as high performance liquid chromatography (HPLC), crystallization and chiral synthesis, have disadvantages including high energy costs, lack of scalability, batch-only processing and reliance on labor intensive processes[106,107]. In contrast, membrane-based separations are promising due to their simplicity, scalability, decreased energy requirements and ability to operate continuously.

1-phenylethanol is an essential intermediate in pharmaceutical syntheses; however, the optical resolution of 1-phenylethanol is currently limited to enantioselective synthesis[108], electrochemical oxidation[109], and size-selective membrane separation via enantioselective complexation and decomplexation[110]. In the size-selective membrane separation, racemic mixture is mixed with chiral host which enantioselectively form a complex with one enantiomer. And then, the uncomplexed enantiomer permeates through a polymeric nanofiltration membrane. The complexed enantiomer is decomplexed by a decomplexing solvent and separated from the chiral host.

Herein we report on the transport of 1-phenylethanol through novel supported liquid crystal membranes (SLCMs). Chiral liquid crystalline (LC) phases were produced by doping

achiral nematic LC materials (4-cyano-4'-pentylbiphenyl – 5CB) with cholesterol based chiral dopants (cholesteryl oleyl carbonate – COC). Methods for the production of these membranes were previously developed by our laboratory for the preparation of achiral SLCMs [43]. This is the first use of cholesteric liquid crystals as the selective phase in enantiomer separation membranes. We also report the novel application of a non-chiral HPLC-Circular Dichroism technique to the characterization of enantiomer selectivity and transport in membranes.

Several analytical techniques have been employed to determine the concentrations of enantiomers in solution[111]. These include liquid chromatography, capillary electrophoresis, and circular dichroism (CD). In liquid chromatography, one specific enantiomer has a stronger affinity with a chiral column than other enantiomer, resulting in peak separations with different retention times in a chromatogram. The capillary electrophoresis technique demands chiral selector such as cyclodextrin and protein for chiral separations under an electric field.[112]

Studies of enantiomer selectivity in membrane transport applications have used chiral phase based HPLC almost exclusively[113,114]. This method is limited in application because the chiral columns are molecule specific and are only capable of separating a limited number of different enantiomeric analytes. Herein we present a quantitative analysis method for the optical resolution of enantiomeric mixtures in solution using a combination of non-chiral HPLC and CD detection. The proposed technique allows significant versatility in the different enantiomer molecules to be analyzed without the necessity of purchasing multiple expensive chiral HPLC columns.

Circular dichroism (CD) is a measure of the difference in the absorbance of right- and left-handed circularly polarized light through an enantiomeric material[115]. A CD detector (Figure 5.1) measures dichroic and UV signals at a given wavelength allowing the calculation of an anisotropy factor *g* (the ratio of the dichroic and UV signals).

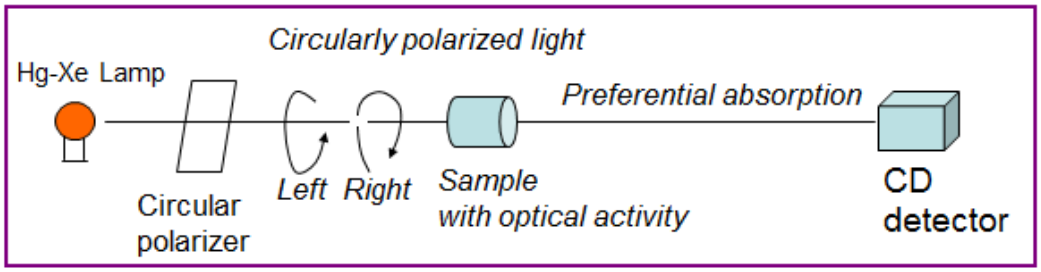

$$\theta(\text{rad cm}^{-1}) = \frac{2.303(A_L - A_R)}{4l}$$

θ; ellipticity

l; path length through the sample

A; absorption

Figure 5.1: Circular dichroism detection for an enantiomeric sample

The anisotropy factor is dependent on the optical purity of the analyte and is independent of analyte concentration. This technique has previously been used to evaluate drug purities and protein secondary structure and stability[116]. Despite extensive studies using CD, there have thus far been no reported applications of CD for the characterization of permeation in membrane materials.

5.3 Experimental

5.3.1 Materials

4-cyano-4'-pentylbiphenyl (5CB) was purchased from Wako Chemicals (Japan) and were used without further purification; 5CB exhibits phase transition temperatures of 24 ℃ (crystal-nematic) and 35 ℃ (nematic-isotropic). Cholesteryl oleyl carbonate (COC), R-1-phenylethanol and S-1-phenylethanol were purchased from Sigma Aldrich and used without further purification. Cellulose nitrate membranes (pore size 0.45 μm, porosity 70~80 %, diameter 47 mm) were used as membrane supports and were obtained from Whatman (USA). 18.2 MΩ deionized water was produced by an E-pure deionization system (Barnstead, USA). The Ultra aqueous C18 HPLC column (4.6 x 150 mm, particle size; 5 μm) was purchased

from Restek (USA). All chemicals were of reagent grade and used without further purification. HPLC grade methanol and water (Sigma Aldrich) were used as the HPLC mobile phase.

5.3.2 Equipment

Analysis of enantiomer solutions was carried out using a High Performance Liquid Chromatography (HPLC) system (Shimadzu, Japan) consisting of a LC-20AB binary pump unit, a CBM-20A communication unit, and a column oven (Figure 5.2). The injected aqueous sample, 20 µl, was separated through a non-chiral Ultra Aqueous C18 column with a methanol/water (50:50) mobile phase for better peak resolution. The column temperature was controlled at 21.8 ℃ (ambient).

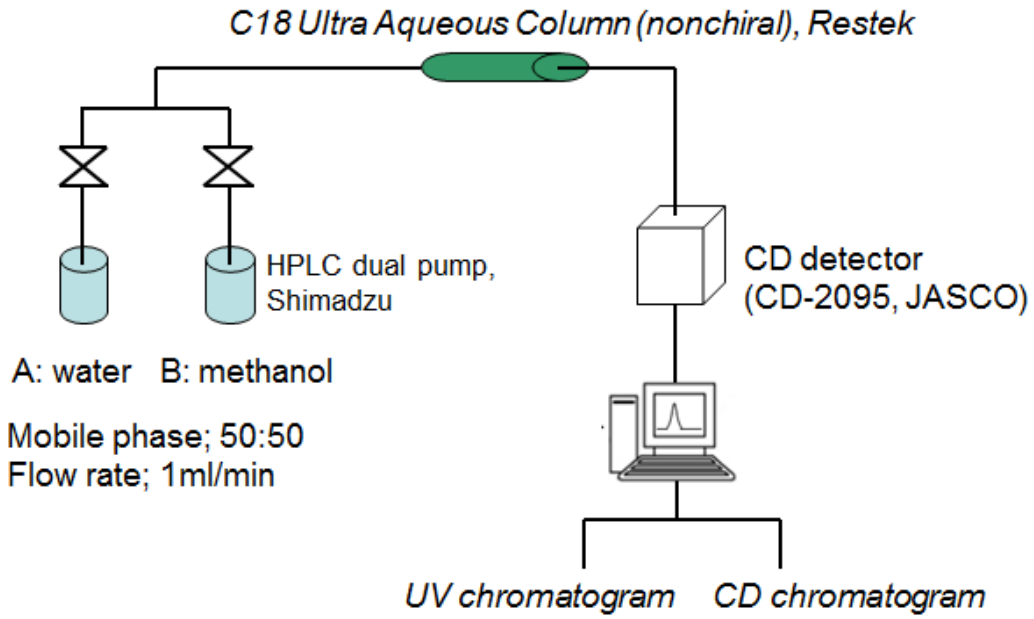

Figure 5.2: HPLC-CD detection system with a nonchiral column

Simultaneous CD and UV detection at 260 nm was performed on a CD-2095 CD detector connected to a computer via an LC-Net II/ADC communicator (Jasco, Japan). The CD spectra of enantiomeric solutes were obtained with a gain of 10 x in the wavelength

ranging from 220 to 420 nm after preheating the detector for 20 min to obtain stable CD and UV signals. The spectra and chromatograms were collected and analyzed using Spectra Manager software (Jasco).

5.3.3 Membrane Preparation

Porous supported liquid crystal membranes (SLCMs) were prepared by impregnating porous cellulose nitrate membranes with a mixture of 5CB and COC via vacuum filtration. The 5CB and COC LCs were coated on the membrane support by filtering the 23 % (w/v) LC chloroform solution through the support. The resulting membranes containing immobilized LCs were immersed in deionized water for 3 hours at room temperature and then dried under vacuum for 1 hour at 60 ℃. The membranes were trimmed to size and sandwiched between two rings of aluminum tape to provide added support. Scanning electron microcopy (SEM) images (Figure 5.3) confirmed that the SLCMs are porous and exhibit a decrease in pore diameter compared to the unfilled cellulose nitrate membrane support.

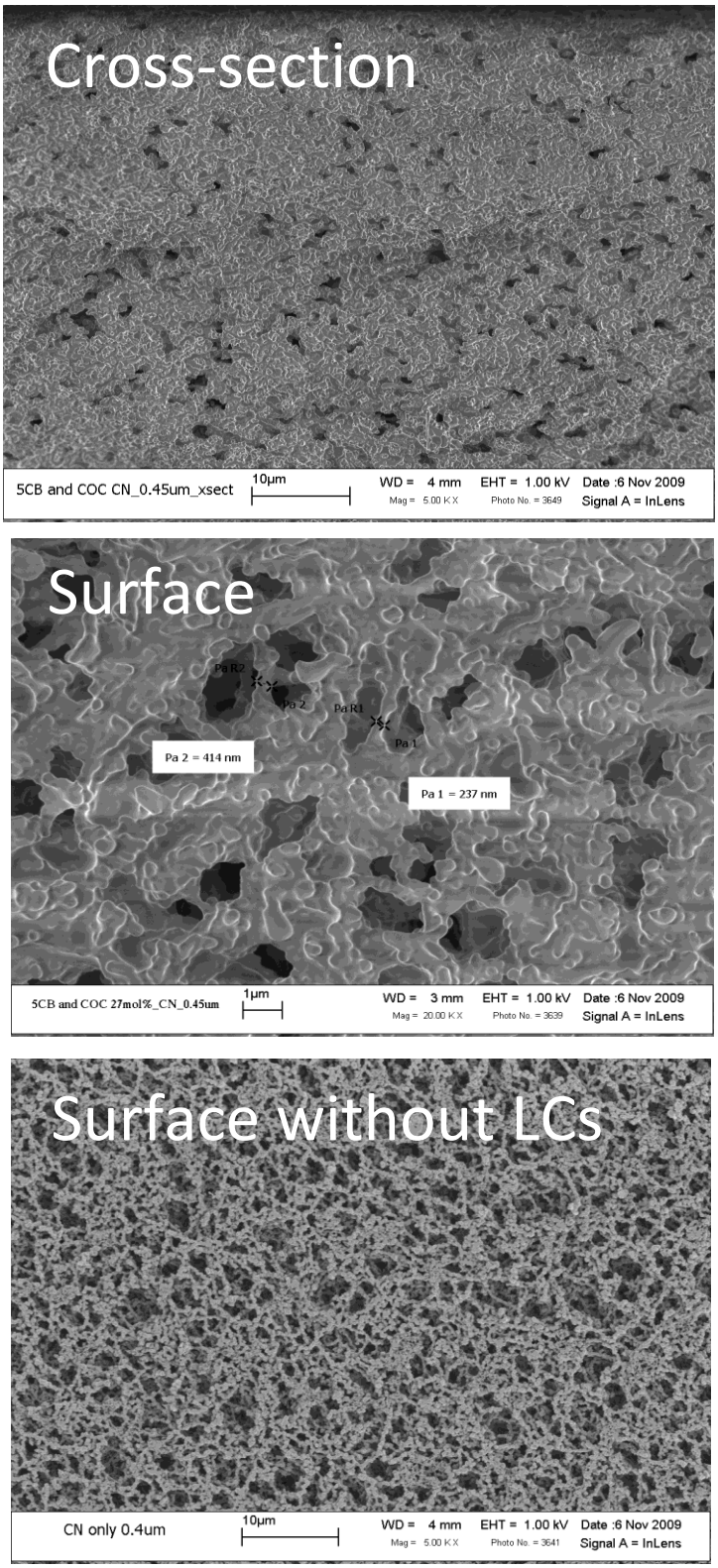

Figure 5.3: Porous supported liquid crystal membranes (SLCMs) prepared with 5CB and COC chloroform solution 27w/v % and cellulose nitrate membrane support without liquid crystals

5.3.4 Membrane Performance Parameters

The flux J across the membrane is obtained from the Fick' first law:

$$J = \frac{DH}{l}(C_A - C_B) \qquad (5.1)$$

where D is the diffusivity, H is the partition coefficient, l is the membrane thickness, C_A and C_B are the concentrations in the feed side and the receiving side, respectively.

From the mass balance in the receiving side:[49]

$$V_B \frac{dC_B}{dt} = +AJ = A\left(\frac{DH}{l}\right)(C_A - C_B) \qquad (5.2)$$

where V_B is the volume in the receiving side, A is the membrane area.

The membrane permeability, also called the permeation coefficient, is derived from eq. 5.2:[49]

$$P = (D \times H) = \frac{dC_B}{dt}\frac{V_B l}{A \times (C_A - C_B)} \qquad (5.3)$$

where P is the permeability (m^2/s), V_B is the volume of receiving side (m^3), l is the membrane thickness (m), A is the permeation area (m^2), t is the permeation time (s), and C_A and C_B are the concentrations of analyte in feed and receiving side respectively (mol/m^3).

The enantiomeric excess (*ee*) is defined as the ratio between the concentration difference and the total concentration of both enantiomers in the receiving side:[117]

$$ee = \frac{C_R - C_S}{C_R + C_S} \times 100 \qquad (5.4)$$

The optical selectivity is defined as the ratio of enantiomer fluxes and can be calculated from the relative slopes of the permeation plots (amount transported versus time) if the values of membrane thickness and feed side concentration are the same in both cases.

5.4 Results

5.4.1 Liquid Crystal Phase Transitions

Cholesteric LCs such as cholesteryl oleyl carbonate (COC) (Figure 2.11) induce a chiral nematic (cholesteric) phase in the nematic phase of 5CB in which the helical sense

depends on the handedness of chiral dopants. It is known that a mixture of 5CB and COC exhibits a left-handed cholesteric phase regardless of the concentration of chiral dopant[7,8].

To verify the existence of a cholesteric phase and to determine the LC transition temperature, a mixture of 5CB and COC (28mol %) was studied using polarized optical microscopy and a temperature-controlled hot stage. The cholesteric to isotropic transition, in which the light became extinct under crossed-polarization due to the lack of birefringence, was observed at 37 ℃. Below the transition temperature, focal conic structures were observed, which indicate the presence of a cholesteric phase in the presence of untreated substrates. It has been reported that transition temperatures for LCs in confined geometries decrease slightly or do not change.[43,57] We have previously reported that LCs embedded in cellulose nitrate (CN) supports exhibited only small variations from the bulk transition temperature.[43] As a result, we assume that the transition temperature of the 5CB-COC mixture embedded in the CN support is approximately 37 ℃.

5.4.2 Selection of CD Wavelength for the detection of 1-Phenylethanol

In order to obtain the highest sensitivity, we determined the CD wavelength at which the highest value of the anisotropy factor (g) was observed. This ensured that the lowest possible detection limits were achieved.[118] The CD and UV spectra of 1-phenylethanol were measured at stopped flow at a retention time of 7 minutes, when the CD and UV peaks appeared in chromatograms while monitoring at a wavelength of 260 nm (Figure 5.4).[119] Based on the CD and UV peaks (Figure 5.5), wavelengths of 254, 260, and 268 nm were further studied to determine the highest CD intensity and *g* values, as the CD spectra for the two enantiomers exhibit opposite signal signs (negative and positive). For 1-phenylethanol, and under the conditions of this experiment (e.g. flow rate, temperature, concentration, amount injected) it was determined that a wavelength of 260 nm resulted in the highest values for both the CD intensity and the anisotropy factor (Table 5.1).

Table 5.1: Anisotropy factor (*g*), CD and UV intensity measured at different wavelengths

Wavelength	**254 nm**	**260 nm**	**268 nm**
CD (mdeg)	-4.152	-5.00725	-1.827
UV (abs)	0.5026	0.44304	0.287
g	-8.26104	-11.302	-6.36585

Aqueous samples of S-1-phenylethanol (37 %, 0.4 mg/l) were injected for each measurement. A background spectrum was measured with the HPLC mobile phase (50 % methanol aqueous) at stopped flow. CD and UV values represent peak areas in chromatograms. *g* is a ratio of the CD and UV peak areas.

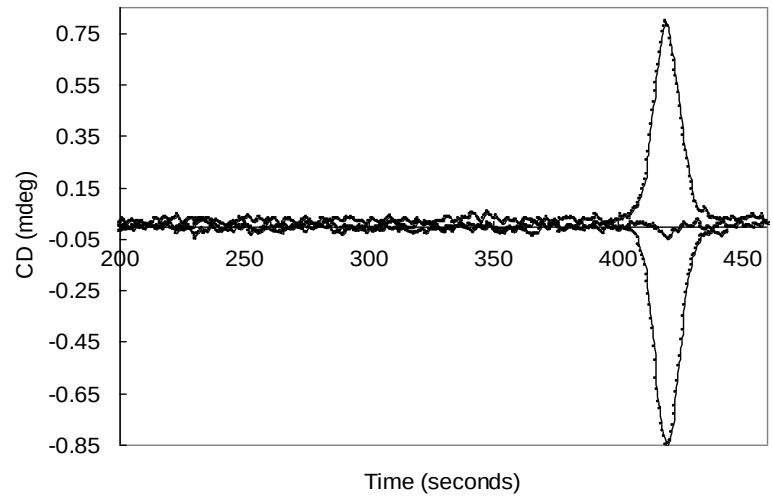

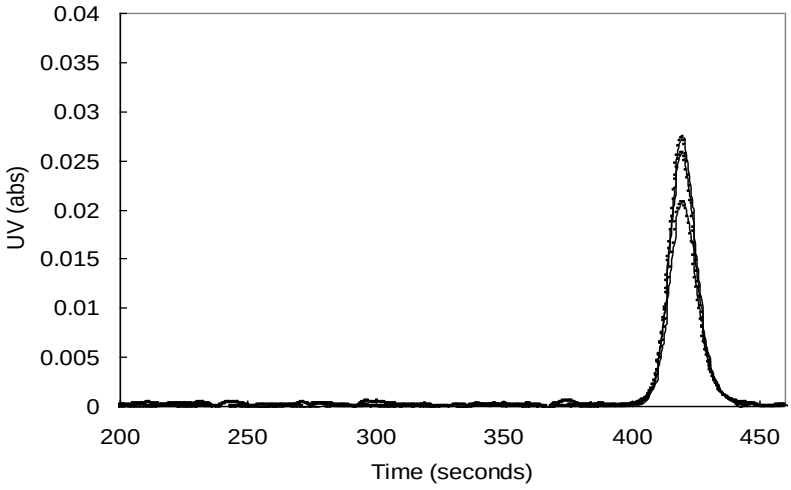

Figure 5.4: CD (top) and UV (bottom) chromatograms for pure R- and S-1-phenylethanol with the same solute concentration (0.4 mg/ml) and a racemic mixture. Positive and negative peaks represent S-1-phenylethanol excess and R-1-phenylethanol excess, respectively. For the racemic mixture, the CD peak was compensated and close to zero, but the R-, S-, and racemic mixture UV peaks exhibited similar positive intensities.

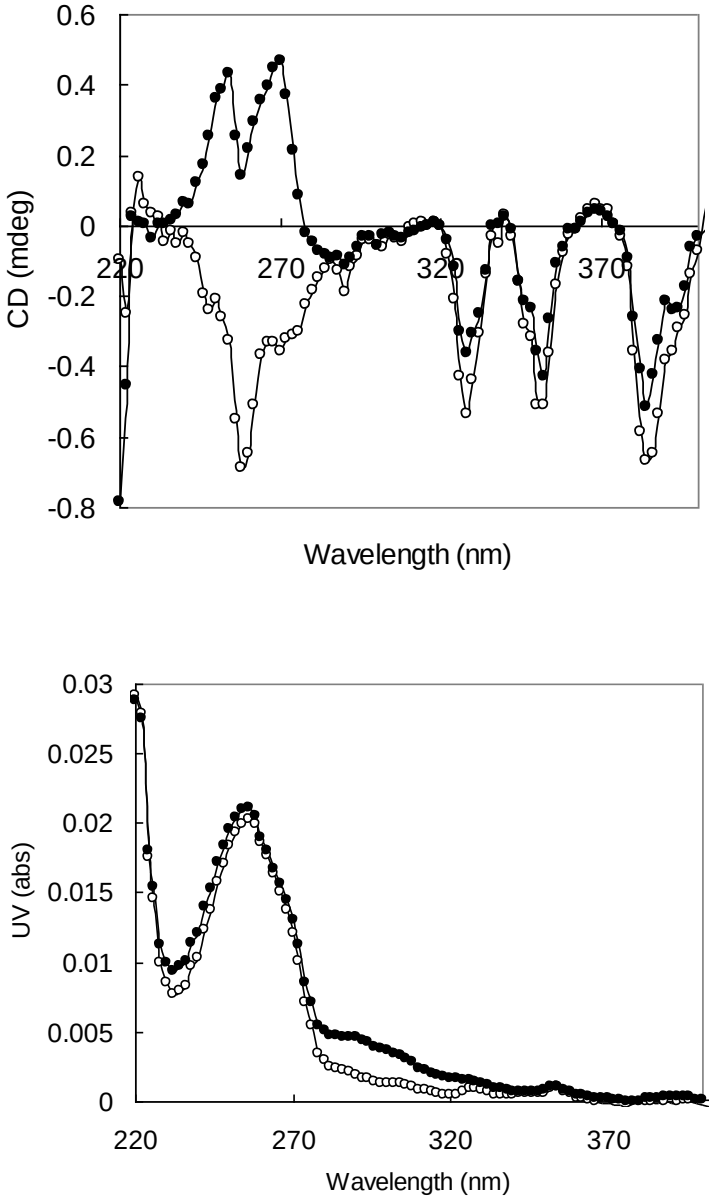

Figure 5.5: CD (top) and UV (bottom) spectra of 1-phenylethanol enantiomers (S- (●) and R- (○))

5.4.3 Dependence of anisotropy factor (*g*) on enantiomeric excess (ee) and solute concentration

We observed a linear relationship between the anisotropy factor, *g*, and the enantiomeric excess, *ee*, which enabled the calculation of *ee* at different concentrations, since *g* is independent of solute concentration. The anisotropy factors of 1-phenylethanol samples with *ee* ranging from -100 % to +100 % were investigated. Each data point was averaged over three runs (reproducible within 4 % - Table 5.2). A linear relationship was obtained regardless of sample concentration by plotting *g* against the *ee* (Figure 5.6). The enantiomer compositions for the samples separated through the membranes are obtained from the plot.

Table 5.2: G factor (*g*, a ratio of CD and UV signals) as a function of enantiomeric excess (*ee*)

ee (%)	***G***	**% S.D. (n=3)**
100	28.07	3.6
50	14.64	3.4
25	4.98	2.3
0	-4.33	2.1
-25	-11.3	2.6
-50	-17.73	3.2
-100	-36.98	3.4

g was calculated from UV and CD peak areas detected at 260 nm.

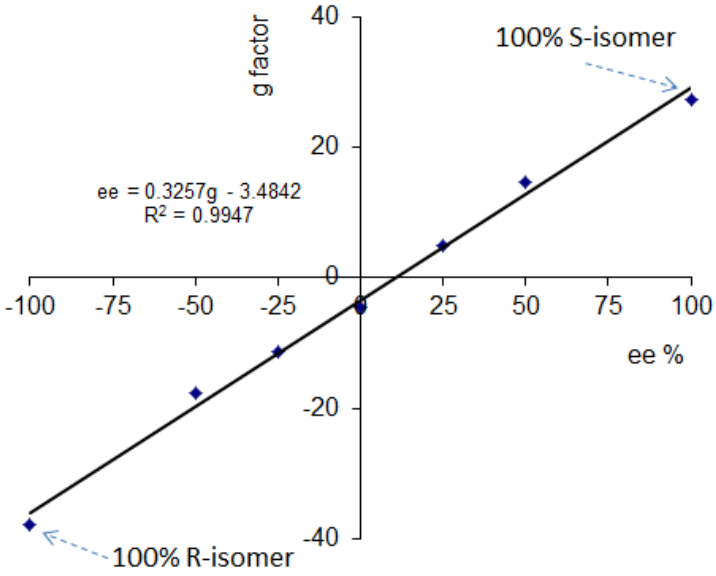

Figure 5.6: Linear dependence of the anisotropy factor (*g*) on the enantiomeric excess (*ee*) or enantiomer composition of 1-phenylethanol solutions

The independence of the anisotropy factor on solute concentration was confirmed using aqueous S-1-phenylethanol solutions of varying concentration. Figure 5.7 clearly shows that *g* is nearly independent of total solute concentration with an average value of $g = 27.3$ and a standard deviation of 2.2 %. The UV absorbance depends linearly on solute concentration according to the Beer-Lambert law over the concentration range studied.[119,120] Actual membrane permeation experiments were performed at lower concentrations, further ensuring the validity of the Beer-Lambert relationship in this case.

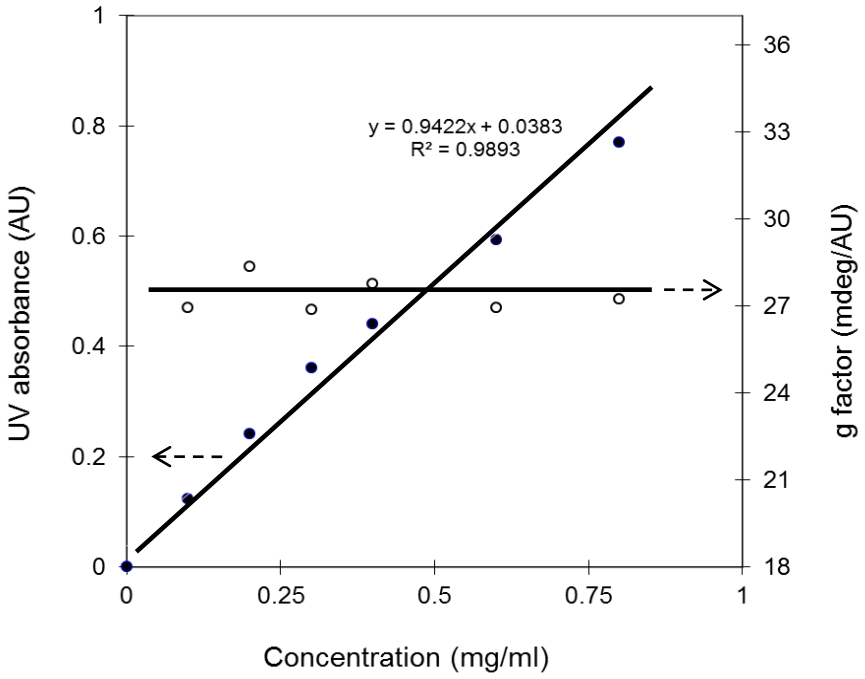

Figure 5.7: Dependence of the anisotropy factor (g – ●) and UV absorbance (○) on the concentration of a S-1-phenylethanol aqueous solution. Total UV absorbance and g were calculated from the peak areas in the chromatogram.

5.4.4 1-Phenylethanol Enantiomer Transport in 5CB/COC and pure 5CB SLCMs

5CB/COC supported liquid crystal membranes (SLCMs) produced using 23 w/v% chloroform/LC solutions with an effective permeation area of 7.55 cm^2 were placed between two glass half cells. The feed cell was filled with 150 ml of a 10 mM aqueous solution of a racemic mixture of 1-phenylethanol, and the receiving cell was filled with 150 ml of deionized water. The membrane permeation cell was immersed in a recirculating water bath to control the system temperature, and the solution in each half cell was stirred at 250 rpm to prevent concentration gradients. Transport experiments were performed in the cholesteric phase, at 33 ℃, and the isotropic phase, at 41 ℃ (Figure 5.8). During the experiments, samples from the receiving side were taken periodically and injected into the HPLC. In experiments performed at 33 ℃, the first UV peak was observed after 20 minutes permeation

time and had a measured peak area of 0.015, which corresponded to 0.02 μg 1-phenylethanol in the injected sample of 20 μl. The first CD peak was observed after 3 hours and had a measured peak area of -0.454, indicating an enantiomeric excess (ee) of 12 %. The first CD peak would appear earlier for samples with higher *ee*, as CD intensity increases with increasing *ee*. Time-transport curves of 1-phenylethanol exhibit decreased S-enantiomer transport at 33 ℃ (cholesteric phase) due to the left-handed helical structure of the LC phase. In comparison, there is little difference in R and S-isomer transport at 41 ℃ when the LC forms an isotropic phase (Figure 5.8).

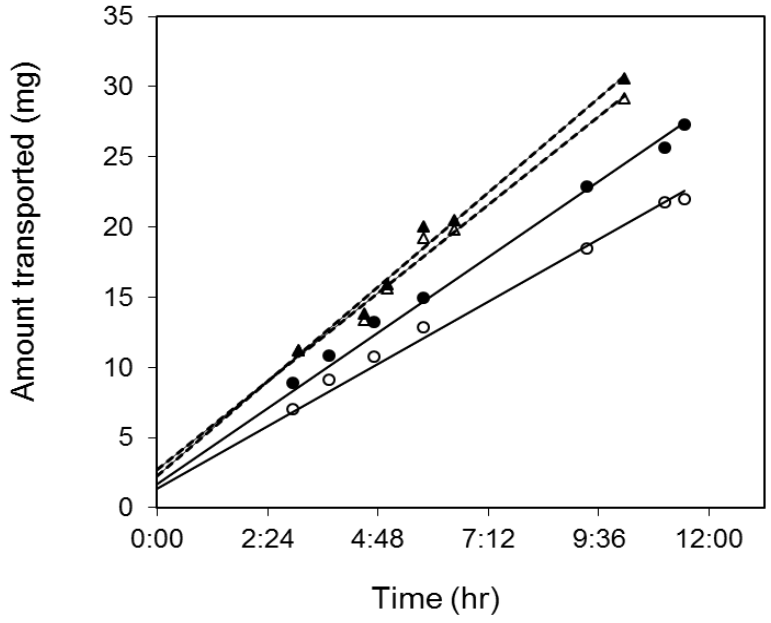

Figure 5.8: 1-phenylethanol transport through a 5CB/COC-embedded cellulose nitrate membrane in the cholesteric phase (33 ℃: solid lines; S - ○; R - ●) and the isotropic phase (41 ℃: dotted line; S - Δ; R - ▲). Data are plotted from a single permeation experiment at different time points. Averaged values from multiple experiments are presented in Table 5.3.

Permeability, enantiomeric excess, and enantioselectivity were calculated for comparison with the performance of other reported membranes, and are listed in Table 5.3. 1-

phenylethanol enantioselectivity in the cholesteric phase ranged between 1.17 and 1.27 (Figure 5.9) and is comparable to those reported for other porous enantioselective membranes (1.11~1.33)[105]. The permeability ($2.7x10^{-9}$ m^2/s or $2.3x10^{-7}$ m/s) was one to two orders of magnitude higher than has been reported for other porous membranes ($2.7x10^{-11}$ m^2/s in regenerated cellulose membranes with <1 nm pore size[121] and $2.1x10^{-10}$ m^2/s in supported cyclodextrin grafted ceramic membranes[105]) and liquid embedded non-porous membranes ($5.0x10^{-10}$ m/s in a liquid membrane containing crown ether carriers[122]).The 5CB/COC membrane separation resulted in an enantiomeric excess between 7 and 11, in the same range as those reported for other porous membranes[123]; however, no decrease in either permeability or selectivity was observed over 10 hours (Figure 5.10). Enantioselectivity decreased as temperature increased (Figure 5.9), exhibiting the expected inverse relationship between permeability and selectivity.[124] We attribute the decrease in selectivity with increasing temperature to reduced interactions, such as van der Waals and hydrogen bonding, between diffusing molecules and LC phase. Just above the isotropic phase transition temperature (37 ℃), a selectivity of 1.06 was observed, decreasing further to 1.01 at a temperature of 48 ℃. This corresponded to a decrease in enantiomeric excess to 1.7 at 41 ℃ (Figure 5.10). The 5CB/COC mixture, with left-handed chirality, exhibited increased interactions with the S-1-phenylethanol leading to slower S-enantiomer transport and, as expected, selectivity for R-1-phenylethanol.

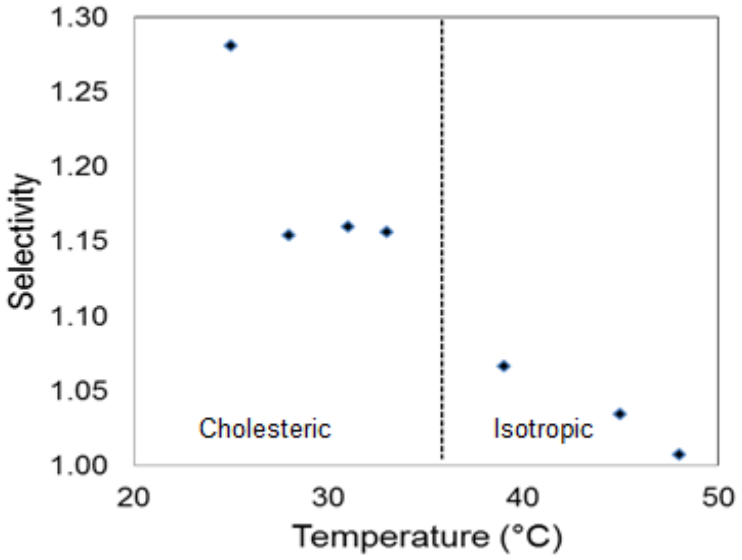

Figure 5.9: Selectivity for 1-phenylethanol enantiomers transport in 5CB/COC (28 mol%) membranes. Data are average values from two independent measurements

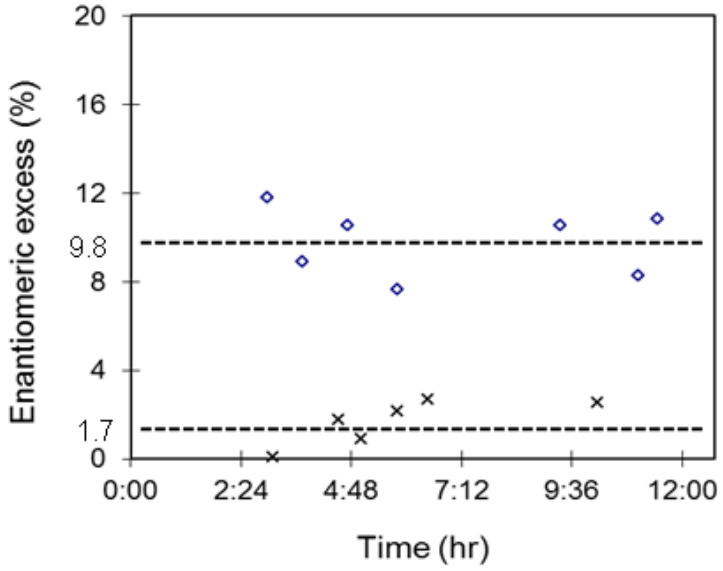

Figure 5.10: Enantiomeric excess (*ee*) for a 1-phenylethanol enantiomer separation using a 5CB/COC (28 %) embedded cellulose nitrate membrane in the cholesteric phase (◊) and the isotropic phase (x). *ee* = $(A_R-A_S)/(A_R+A_S)*100$

Table 5.3: Permeability (P) and selectivity (S) of 1-phenylethanol enantiomers in the cholesteric (33 ℃) and isotropic (41 ℃) phases of 5CB/COC (28 %) membranes and in the nematic phase (33 ℃) of 5CB membranes

	Pore size (theoretical)		P x 10^9 (m^2/s) 33 ℃	P x 10^9 (m^2/s) 41 ℃	Selectivity 33 ℃	Selectivity 41 ℃
5CB/COC	0.33 μm	R	1.46±3 %	1.84±4 %	1.17	1.07
		S	1.24±3 %	1.74±3 %		
5CB	0.33 μm	R	2.70±4 %		1.02	
		S	2.63±5 %			

5CB/COC and 5CB membranes were prepared from 23 w/v% chloroform solution and 51 mg ± 4 (n=5) of the liquid crystal mixture was impregnated in a cellulose nitrate membrane support with a diameter of 3.1 cm. The theoretical pore size was calculated assuming a cylindrical pore configuration and liquid crystals layered on the inner surface with a density of 5CB ($1g/cm^3$)[73] and 70 % porosity of cellulose nitrate membrane.

For comparison, permeability measurements were taken using an undoped pure 5CB SLCMs (Table 5.3). In the absence of chiral dopant (COC), 5CB adopts a non-chiral nematic phase. The permeabilities for the R-and S-1-phenylethanol in the pure 5CB SLCMs were 85 % and 110 % higher, respectively, than in the 5CB/COC membrane containing 28 % COC at the same temperature. The pure 5CB membrane also exhibited negligible selectivity.

5.4.5 Activation Energies for Permeation of 1-phenylethanol Enantiomers

The temperature dependence of 1-phenylethanol enantiomer transport in 5CB/COC SLCMs was determined and used to calculate the activation energy for permeation in the cholesteric and isotropic phases. The activation energy for permeation is a measure of the interaction strength between 1-phenylethanol isomers and the LC phase during permeation

through the 5CB/COC membrane, and can be calculated using an Arrhenius relation from the slope of a plot of ln(P) vs 1/T:

$$P = P_0 \exp\left(\frac{-E_a}{RT}\right) \qquad (5.5)$$

where P is the permeation coefficient (cm^2/s), R is the ideal gas constant (8.314 J/mol K), T is the temperature (K), E_a is the activation energy for permeation (kJ/mol), and P_0 is the Arrhenius constant (cm^2/s).

The Arrhenius plot for permeation of 1-phenylethanol in 5CB/COC (28 mol%) membranes is displayed in Figure 5.11. Permeabilities for R- and S-enantiomers increased with temperature, exhibiting Arrhenius-like behavior, and different slopes are observed for the R- and S-enantiomers in both the cholesteric and isotropic phases. The activation energies for permeation are significantly lower in the isotropic phase than in the cholesteric phase (Table 5.4). The increased activation energy for permeation in the cholesteric phase is due to increased interactions between the diffusing enantiomer molecules and the helical LC phase coating the pore walls. In contrast, the lack of an ordered helical structure results in lower activation energies in the isotropic phase. S-1-phenylethanol exhibited higher activation energies than R-1-phenylethanol in both the isotropic and cholesteric phases indicating that the S-enantiomer interacts more strongly with the 5CB/COC phases. As a result, lower permeabilities were observed for the S-enantiomer through 5CB/COC membranes. The higher activation energies for permeation observed for 1-phenylethanol enantiomers in 5CB/COC SLCMs suggest that the ordered cholesteric liquid crystal phase is necessary to achieve higher enantioselectivities.

Table 5.4: Activation Energies for 1-phenylethanol enantiomer transport in 5CB/COC (28 mol%) membranes

	Activation Energy (kJ/mol)	
	R-enantiomer	S-enantiomer
Cholesteric	58.0 ± 4.2	67.9 ± 5.5
Isotropic	10.1 ± 1.7	15.3 ± 1.5

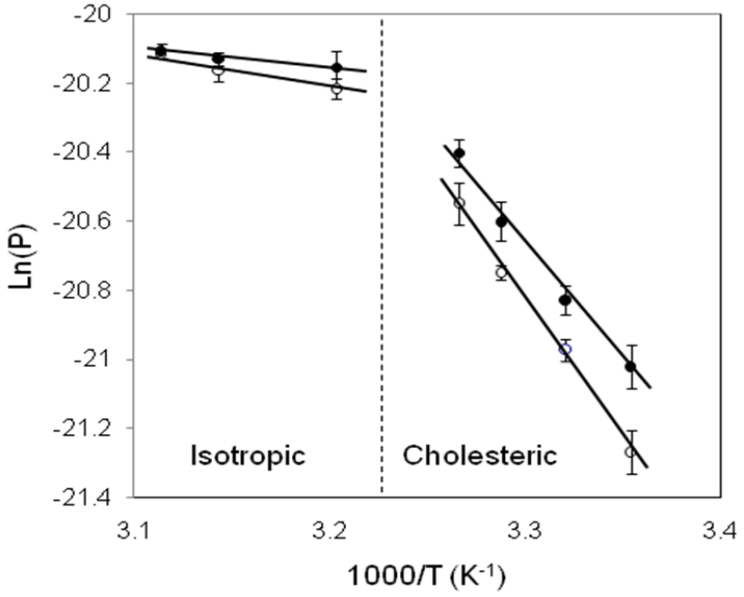

Figure 5.11: Arrhenius plot of permeability for 1-phenylethanol enantiomer transport in 5CB/COC (28 mol%) membranes. White and black symbols represent S-enantiomer and R-enantiomer, respectively. Error bars represent one standard deviation determined from two independent measurements.

5.5 Conclusions

Preliminary results for the stereoselective transport of 1-phenylethanol enantiomers through novel enantioselective membranes based on cholesteric liquid crystals were obtained using non-chiral phase based HPLC combined with circular dichroism and UV-VIS spectrometry. The enantioselective membranes were composed of cellulose nitrate supports impregnated with 5CB/COC LC mixtures. S-1-phenylethanol exhibited slower permeation

than R-1-phenylethanol, likely due to favorable interactions between the left-handed cholesteric LC phase and the left-handed S-1-phenylethanol molecules. A similar selective adsorption mechanism of enantiomers has been reported previously for chromatographic separations using cholesteric LC phases.[39,6] Significantly higher activation energies for permeation were observed in the cholesteric phase, indicating increased interactions between diffusing molecules and the helically ordered LC phase. The higher activation energies observed for S-enantiomers compared to R-enantiomers are consistent with the lower permeabilities observed for the S-enantiomers. As expected, the enantioselectivity exhibited an inverse relationship with permeability, and selectivities as high as 1.27 were obtained in the cholesteric phase at room temperature. Selectivities decreased rapidly above the isotropic phase transition due to the absence of an ordered helical phase. In comparison, 5CB membranes without chiral dopant exhibited no enantioselectivity in either the nematic or isotropic phases. It is clear that the presence of a helically ordered chiral LC phase is necessary to achieve significant enantioselectivity in these systems.

The development of a combined nonchiral HPLC and CD detection method (HPLC-CD) allowed us to simultaneously determine the optical purity and the concentration of enantiomers permeating through chiral resolution membranes using the anisotropy factor (*g*) and the UV intensity. To our knowledge, this is the first application of nonchiral HPLC with CD detection to quantify enantiomer transport through membranes. The HPLC-CD method is more versatile than HPLC detection methods that rely on chiral stationary phases because it does not require the use of specific chiral columns for the resolution of different enantiomers. The large spectral range (220~420 nm)[118] of the CD signal enables the detection of a wide variety of enantiomer molecules, and the precision and sensitivity of the nonchiral HPLC-CD detector has been shown to be comparable to chiral HPLC detection systems.[115,118]

Chapter 6. Enantioselective Separations using Chirally Doped Liquid Crystalline Membranes

6.1 Introduction

Enantioselective membranes are classified into dense (or nonporous) and porous membranes (Figure 6.1).[123] In the dense membranes such as liquid phase membranes, one enantiomer is selectively soluble by a complexation with chiral selectors such as crown ether, enzyme[113], antibody, and chiral side group[125]. The dense membranes show high selectivity, but low stability which limits its applications to a large scale production. On the other hand, the porous membranes perform enantiomer separations based on selective adsorption between enantiomer and pore surface with chiral selectors such as cyclo dextrin[105] and DNA[126].

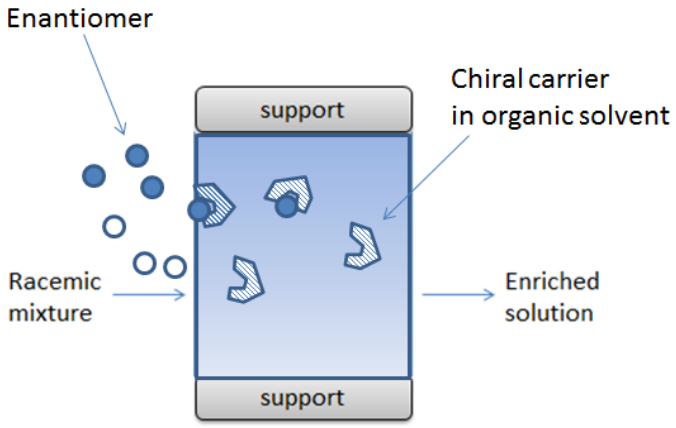

(a) Dense membrane

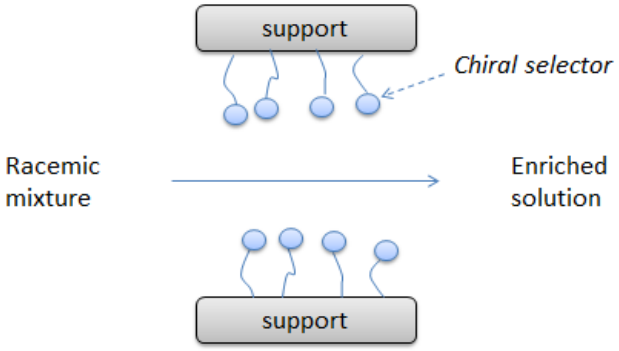

(b) Porous membrane

Figure 6.1: Enantioselective separations through dense and porous membranes in liquid phase

However, the chiral selectors such as enzyme and antibody have limited life time and the cyclo dextrin embedded membranes require a decomplexation process due to its strong interaction with the enantiomer by hydrophobic, electrostatic, and hydrogen bonding interactions[123]. Thus, new membrane materials for enantiomer separations are still required.

Small molecule thermotropic liquid crystals (LCs) exhibit self-assembled orientations such as smectic, nematic, and isotropic phase depending on temperature changes. With an addition of chiral dopants, LC molecules in the nematic phase oriented along one direction are reoriented in a helical way known as cholesteric liquid crystal (ChLC) phase. A ChLC phase has been widely studied in display application due to its optical activity showing different colors depending on helical pitch changes controlled by chiral dopants.[46,7] However, the separation applications of ChLC phase have been little known in gas chromatographic separation technique[5,6], even no membrane separation. The enantioselective separation abilities of ChLC phase have been reported[5,6] in chromatographic separations. The ChLC phase was applied as a stationary phase in chromatographic separations, but the cholesteric phase was limited to high temperatures, 120~175 ^{o}C, which does not allow enantiomer separations in the aqueous phase.

Herein we report a novel ChLC embedded polymer membranes, which features transport phenomena of membrane chromatography (Figure 6.2) through the membrane pores. In porous membranes, the transport of solutes take place through the membrane pores and is dependent on different types of interactions such as ion exchange, affinity, hydrophobic and hydrophilic interactions.[127,128,129] The ChLC phase induced by adding cholesterol-based chiral dopants in nematic LC phase exhibits left-handed chirality[7,8] at low temperature below 40 ℃ and left-handed enantiomers transport slower than right-handed enantiomers due to the interactions between the left-handed enantiomer and the left-handed chiral phase in the membrane. Membrane chromatography separations[127,128,129] not only overcome pressure drop and slow process over conventional chromatography separations, but

provide high permeability compared to nonporous membrane separations. This can lead to membrane separations suitable for large-scale enantiomer production.[124]

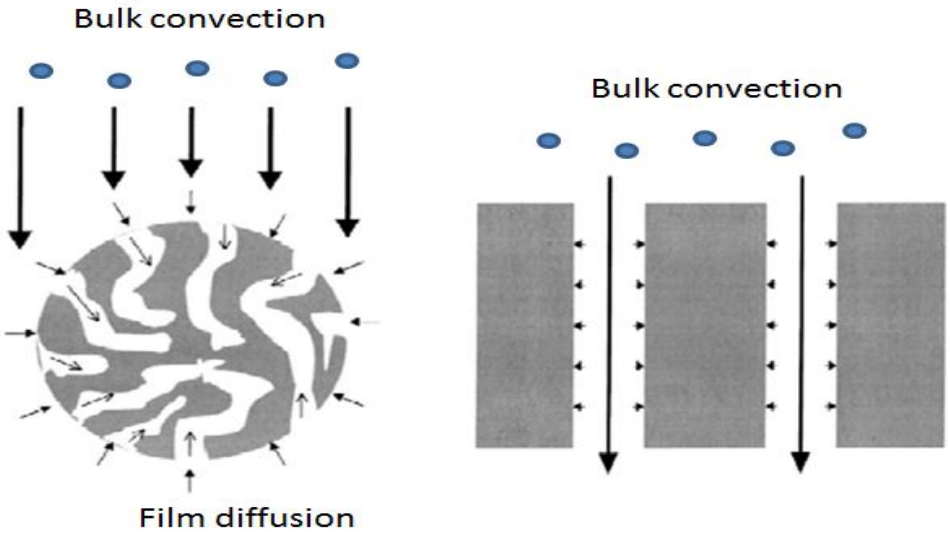

(a) Packed bed chromatography (b) Membrane chromatography

Figure 6.2: Transport in packed bed chromatography and membrane chromatography[128]

6.2 Experimental

6.2.1 Materials

4-cyano-4'-pentylbiphenyl (5CB) was purchased from Wako Chemicals (Japan), and exhibits phase transition temperatures of 24 °C (crystal-nematic) and 35 °C (nematic-isotropic). Cholesteryl nonanoate (CN), cholesteryl oleyl carbonate (COC) (Figure 2.11), R- and S-1-phenylethanol isomers were purchased from Sigma Aldrich. Cellulose nitrate membranes (pore size 0.45 μm, porosity 70~80 %, diameter 47 mm) for use as membrane supports were obtained from Whatman (USA). 18.2 MΩ deionized water was produced by an E-pure deionization system (Barnstead, USA). A nonchiral C18 HPLC column (4.6 x 150 mm, particle size; 5 μm) was purchased from Restek (USA). All chemicals were of reagent

grade and used without further purification. HPLC grade methanol and water (Sigma Aldrich) were used as the HPLC mobile phase.

6.2.2 Equipment

Analysis of enantiomer solutions was carried out using a high performance liquid chromatography (HPLC) system (Shimadzu, Japan) consisting of a LC-20AB binary pump unit, a CBM-20A communication unit, and circular dichroism (CD) detector (CD-2095, Jasco). The CD detector enables to determine enantiomer compositions by measuring CD and UV signals simultaneously without the use of expensive chiral column.[115]

The aqueous sample, 20 μl, was injected into the HPLC-CD detection system with a methanol/water (50:50) mobile phase for 1-phenylethanol isomer aqueous samples monitored at 260 nm. The column temperature was controlled at 21.8 °C (ambient). CD spectra of enantiomeric solutes were obtained with a gain of 10 x in the wavelength ranging from 220 to 420 nm after preheating the detector for 20 min to obtain stable CD and UV signals. The spectra and chromatograms were collected and analyzed using Spectra Manager software (Jasco). Enantiomer compositions were obtained from a g-factor (a ratio of CD to UV) and enantiomer concentrations were obtained from UV intensity.

6.2.3 Membrane Preparation

Porous supported liquid crystal membranes (SLCMs) were prepared by impregnating porous cellulose nitrate membranes with a mixture of 5CB and chiral dopants, CN or COC, via vacuum filtration. The LC mixtures were coated on the membrane support by filtering LC in chloroform solution with different concentrations through the support in order to control membrane pore size. The resulting membranes containing immobilized LCs were dried

overnight at a room temperature. The membranes were trimmed to size and sandwiched between two rings of aluminum tape to provide added support.

6.3 Results and Discussion

The membrane permeation behavior of two chiral solutes, phenylglycine and 1-phenylethanol, was examined. These were selected based on their solubility in the cholesteric LC materials: preliminary experiments showed that phenylglycine is insoluble in the LC materials, while 1-phenylethanol exhibits limited solubility. We expected that there would be transport of the phenylglycine only in the case of a porous LC membrane. The 1-phenylethanol should exhibit transport through non-porous LC membranes based on a sorption-diffusion mechanism. The phenylglycine is permeated through the membrane pores by interactions with LC surface and the 1-phenylethanol is permeated by absorption into the LC phase and diffusion through LC phase.

6.3.1 Phenylglycine Enantiomer Separations and Porous Liquid Crystal Membrane

Nonporous and the porous membranes were prepared using cellulose nitrate membranes with average pore sizes of 0.2 μm and 0.45 μm, respectively. Theoretical pore diameters (Table 6.1) were calculated assuming uniform coating of cylindrical pores in the cellulose nitrate membrane. The theoretical pore size decreases as the amount of impregnated LC increases. In the case of the nonporous membranes made using the 0.2 μm support, 95 % of the available pore volume was filled with LC.

The embedded amount of LC mixture of 5CB and CN (17 mol%) in cellulose nitrate membranes (0.45 μm pore) was dependent on the chloroform solution concentration (Figure 6.3). The amount of LC deposited in the cellulose nitrate membrane increased with increasing LC concentration in the chloroform solution, reaching a plateau after 25 %w/v concentration. In membrane separation experiments using phenylglycine racemic mixtures through

membranes, phenylglycine was transported through the porous 5CB and CN (17 mol%) embedded membranes (0.45 μm pore, less than 70 mg LC embedded,) but was not transported through the nonporous LC membranes (0.2 μm pore, more than 95 mg LC embedded.) The lack of phenylglycine transport confirms that the 0.2 μm pore cellulose nitrate supports embedded with more than 95 mg LC are non-porous, and that phenylglycine exhibits negligible solubility in the LC mixture. In addition, under a cross-polarization the birefringence was not observed in the porous LC membranes (0.45 μm; below 70 mg) as the pores still have voids due to less LC amount, but observed in the nonporous LC membranes (0.2 μm; above 96 mg), which suggest that the LC membranes with the LC amount below 70 mg have the transport channel (pore).

Table 6.1: Phenylglycine transport through 5CB and CN (17 mol%) membrane at 37 ℃

Support Pore (μm)	LC (mg)	$V_{occupied}$ (%)	Membrane Pore, μm (theoretical)	Permeability (m^2/s)	Selectivity
0.2	96	95	0	0	0
0.45	70	68	0.27	4.36E-10	1.19
	65	49	0.28		
	40	39	0.36	9.78E-10	1.15
	25	24	0.39		

Based on the density of 5CB (1 g/cm^3)[73], the occupied LC volume fraction of the cellulose nitrate membrane was obtained.

Permeability increased and selectivity decreased with increasing theoretical pore size in the LC embedded membrane (Figure 6.4) due to an increased chance of interaction between the enantiomers and LC phase in the narrower pores, as depicted in Figure 6.5. The 5CB and CN membranes showed selectivity towards R-phenylglycine due to increased interaction between lefthanded L-phenylglycine and the lefthanded cholesteric LC surface.

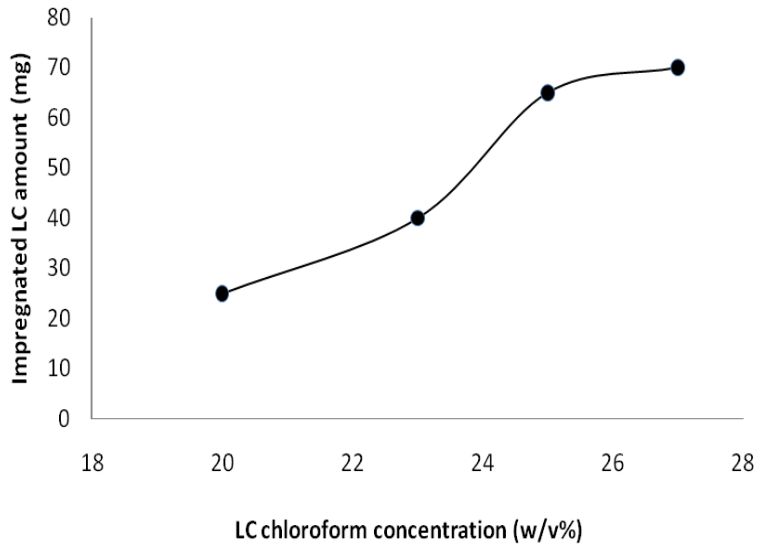

Figure 6.3: LC chloroform solution concentration vs. impregnated LC amount

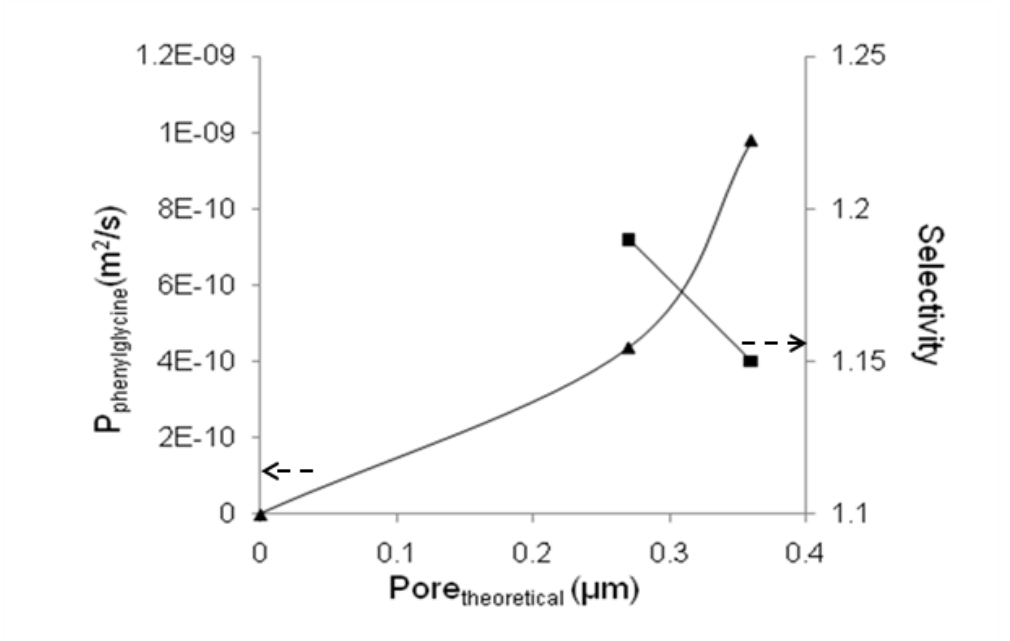

Figure 6.4: Phenylglycine permeability(▲) and selectivity(■) in different theoretical pore size of LC embedded membranes (0.45 μm). Membrane with pore size of zero was made from cellolose nitrate membrane of 0.2 μm pore.

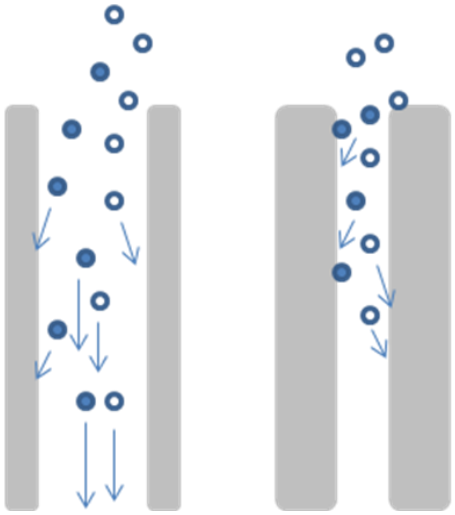

(a) 0.36 µm pore (b) 0.27 µm pore

Figure 6.5: Schematic representation of R and S-isomers interactions with LC phase in pores for (a) 0.36 µm pore size membrane and (b) 0.27 µm pore size membrane

6.3.2 1-phenylethanol Enantiomer Separation with Porous LC Membrane

Porous and non-porous LC membranes were produced using a mixture of 5CB and 17 mol% CN. Porosity was verified by phenylglycine transport experiments and polarized optical microscopy. The transport of a racemic mixture of 1-phenylethanol enantiomer was examined in order to study enantioselective transport in the chiral nematic LC phase. In contrast to phenylglycine, 1-phenylethanol enantiomers permeated through the nonporous LC membrane (0.2 µm pore, more than 96 mg LC embedded) with a theoretical pore size of zero (Table 6.2) by a sorption-diffusion mechanism. This was expected, as 1-phenylethanol enantiomers are soluble in the LC materials based their relatively lower water solubility due to the lower number of hydrogen donors available to interact with water molecules. However, 1-phenylethanol enantiomers exhibited no enantioselectivity in the non-porous membranes (selectivity 1.01). This is in disagreement with the theoretical predictions of Frezzato et al.[130,131], who predicted faster diffusion of one enantiomer in a chiral matrix. In contrast, 1-phenylethanol exhibited enantiselectivity in porous LC membranes with less than 70 mg LC

embedded, leading to an excess of R-1-phenylethanol due to the interactions between the lefthanded S-1-phenylethanol and the lefthanded cholesteric phase coating the pore walls. In the same way as phenylglycine, 1-phenylethanol permeability was increased and selectivity was decreased with increasing pore size of the porous LC membrane due to the decreased chance of interactions between enantiomer and LC phase in the larger pore.

Table 6.2: 1-phenylethanol transport through 5CB and CN (17 mol%) membrane at 37 ℃

Support Pore (μm)	LC (mg)	$V_{occupied}$ (%)	Membrane Pore, μm (theoretical)	Permeability (m^2/s)	Selectivity
0.2	96	95	0	2.74E-09	1.01
0.45	70	68	0.27	2.95E-09	1.17
	65	49	0.28		
	40	39	0.36	3.67E-09	1.14
	25	24	0.39		

6.3.3 1-phenylethanol Transport in the Nematic, Cholesteric and Isotropic Phases

1-phenylethanol enantiomer separations were examined in different LC phases. LC membranes showed an optical resolution with a selectivity of 1.17 (Table 6.3 and Figure 6.6) in the cholesteric phase, but showed a decreased selectivity of 1.08 (Figure 6.7) in the isotropic phase where only molecular chirality of CN exists and it is in a higher temperature than the cholesteric phase. The 5CB/COC membranes also showed the lower selectivity in the isotropic phase than in the cholesteric phase. Rod-like 5CB LC membrane with no chiral dopant showed no selectivity and higher permeability than 5CB/CN membrane even at a lower temperature due to the absence of phase chirality and molecular chirality (Table 6.3 and Figure 6.6). Therefore, the cholesteric LC phase induced by chiral dopants in the nematic phase resulted in interactions between lefthanded enantiomer and lefthanded LC phase.

Additionally, the higher temperatures in the isotropic phase weaken the interactions such as hydrogen bond and van der Waals between solutes and LC.

A chiral recognition occurs by hydrogen bonding interactions in chiral selectors such as crown ether[132] and cyclo dextrin[105,121]. In order to identify the chiral recognition interactions in the LC mixtures, we employed cholesteryl chloride (CC) chiral dopant which has no hydrogen bond acceptor. The 5CB/CC membrane showed a decreased selectivity of 1.10 in the cholesteric phase which is lower than 5CB/CN membrane with two hydrogen acceptors in CN. In addition, the higher permeability and less interaction between enantiomers and LC phase was observed in 5CB/CC membranes due to the absence of H bond acceptor of LC phase despite the lower temperature than the 5CB/CN membrane (Table 6.3).

Table 6.3: Permeability and selectivity in different phases of LC membranes

25 w/v%	P (m^2/s)	Selectivity	Phase
5CB	3.55E-09	1.03	Nematic (30 ℃)
5CB/CN	2.57E-09	1.17	Cholesteric (37 ℃)
	4.60E-09	1.08	Isotropic (46 ℃)
5CB/COC	2.11E-09	1.17	Cholesteric (31 ℃)
	2.59E-09	1.07	Isotropic (41 ℃)
5CB/CC	3.04E-09	1.1	Cholesteric (33 ℃)

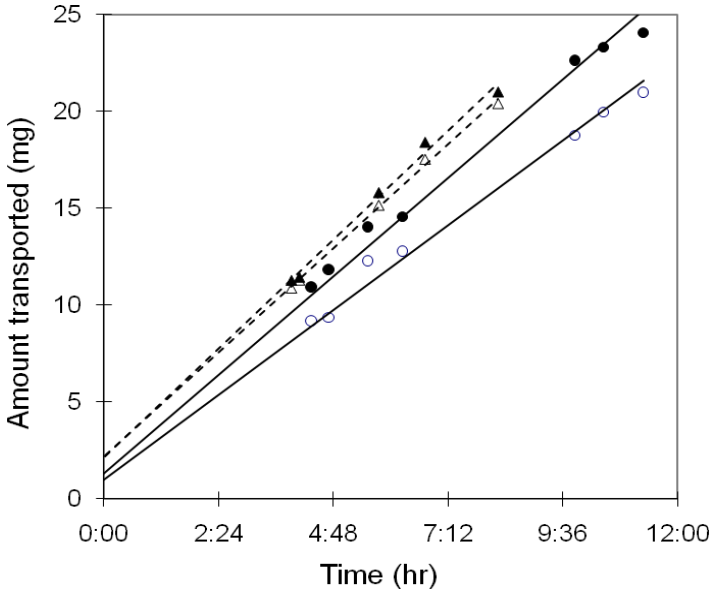

Figure 6.6: 1-phenylethanol transport through 5CB and CN (17 mol%) embedded cellulose nitrate membrane in the cholesteric (solid line) and nematic phase (dashed line)

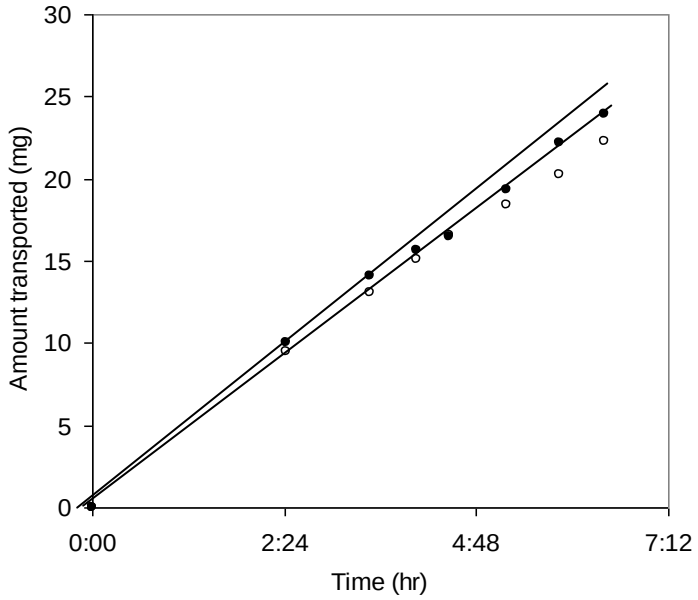

Figure 6.7: 1-phenylethanol transport through 5CB and CN (17 mol%) embedded cellulose nitrate membrane at 46 ℃ (isotropic phase) made from 25 w/v% solution

6.3.4 Activation Energy of 1-phenylethanol and phenylglycine enantiomers for Permeation

To study the selective affinity between LC phase and enantiomer, the activation energy for permeation was investigated. The activation energy was obtained from the slope of Arrhenius plot[43] (Figure 6.8) for transport experiments in different temperatures.

$$P = P_0 \exp\left(\frac{-E_a}{RT}\right) \qquad (6.1)$$

where P is permeation coefficient or permeability (cm^2/s), R is ideal gas constant (8.314 J/mol·K), T is temperature (K), E_a is activation energy for diffusion (kJ/mol), and P_0 is Arrhenius constant (cm^2/s).

The permeability was linearly increased with a temperature increase and different slopes were observed for 1-phenylethanol and phenylglycine enantiomers. The lefthanded enantiomers of 1-phenylethanol and phenylglycine showed the higher activation energies of 37.6 and 48.8 kJ/mol than 32.6 and 44.6 kJ/mol of the righthanded enantiomers, respectively. Therefore, lefthanded LC phase has more interactions with lefthanded enantiomer than righthanded enantiomer as a result of more diffusion barrier.

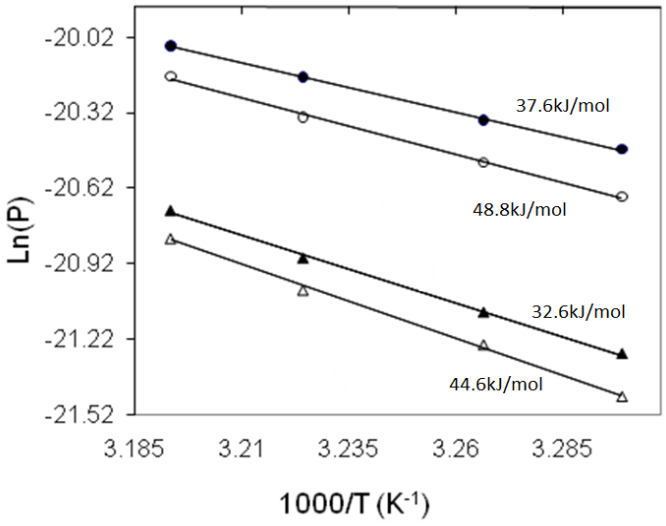

Figure 6.8: Arrehenius plot of permeability for R(●) and S(○) 1-phenylethanol and R(▲) and L(Δ) phenylglycine through 5CB and CN (17 mol%) membrane prepared from 25 w/v% LC chloroform solution

The higher permeabilities were observed in 1-phenylethanol enantiomers compared to phenylglycine enantiomers due to the smaller molecular weight and size of the 1-phenylethanol. The selectivity was decreased with a temperature increase due to reduced interactions such as hydrogen bond and van der Waals and faster diffusion in membrane pores (Figure 6.9). Additionally, the more number of hydrogen bond donor in phenylglycine enantiomers did not result in enhanced enantiomer selectivity.

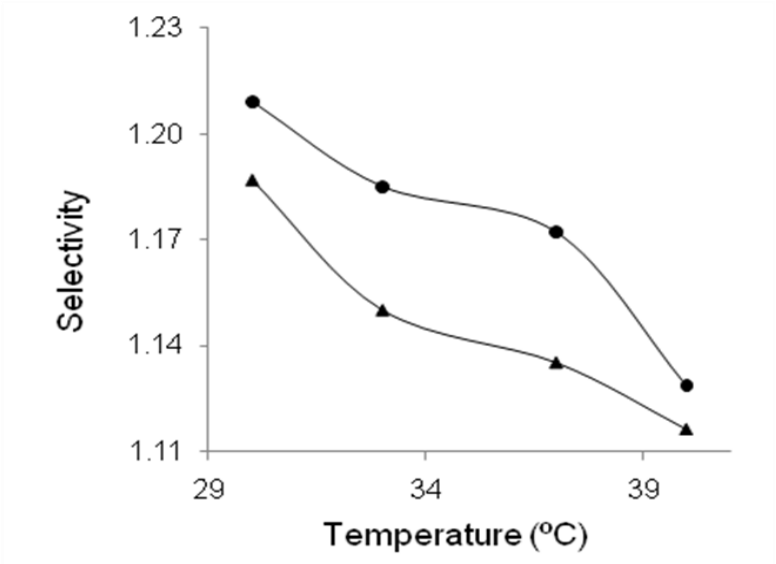

Figure 6.9: Selectivity for 1-phenylethanol(●) and phenylglycine(▲) enantiomers in different temperatures

6.3.5 Selectivity Dependence on Chiral Dopant Composition

The selectivity of 1-phenylethanol separation was investigated at different compositions of chiral dopant with membranes made from 23 w/v% and 25 w/v%. The selectivity was less than 1.1 at 5 mol% CN and increased up to 17 %, and then the graph reached at a plateau showing selectivities of 1.18 and 1.15 at 30 % CN (Figure 6.10). The membranes (0.28 μm theoretical pore) made with 25 w/v% LC solution (65 mg LC at Figure 6.3) exhibited higher selectivity at every CN concentration than the membranes (0.36 μm theoretical pore) made with 23 w/v% LC solution (40 mg LC at Figure 6.3) due to an

increased chance to interact between enantiomers and LC phase in the pores (Figure 6.5). The membranes with 0.28 μm theoretical pore showed lower permeabilities than the membranes with 0.36 μm theoretical pore due to the narrow diffusion path and increased interaction with LC phase.

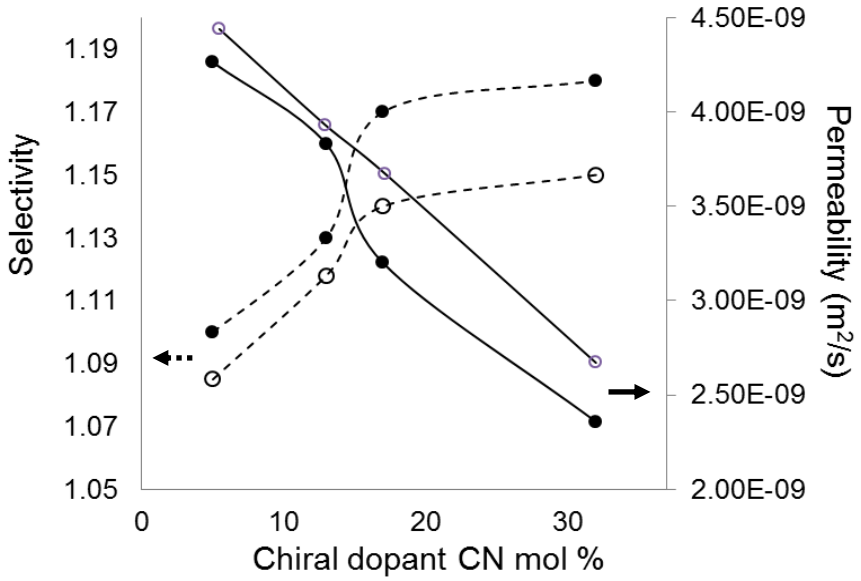

Figure 6.10: Selectivity (dashed lines) and permeability (solid lines) for 1-phenylethanol vs. chiral dopant composition in cholesteric phase (35 ℃). 0.28 μm pore membrane (●); 0.36 μm pore membrane (○)

6.4 Conclusions

We have applied chiral liquid crystalline (LC) materials in enantioselective membrane separations using supported LC membranes (SLCM). The final SLCM pore size could be adjusted by varying the concentration of the LC chloroform solution used for impregnation. Phenlyglycine was transported through porous SLCMs, but did not permeate through nonporous SLCMs due to the negligible solubility of the phenylglycine in the LC materials. In contrast, 1-phenylethanol was readily transported through the nonporous SLCMs, but

exhibited negligible enantioselectivity. The porous SLCMs exhibited enantioselective behavior for 1-phenylethanol similar to that observed for phenylglycine. Enantioselectivity in the porous SLCMs resulted from interactions between the lefthanded L-phenylglycine and L-1-phenylethanol and the lefthanded cholesteric LC surface which led to slower diffusion for the L- enantiomers than the corresponding D- enantiomers. The helical structure preferentially adsorbs the enantiomers fitting the handedness of its helical structure[133] due to interactions between the helical structure (phase chirality) in the cholesteric phase and the enantiomer (molecular chirality).

Studies of enantioselectivity using chiral dopants with different numbers of hydrogen bonding sites indicated that hydrogen bonding interactions enhance enantioselectivity. The 5CB/cholesteryl chloride (CC) membrane exhibited lower enantioselectivity due to the absence of hydrogen bonding interactions between the enantiomer and chiral dopant. The 5CB/CC membranes also exhibited higher permeability compared to the 5CB/CN or 5CB/COC membranes with the same theoretical pore size. Transport studies at temperatures above and below the LC-isotropic phase transitions indicated that the cholesteric phase exhibits higher selectivity and lower permeability than the isotropic phase, likely due to increased interactions between the enantiomers and the helically ordered cholesteric phase.

Enantioselectivities increased with decreasing theoretical pore size for both phenylglycine and 1-phenylethanol enantiomers due to the increased chance of interactions between the enantiomer and the LC surface. According to the activation energy for permeation, both enantiomers exhibited higher activation energies for the lefthanded 1-phenylethanol and phenylglycine enantiomers, indicating slower diffusion for the lefthanded enantiomers due to stronger interactions between the lefthanded enantiomer and the lefthanded LC phase. Enantioselectivity increased with chiral dopant concentration up to 17mol%, after which a plateau was reached; permeability decreased with increasing chiral dopant concentration over the whole range of compositions studied.

Chapter 7. Study on Block Copolymer Phase Separation during Solvent Drying

7.1 Introduction

The equilibrium phase separation behavior and kinetics of block copolymer melts are well established. The phase behavior of the copolymer depends on the interaction parameter (χ), degree of polymerization (N), and chain composition (f).[134] Despite this, there is only a limited understanding of phase separation kinetics and evolving grain structures in block copolymer solution.

It has been reported[135] that casting conditions (concentration, drying rate and temperature) of random and block copolymer systems of BisSF-BPSH (Figure 7.1) exhibited substantial effects on membrane properties and performance, such as proton conductivity. The processing conditions, the casting method, drying temperature, and initial polymer concentration, which effect on block copolymer morphologies, resulted in a profound impact on the proton conductivity.

For BisSF 17k/12k samples, a membrane made using a the batch process, 5 % initial concentration, and low temperatures showed a significantly increased conductivity over a membrane made from a casting process, 12.5 % initial concentration, and higher temperature. This clearly demonstrates that the processing conditions affect membrane permeability.

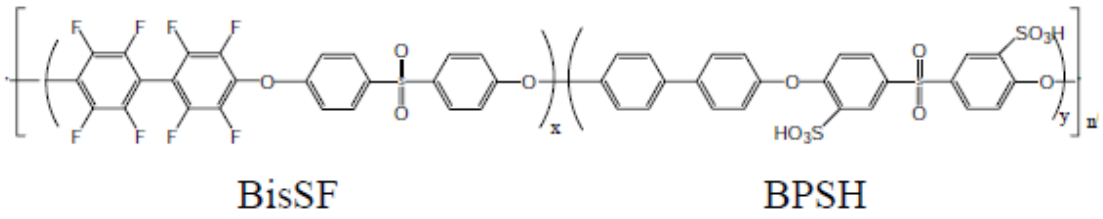

Figure 7.1: Chemical structure of BisF-BPSH (x:y) multiblock, x and y represents block lengths in kg/mole[136]

In order to optimize the performance of a membrane produced by means of solution casting, understanding the kinetics of block copolymer phase separation during the solvent removal process is necessary to efficiently design processes that produce an appropriate microstructure. In previous research[137,138], shallow temperature quenches (vertical line in Figure 7.2) are used to understand block copolymer morphologies from isotropic to ordered structures, but the processes in industry are based on changing the polymer solution concentration during the solvent drying process (horizontal line in Figure 7.2). Herein, we present preliminary research on the phase separation behavior of polymer solution-cast films studied using small angle X-ray scattering (SAXS).

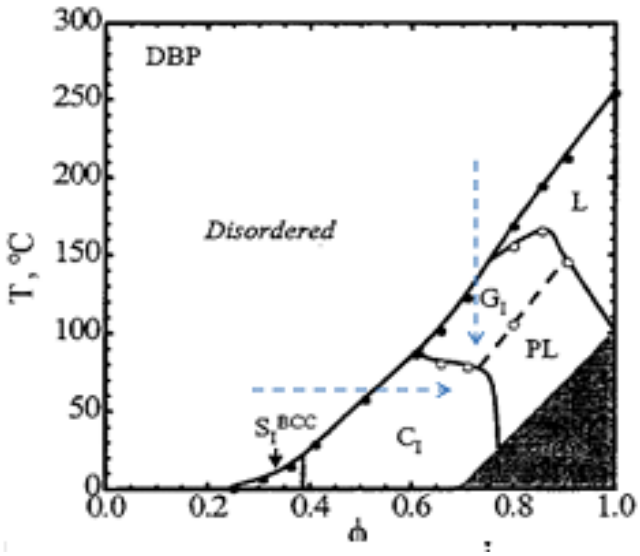

Figure 7.2: Phase diagram[138] for a SI copolymer in DBP with lines showing a temperature quench (vertical) and concentration change (horizontal)

7.2 Experimental

7.2.1 Materials

Poly(styrene-butadiene-styrene) (SBS), poly(styrene-butadiene) (SB), and toluene were purchased from Sigma. SBS consists of 30 wt% styrene block with a molecular weight,

140,000 g/mol and SB consists of 30 wt% styrene block with a molecular weight, 130,000 g/mol. All reagents were used without further purification.

7.2.2 Measurements

10 wt% SB or SBS toluene solutions were mixed using a sonicator at room temperature for 3 hours. The completely dissolved polymer solution was cast onto a petri dish, followed by using drying until it reached at a desired concentration. The sample was sandwiched between two kapton windows and vertically positioned in a sample cell (Figure 7.3) for SAXS measurements while changing temperatures at the same concentration.

In order to carry out SAXS measurements while monitoring solvent at a constant temperature, a sample cell (Figure 7.4) was designed to monitor the sample weight changes using a microbalance (accuracy; 0.001 g). A laptop computer linked with the microbalance recorded the sample weight every five seconds. 10 wt% SB or SBS toluene solution was cast onto a silicon wafer and placed on a sample stage.

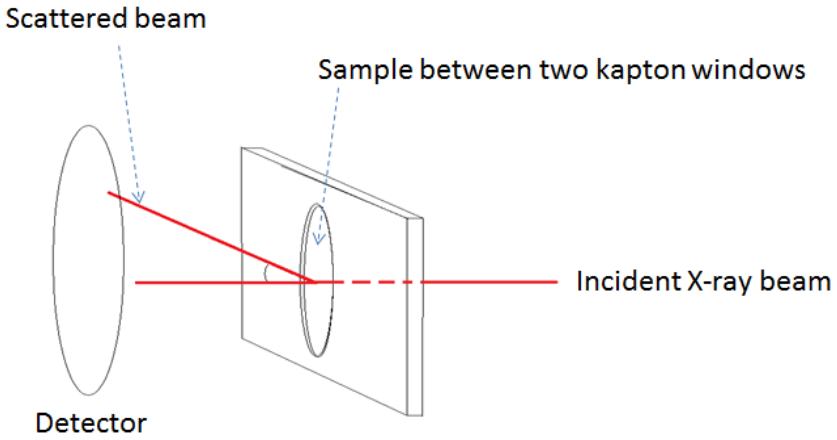

Figure 7.3: SAXS measurement for the polymer solution vertically positioned. The detector measures the scattered beam intensity as a function of angle between scattered beam and incident beam.

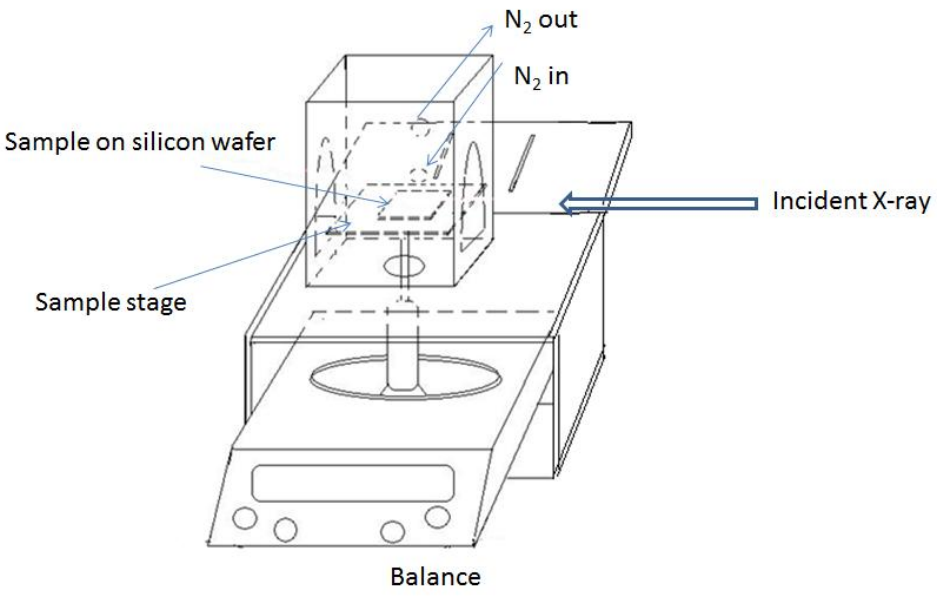

Figure 7.4: Sample cell to allow SAXS measurements while monitoring sample concentrations

7.2.3 SAXS Parameters

The images of the scattered beams are transformed into two-dimensional plots of the scattered beam intensity, I(q), versus scattering vector, $q=4\pi\sin(\theta)/\lambda$ (λ is the wavelength of the X-rays; 2θ is the angle between the incident X-ray beam and the scattered beam). The first peak at low q is called the primary peak. The q-value, q_{max}, at which this peak achieves its maximum is used to calculate the interdomain Bragg Spacing

$$D_{Bragg} = \frac{2\pi}{q_{\max}} \qquad (7.1)$$

In order to determine the relative degree of ordering in a system, the integrated peak intensity of the primary peak is used.

$$I^*(q) = \int I(q)dq \qquad (7.2)$$

Various secondary peaks will appear, having significantly lower intensities than the primary peaks. Depending on the microphase orientations or morphologies, the ratio of peak positions, $n=q_i/q_{max}$ (i=2,3,…; q_{max} corresponds to the primary peak; q_2 for the second peak

and q_3 for the third peak), shows different values. For example (Figure 7.5), peaks are found at n = 1, 2, 3, 4 for lamellae structures while hexagonally packed cylinders give peaks at n = 1, 2, $3^{1/2}$, $7^{1/2}$.

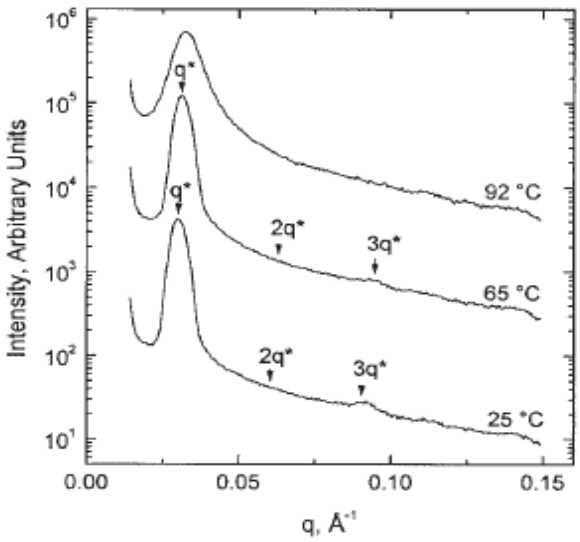

Figure 7.5: X-ray scattering profiles for styrene-isoprene (SI) copolymer in dioctyl phthalate at different temperatures.[139] Peaks are found at n=1,2,3 due to the lamellae structures.

7.3 Results

10 wt% SBS toluene solution was dried at room temperature and sampled at 30 wt%. The sample was vertically placed in the sample cell for SAXS measurements. The primary peak for the sample at 55 ℃ (Figure 7.6) was continuously decreased for 25 min due to the increased mobility between stytene and butadiene blocks. Under heating up to 60 ℃, the peak showed a further decrease due to decreasing order. As time increases while keeping the temperature, the peak reached at its equilibrium state. Primary peaks shifted to higher q at 55 ℃, indicating a decrease in Bragg Spacing (interdomain distance), D_{Bragg}. The shifted peaks were not observed at 60 ℃. For 35 wt% SBS toluene solution, the peak (Figure 7.7) decreased under heating and showed a negligible intensity after 3 hrs. The peak was recovered after cooling, but could not reach the original peak intensity for 6 hrs.

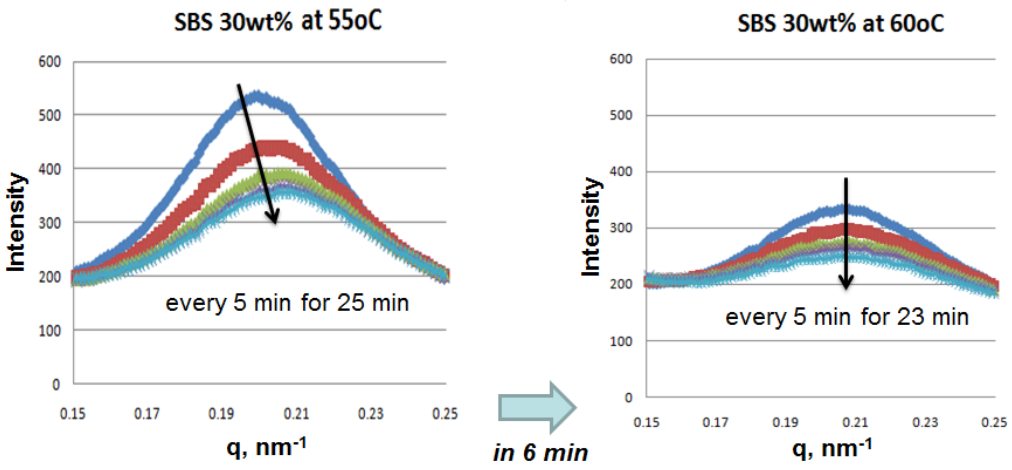

Figure 7.6: SAXS intensity changes at different temperatures

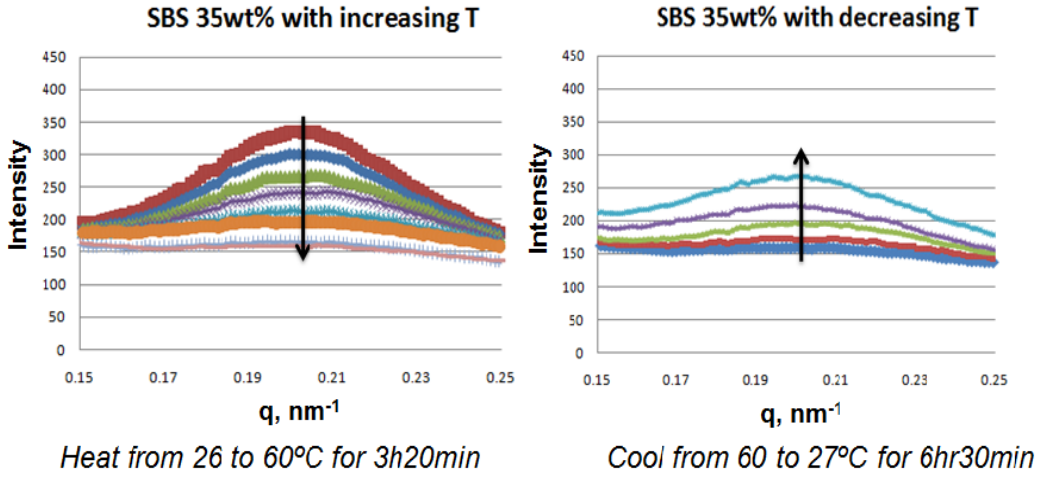

Figure 7.7: SAXS intensity changes while cooling and heating the sample

In the SAXS measurements at various concentrations during drying at a room temperature, the sample cell (Figure 7.4) was used and 10 wt% samples were located onto the silica substrate. Three different drying rates were used, all at room temperature: sweep gas is run through the sample cell; no sweep gas is run through the sample cell; the sample is dried in the presence of excess solvent with no sweep gas to give enough time for equilibrium. The peak (Figure 7.8) appeared for the SB toluene solution after 40 wt% concentration, which

suggests that the isotropic to ordered phase transition occurred at sample concentrations between 30 % and 40 % at a room temperature.

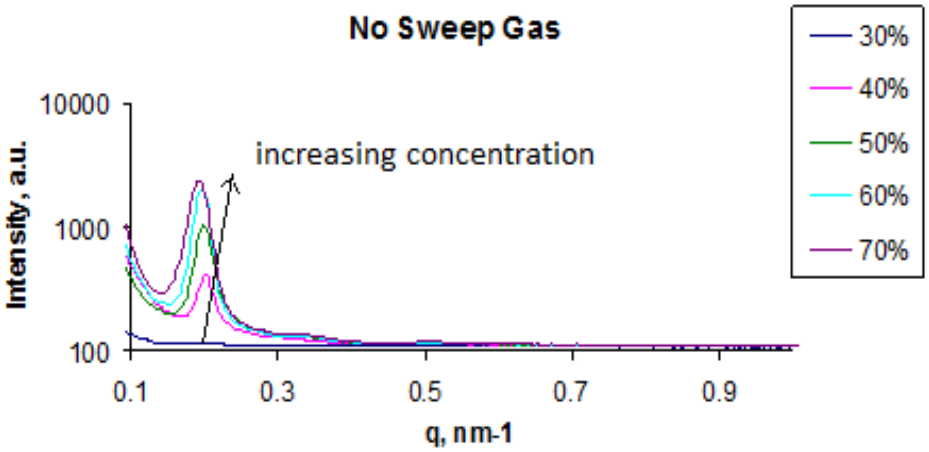

Figure 7.8: Scattering profile of SB in toluene at various concentrations during drying at room temperature without a sweep gas

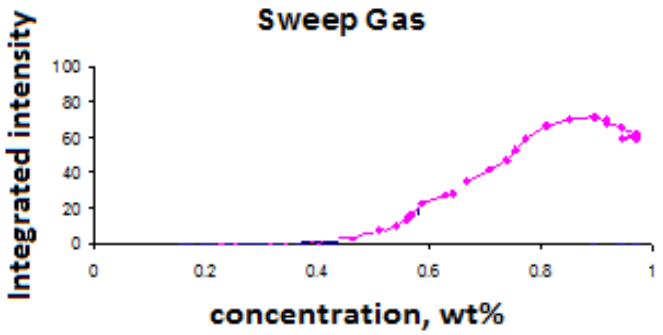

(a) Drying with sweep gas

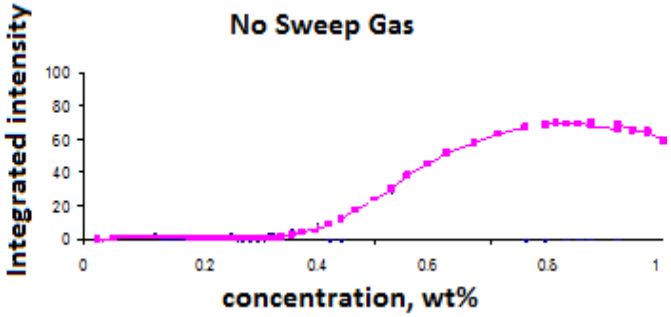

(b) Drying with no sweep gas

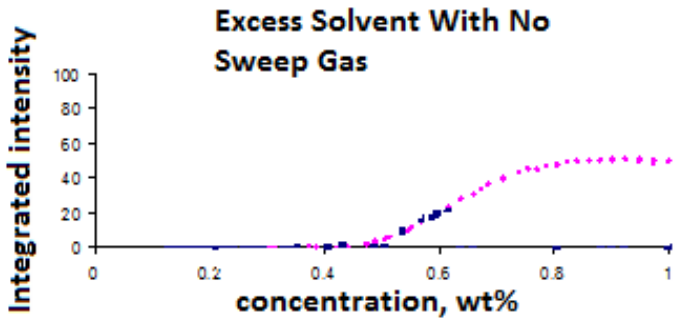

(c) Saturated air with toluene with no sweep gas

Figure 7.9: Integrated primary peak intensity of SB in toluene during drying under various conditions

The integrated primary peak intensity is presented for three different drying conditions (Figure 7.9). The peak appeared before 40 wt% during no sweep gas (Figure 7.9, (b)) due to the more mobility in slow drying compared to the sweep gas condition, but the

slowest drying condition with excess solvent (Figure 7.9, (c)) showed the peak appearance after 40 wt%.

In future work, block copolymer morphologies will be investigated to understand the polymer solution phase behavior at different temperatures during solvent removal. Optimum processing conditions for the production of polymer films will be determined with the phase separation kinetics obtained from the SAXS measurements.

Chapter 8. Conclusions and Future Work

This thesis is directed toward exploring the sorption and diffusion properties in liquid crystal materials. The previous research on liquid crystals for separation applications was conducted in gas phase separations by measuring the weight of absorbed gas molecules. The understanding of transport properties in the liquid crystals remains limited. Therefore, the purpose of this work was to experimentally determine the sorption and diffusion properties of organic solutes in liquid phase separations. In further research, we presented an enantioselective membrane using a cholesteric liquid crystal phase based on the understanding of transport properties from the liquid phase separations.

It is difficult to directly determine the solubility and diffusivity of solutes in liquid crystal materials. We have adopted a time-lag method to determine the diffusivity and solubility of organic solutes through supported liquid crystal membranes. The organic solutes were selected to allow us to study the relative effects of molecular shape and intermolecular interactions (pi-pi interactions, hydrogen bonding, and dipole interactions) on the solubility and diffusivity of organic solutes in liquid crystal materials. Notably, we observed (1) enhanced diffusion of solutes possessing a single hydrogen-bond donor compared to those with multiple hydrogen-bond donors or no hydrogen-bond donors; (2) higher diffusivity and solubility in PCH5 than 8CB due to lower packing density of PCH5; and (3) shape selective sorption of organic solutes in the anisotropic phases of 8CB and PCH5.

Both 8CB and PCH5 liquid crystals embedded cellulose nitrate membranes exhibited permeation selectivities due to inter and intramolecular hydrogen bonding interactions between solute and liquid crystal or water molecule. PCH5 liquid crystalline membranes exhibited enhanced selectivity for hydroxybenzoic acid and aminophenol isomers compared to 8CB membranes due to increased sorption selectivities. Hydroxybenzoic acid and aminophenol isomer separations have not been previously reported in membrane separations.

In order to evaluate the performance of enantioselective membranes, an HPLC-CD detection system has been developed. The HPLC-CD technique relies on the use of circular dichroism (CD) detector in combination with a non-chiral phase based HPLC (HPLC-CD). The HPLC-CD system has significant advantages over conventional chiral column based HPLC detection system as the nonchiral-based HPLC-CD system does not require multiple expensive chiral columns for the detection of different enantiomer molecules. To our knowledge there have been no previous reports of its use for the characterization in membrane separations.

Enantioselective membranes were fabricated by impregnation of a mixture of 5CB and chiral dopant into a polymer support. The cholesteric phase was layered onto the polymer support and the membrane had pores through which enantiomer molecules permeated with interactions between the enantiomer and the liquid crystal phase. Enantiomers of the same handedness as the cholesteric phase have more interactions, resulting in the slower diffusion than other enantiomers. Higher activation energies for permeation through the membrane were observed in the cholesteric phase than in the isotropic phase due to the stronger interactions between the enantiomer and the liquid crystals in the cholesteric phase. As a result, higher selectivities were observed in the cholesteric phase. According to the theoretical pore size, the membranes with the smaller pore size exhibited higher selectivity due to the increased chance of interactions between enantiomer and cholesteric phase, but exhibited lower permeability. In terms of chiral dopant concentration effects on the selectivity, the selectivity was increased until a critical point, 17mol% of chiral dopant.

Future considerations, based on the results of the present research should be directed toward enhancing the stability of the liquid crystal embedded membranes. The liquid crystals were leached out from the cellulose nitrate membrane support, which was monitored on UV spectrometer and HPLC. The stability problem is general in the supported liquid membrane type. During experiments, the liquid crystals leaching from the membrane support were

detected by using a UV spectrometer. Different kinds of membranes should be considered such as polymer dispersed liquid crystal (PDLC) membranes in which liquid crystal droplets are embedded in polymer networks or LC droplet polymers.

The liquid crystals in the cellulose nitrate membrane could not be oriented along with one direction since the pores of the cellulose nitrate membrane are randomly oriented. For enhanced permeability and selectivity, the liquid crystals need to be oriented in one direction by embedding liquid crystals in the membranes with unidirectional pores such as an Anopore aluminium oxide membrane.

For enantiomer separations, the membrane requires a transport channel through which the enantiomers can interact with the cholesteric LC surface. In the future, chiral dopants with more hydrogen acceptors should be developed to enhance the enantioselectivity. In addition, techniques to make membranes with smaller pore sizes and to prevent LC loss from the membrane are needed.

References

1 Branco, L. C.; Crespo, J. G.; Alfonso, C. A. M. *Angew. Chem. Int. Ed.* **2002**, *51*, 2771-2773.
2 Park, Y.; Skelland, A. H. P.; Forney, L. J.; Kim, J. *Water Research* **2006**, *40*, 1763-1772.
3 Villaluenga, G. P. G.; Tabe-Mohammadi, A. *J. Mem. Sci.* **2000**, *169*, 159-174.
4 Maruyama, A.; Adachi, N.; Takatsuki, T.; Torii, M.; Sanui, K.; Ogata, N. *Macromolecules* **1990**, *23*, 2748-2752.
5 Xiaotian, Q.; Zaide, Z.; Minggui, X.; Yongchang, Z.; Ying, T. *Talanta* **1998**, *46*, 45-51.
6 Onuchak, L. A.; Stepanova, R. F.; Kudryashov, S. Y.; Akopova, O. B. *Russ. J. Phys. Chem. A* **2008**, *82(2)*, 269-275.
7 Gvozdovskyy, I.; Lisetski, L. *Mol. Cryst. Liq. Cryst.* **2007**, *475*, 113-122.
8 Kozawaguchi, H.; Wada, M. *Jpn. J. Appl. Phys.* **1975**, *14(5)*, 657-660.
9 Gin, D. L.; Lu, X.; Nemade, P. R.; Pecinovsky, C. S.; Xu, Y.; Zhou, M. *Adv. Funct. Mater.* **2006**, *16*, 865-878.
10 Gin, D. L.; Gu, W.; Pindzola, B. A.; Zhou, W. *Acc. Chem. Res.* **2001**, *34*, 973-980.
11 Bunjes, H.; Rades, T. *J. Pharm. Pharmacol.* **2005**, *57*, 807-816.
12 Eelkema, R.; Feringa, B. L. *Org. Biomol. Chem.* **2006**, *4*, 3729-3745.
13 Goodby, J. W. *J. Mater. Chem.* **1991**, *1*, 307-318.
14 Artsyukhovich, A.; Broekman, L. D.; Salmeron, M. *Langmuir* **1999**, *15*, 2217-2223.
15 Chandrasekhar, S. Liquid Crystals. 2nd ed. **1992**, Cambridge University Press.
16 Chilaya, G. Partially Ordered System: Chirality in Liquid Crystals **2001**, Springer New York.
17 Lin, S. Y.; Lin, H. L.; Li, M. J. *Eur. J. Pharm. Sci.* **2002**, *17*, 153-160.
18 Lin, S. Y.; Chen, K. S.; Lin, Y. Y. *J. Controlled. Rel.* **1998**, *55*, 13-20.
19 Lin, S. Y.; Lin, H. L.; Li, M. J. *J. Mem. Sci.* **2003**, *225*, 135-143.
20 Nozawa, I.; Suzuki, Y.; Sato, S.; Sugibayashi, K.; Morimoto, Y. *J. Biomed. Mater. Res.* **1991**, *25*, 243-254.
21 Nozawa, I.; Suzuki, Y.; Sato, S.; Sugibayashi, K.; Morimoto, Y. *J. Biomed. Mater. Res.* **1991**, *25*, 577-588.
22 Dinarvand, R.; Khodaverdi, E.; Atyabi, F. *Mol. Cryst. Liq. Cryst.* **2005**, *442*, 19-30.
23 Inui, K.; Okazaki, K.; Miyata, T.; Uragami, T. *J. Mem. Sci.* **1998**, *143*, 93-104.
24 Inui, K.; Miyata, T.; Uragami, T. *J. Poly. Sci.: Part B: Poly. Phys.* **1998**, *36*, 281-288.
25 Okuno, H.; Nishida, T.; Uragami, T. *J. Poly. Sci.: Part B: Poly. Phys.* **1995**, *33*, 299-307.
26 Inui, K.; Miyata, T.; Uragami, T. *J. Poly. Sci.: Part B: Poly. Phys.* **1997**, *35*, 699-707.
27 Hsu, E. C. H.; Johnson, J. F. *Mol. Cryst. Liq. Cryst.* **1974**, *27*, 95-104.
28 Lin, S. Y.; Tseng, H. Y.; Li, M. J.; *Appl. Phys. A* **2000**, *70*, 663-668.
29 Drzaic, P. S. *Liq. Cryst.* **2006**, *33(11-12)*, 1281-1296.
30 Higgins, D. A.; Hall, J. E.; Xie, A. *Acc. Chem. Res.* **2005**, *38*, 137-145.
31 Kajiyama, T.; Nagata, Y.; Maemura, E.; Takayanagi, M. *Chem. Lett.* **1979**, 679-682.
32 Chen, G.; Springer, J. *Mol. Cryst. Liq. Cryst.* **2000**, *339*, 31-44.
33 Chen, D.; Hsiue, G. *Mol. Cryst. Liq. Cryst.* **1993**, *237*, 85-95.
34 Hsiue, G.; Chen, D.; Hsieh, C. *Mol. Cryst. Liq. Cryst.* **1994**, *241*, 187-193.
35 Chen, G.; Springer, J. *Macromol. Chem. Phys.* **2000**, *201*, 1552-1559.
36 Ghosal, K.; Freeman, B. D. *Polymer Adv. Tech.* **1994**, *5*, 673-697.
37 Witkiewicz, Z. *J. Chromatogr.* **1982**, *251*, 311.
38 Witkiewicz, Z. Liquid Crystals: Applications and Uses, World Scientific Publishing, Singapore, **1991**.

39 Witkiewicz, Z.; Oszczudlowski, J.; Repelewicz, M. *J. Chromatogr. A* **2005**, *1062*, 155-174.
40 Zielinski, W. L.; Johnston, K.; Muschik, G. M. *Anal. Chem.* **1976**, *48(6)*, 907-911.
41 Sakagami, S.; Nakamizo, *Chem. Soc. Jap.* **1984**, *57*, 1157-1158.
42 Medina, I. *Liq. Cryst.* **1992**, *12(6)*, 989-995.
43 Han, S.; Martin, S. M. *J. Phys. Chem. B* **2009**, *113*, 12696-12703.
44 Miyako, E.; Maruyama, T.; Kamiya, N.; Goto, M. *Chem. Eur. J.* **2005**, *11*, 1163-1170.
45 van Delden, R. A.; Feringa, B. L. *Angew. Chem. Int. Ed.* **2001**, *40*, 3198-3200.
46 Goodby, J. W. *Science*, **1986**, *231*, 350-355.
47 Kocherginsky, N. M.; Yang, Q.; Seelam, L. *Sep. Pur. Tech.* **2007**, *53*, 171-177.
48 van Laarhoven, J. A. H.; Kruft, M. A. B.; Vromans, H. *Int. J. Pharm.* **2002**, *232*, 163-173.
49 Mukoma, P.; Jooste, B. R.; Vosloo, H. C. M. *J. Mem. Sci.* **2004**, *243*, 293-299.
50 Liang, S.; Zhang, L.; Xu, J. *J. Mem. Sci.* **2007**, *287*, 19-28.
51 Sanchez, J.; Gijiu, C. L.; Hynek, V.; Muntean, O.; Julbe, A. *Sep. Pur. Tech.* **2001**, *25*, 467-474.
52 Morgan, D.; Ferguson, L.; Scovazzo, P. *Ind. Eng. Chem. Res.* **2005**, *44*, 4815-4823.
53 Sawada, A.; Naemura, S. *Jpn. J. Appl. Phys.* **2002**, *41*, 195-197.
54 Rozanski, S. A. *Syn. Metals* **2000**, *109*, 245-248.
55 Vilfan, M.; Apih, T.; Sebastiao, P. J.; Lahajnar, G.; Zumer, S. *Phys. Rev. E* **2007**, *76*, 051708.
56 Rutherford, S. W.; Do, D. D. *Adsorption*, **1997**, *3*, 283-312.
57 Crandall, K. A.; Rosenblatt, C.; Aliev, F. M. *Phys. Rev. E* **1996**, *53*, 636-640.
58 Vilfan, M.; Vrbancic-Kopac, N.; Ziherl, P.; Crawford, G. P. *Appl. Magn. Reson.* **1999**, *17*, 329-344.
59 Denolf, K.; Cordoyiannis, G.; Glorieux, C.; Thoen, *J. Phys. Rev. E* **2007**, *76*, 051702.
60 Glemza, A. J.; Koehler, J. A.; Brune, B. J.; Payne, G. F. *Ind. Eng. Chem. Res.* **1998**, *37*, 3685-3690.
61 Park, H.; Yoon, S.; Lee, J.; Chough, S. J. Appl. Pol. Sci. **2007**, 105, 2824-2829.
62 Berthelot, M.; Laurence, C.; Foucher, D.; Taft, R. W. *J. Phys. Org. Chem.* **1996**, *9*, 255-261.
63 Berthelot, M.; Laurence, C.; Lucon, M.; Rossignol, C.; Taft, R. W. *J. Phys. Org. Chem.* **1996**, *9*, 626.
64 Thote, A. J.; Gupta, R. B. *Ind. Eng. Chem. Res.* **2003**, *42*, 1129-1136.
65 Thote, A. J.; Gupta, R. B. *Fluid Phase Equil.* **2004**, *220*, 47-55.
66 Eaton, D. R.; Sandercock, A. C. *J. Phys. Chem.* **1982**, 86, 1371-1375.
67 Eaton, G.; Pena-Nunez, A. S.; Symons, M. C. R. *J. Chem. Soc., Faraday Trans. 1* **1988**, *84(6)*, 2181-2193.
68 Funasaka, W.; Fujimura, K.; Kushida, S. *J. Chromatogr.* **1972**, *64*, 95-101.
69 Belaidi, D.; Sebih, S.; Boudah, S.; Guermouche, M. H.; Bayle, J. P. *J. Chrom. A* **2005**, *1087*, 52-56.
70 Vilfan, M.; Apih, T.; Gregorovic, A.; Zalar, B.; Lahajnar, G.; Zumer, S.; Hinze, G.; Bohmer, R.; Althoff, G. *Magn. Reson. Imaging* **2001**, *19*, 433-438.
71 Zhang, J.; MacGregor, R. P.; Balcom, B. J. *Chem. Phys. Lett.* **2008**, *461*, 106-110.
72 Blinc, R.; Marin, B.; Pirs, J.; Doane, J. W. *Phys. Rev. Lett.* **1985**, *54*, 438-440.
73 Belyaev, V. V.; Grebenkin, M. F.; Petrov, V. F. *Russ. J. Phys. Chem.* **1990**, *64(4)*, 509-511.
74 Afonso, C. A. M.; Crespo, J. G. *Angew. Chem. Int. Ed.* **2004**, *43*, 5293-5295.
75 Yang, W. C.; Yu, X. D.; Yu, A. M.; Chen, H. Y. *J. Chromatogr. A* **2001**, *910*, 311.
76 Rastogi, S. C. *J. Sep. Sci.* **2001**, *24*, 173.

77 Hu, Z.; Jia, L.; Zhang, Z. *Anal. Lett.* **1996**, *29(14)*, 2573-2586.
78 Dzygiel, P.; Wieczorek, P.; Mathiasson, L.; Jonsson, J. A. *Anal. Lett.* **1998**, *31(7)*, 1261-1274.
79 Bhandare, A. A.; Argekar, A. P. *J. Mem. Sci.* **2002**, *201*, 233-237.
80 Oweimreen, G. A. *J. Phys. Chem. B* **2001**, *105*, 8417-8419.
81 Watson, S. J.; Gleeson, H. F.; D'Emanuele, A. *Mol. Cryst. Liq. Cryst.* **2001**, *367*, 435-443.
82 Press, M. J.; Arrott, A. S. *Phys. Rev. A* **1973**, *8*, 1459.
83 Chan, M. L.; Chan, T. C. *J. Phys. Chem.* **1995**, *99*, 5765-5768.
84 Plessis, J. D.; Pugh, W. J.; Judefeind, A.; Hadgraft, J. *Eur. J. Pharm. Sci.* **2001**, *13*, 135-141.
85 Inui, K.; Miyata, T.; Uragami, T. Macromol. *Chem. Phys.* **1998**, *199*, 589-595.
86 Mota, F. L.; Queimada, A. J.; Pinho, S. P.; Macedo, E. A. *Ind. Eng. Chem. Res.* **2008**, *47*, 5182-5189.
87 Korenman, Y. I.; Taldykina, S. N.; Usenko, E. A. Deposited Doc. **1976**, 2556-76.
88 Tsujino, Y.; Hieda, Y.; Kimura, K.; Dekio, S. *Foren. Sci. Int.* **2003**, *133*, 141-145.
89 Hu, C.; Chen, Z.; Shen, A.; Shen, X.; Li, J.; Hu, S. *Carbon*, **2006**, *44(3)*, 428-434.
90 Thomas, M.; Richardson, H. H. Vib. *Spectroscopy*, **2000**, *24*, 137-146.
91 Anslyn, E. V.; Dougherty, D. A. Modern Physical Organic Chemistry. University Science Books. **2005**, pp155.
92 Wacrenier, J. M.; Druon, C.; Lippens, D. *Mol. Phys.* **1981**, *43*, 97.
93 Martienssen, W.; Warlimont, H. Handbook of condensed matter and materials data. Springer. **2005**, pp 950.
94 Digest of Literature on Dielectrics, 38, 1974, National Academy of Sciences, Washington, D.C.
95 Chan, T. C. *J. Chem. Phys.* **1984**, *80(11)*, 5862-5864.
96 Swislocka, R.; Oleksinski, E.; Regulska, E.; Kalinowska, M.; Lewandowski, W. *J. Mol. Str.* **2007**, *834-836*, 380-388.
97 Maistrenko, V. N.; Sapel'nikova, S. V.; Kudasheva, F. Kh.; Amirkhanova, F. A. J. *Anal. Chem.* **2000**, *55(6)*, 586-589.
98 Wilke, C. R.; Chang, P. C. Am. *Inst. Chem. Eng. J.* **1955**, *1*, 264.
99 Niesner, R.; Heintz, A. *J. Chem. Eng. Data* **2000**, *45*, 1121-1124.
100 Logan, B. E. Environmental Transport Processes. Wiley-Interscience. **1998**, pp 66-71.
101 Capar, M. I.; Cebe, E. Chem. *Phys. Lett.* **2005**, *407*, 454-459.
102 Jadzyn, J.; Dabrowski, R.; Lech, T.; Czechowski, G. *J. Chem. Eng. Data* **2001**, *46*, 110-112.
103 Cheung, D. L.; Clark, S. J.; Wilson, M. R. Chem. *Phys. Lett.* **2002**, *356*, 140-146.
104 Hayduk, W.; Minhas, B. S. *Canadian J. of Chem. Eng.* **1982**, *60*, 295-299.
105 Krieg, H. M.; Breytenbach, J. C.; Keizer, K. *J. Mem. Sci.* **2000**, *164*, 177-185.
106 Aoki, T.; Tomizawa, S.; Oikawa, E. *J. Mem. Sci.* **1995**, *99*, 117-125.
107 Rmaile, H. H.; Schlenoff, J. B. *J. Am. Chem. Soc.* **2003**, *125*, 6602-6603.
108 Matsumoto, T.; Ito, M.; Fukuda, H.; Kondo, A. *Appl. Microbiol. Biotechnol.* **2004**, *64*, 481-485.
109 Kataky, R.; Murphy, L.; Lancon, A. D.; Kalakuntla, S.; Lopes, P. *J. Electroanal. Chem.* **2009**, *633*, 57-62.
110 Sereewatthanawut, I.; Boam, A. T.; Livingston, A. G. *Macromole. Symp.* **2008**, *264*, 184-188.
111 Ward, T. J.; Baker, B. A. *Anal. Chem.* **2008**, *80*, 4363-4372.
112 Gubitz, G.; Schmid, M. G. *Electrophoresis* **2004**, *23*, 3981–3996.

113 Miyako, E.; Maruyama, T.; Kamiya, N.; Goto, M. *J. Am. Chem. Soc.* **2004**, *126*, 8622-8623.
114 Teraguchi, M.; Suzuki, J.; Kaneko, T.; Aoki, T.; Masuda, T. *Macromolecules* **2003**, *36*, 9694-9697.
115 Miller, M. T.; GE, Z.; Mao, B. *Chirality* **2002**, *14*, 659-664.
116 Kelly, S. M.; Price, N. C. *Curr. Prot. Pept. Sci.* **2000**, *1(4)*, 349-384.
117 Xie, R.; Chu, L.; Deng, J. *Chem. Soc. Rev.* **2008**, *37*, 1243-1263.
118 Bertucci, C.; Andrisano, V.; Cavrini, V.; Castiglioni, E. *Chirality* **2000**, *12*, 84-92.
119 Reetz, M. T.; Kuhling, K.M.; Hinrichs, H.; Deege, A. *Chirality* **2000**, *12*, 479-482.
120 Ingle, J. D. J.; Crouch, S. R. Spectrochemical analysis, Prentice Hall, New Jersey **1988**.
121 Xiao, Y.; Lim, H. M.; Chung, T. S.; Rajagopalan, R. *Langmuir* **2007**, *23*, 12990-12996.
122 Demirel, N.; Bulut, Y.; Hosgoren, H. *Chirality* **2004**, *16*, 347-350.
123 Yang, M.; Chu, L.; Wang, H.; Xie, R.; Song, H.; Niu, C. H. *Adv. Funct. Mater.* **2008**, *18*, 652-663.
124 van der Ent, E.M.; van't Riet, K.; Keurentjes, J. T. F.; van der Padt, A. *J. Mem. Sci.* **2001**, *185*, 207-221.
125 Aoki, T.; Ohshima, M.; Shinohara, K.; Kaneko, T.; Oikawa, E. *Polymer* **1997**, 38(1), 235-238.
126 Matsuoka, Y.; Kanda, N.; Lee, Y. M.; Higuchi, A. J. *Mem. Sci.* **2006**, 280, 116-123.
127 Ghosh, R. *J. Chromatogr. A* **2001**, *923*, 59-64.
128 Ghosh, R. *J. Chromatogr. A* **2002**, *952*, 13-27.
129 Ghosh, R. *J. Mem. Sci.* **2009**, *344*, 107-111.
130 Frezzato, D.; Moro, G. J.; Zannoni, C. *J. Chem. Phys.* **2005**, *122*, 164904.
131 Frezzato, D.; Zannoni, C.; Moro, G. J. *J. Chem. Phys.* **2006**, *125*, 104903.
132 Aydin, L.; Aral, T; Karakaplan, M.; Hosgoren, H. *Tetrahedron: Asymmetry* **2009**, *20(2)*, 179-183.
133 Courty, S.; Tajbakhsh, A. R.; Terentjev, E. M. *Phys. Rev. E* **2006**, *73*, 011803.
134 Matsen, M. W.; Bates, F. S. *Macromolecules* **1996**, *29*, 1091-1098.
135 Huang, J.; Baird, D. G.; Fan, G.; Zhang, Z.; Badami, A.; Takamuku, S.; McGrath, J. E. Continuous film casting and evaluation of polymer membranes for fuel cells, **2007** Society of Plastics Engineers Annual Conference, Cincinnati, OH.
136 Yu, X.; Roy, A.; Dunn, S.; Yang, J.; McGrath, J. E. *Macromolecular Symposia* **2006**, *245/246*, 439-449.
137 Chastek, T. Q.; Lodge, T. P. *J. Poly. Sci.: Part B: Physics* **2006**, *44*, 481-491.
138 Lodge, T. P.; Pudil, B.; Hanley, K. J. *Macromolecules* **2002**, *35*, 4707-4717.
139 Chastek, T. Q.; Lodge, T. P. *J. Polym. Sci. Part B* **2005**, *43*, 405.